uOttawa

L'Université canadienne
Canada's university

FACULTÉ DES ÉTUDES SUPÉRIEURES ET POSTOCTORALES

uOttawa

L'Université canadienne
Canada's university

FACULTY OF GRADUATE AND POSDOCTORAL STUDIES

Forouzan Sadeghi
AUTEUR DE LA THÈSE / AUTHOR OF THESIS

M.A.Sc. (Chemical Engineering)
GRADE / DEGREE

Department of Chemical Engineering
FACULTÉ, ÉCOLE, DÉPARTEMENT / FACULTY, SCHOOL, DEPARTMENT

Development of Nanocomposite Materials for Gas Separation Membranes

TITRE DE LA THÈSE / TITLE OF THESIS

Dr. B. Kruczek
DIRECTEUR (DIRECTRICE) DE LA THÈSE / THESIS SUPERVISOR

Dr. A. Tremblay
CO-DIRECTEUR (CO-DIRECTRICE) DE LA THÈSE / THESIS CO-SUPERVISOR

EXAMINATEURS (EXAMINATRICES) DE LA THÈSE / THESIS EXAMINERS

Dr. C. Lan

Dr. H. Tezel

Gary W. Slater
Le Doyen de la Faculté des études supérieures et postdoctorales / Dean of the Faculty of Graduate and Postdoctoral Studies

DEVELOPMENT OF NANOCOMPOSITE MATERIALS FOR GAS SEPARATION MEMBRANES

by

FOROUZAN SADEGHI

Thesis submitted to the
Faculty of Graduate and Postdoctoral Studies
in partial fulfillment of requirements for the degree of

Master of Science
In Chemical Engineering

Department of Chemical Engineering
Faculty of Engineering
University of Ottawa

May 2007

Your file Votre référence
ISBN: 978-0-494-34107-0
Our file Notre référence
ISBN: 978-0-494-34107-0

STATEMENT OF CONTRIBUTION OF COLLABORATORS

I hereby declare that I am the sole author of this thesis. All the experiments and discussions were performed by me under the supervision and training received from professors Andre Y. Tremblay and Boguslaw Kruczek.

Signature

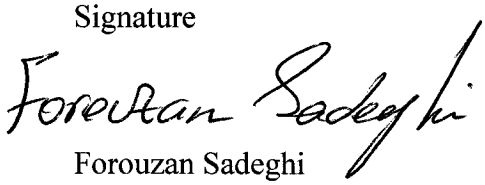

Forouzan Sadeghi

Date: May 14, 2007

To my father

ABSTRACT

The objective of this study is to improve the compatibility of nanoparticles in composite materials. This was achieved by developing a method in which an inorganic precursor contained in a stable water/oil (W/O) emulsion was mixed with a polymer solution containing a second inorganic precursor. Inorganic polymerization occurred in the aqueous domain of the W/O emulsion. The in-situ synthesis of the precursor was performed in order to enhance the nanoscale compatibility between the inorganic material and polymer. This technique produced materials which we have named: emulsion polymerized mixed matrix (EPMM) materials.

A series of poly (2,6-dimethyl-1,4-phenylene oxide) (PPO)-based organic-inorganic membranes were prepared by employing this method. A W/O emulsion containing aluminium hydroxonitrate was added to a PPO solution containing tetraethyl orthosilicate (TEOS). Droplet sizes in the W/O emulsions, observed by dynamic light scattering (DLS) ranged from 254 to 344 nm.

Scanning electron micrography (SEM), electron diffractive X-Ray (EDX), thermogravimetric analysis (TGA), differential scanning calorimetry (DSC) and gas permeation and separation measurements were carried out to characterize the EPMM membranes. SEM indicated the presence of inorganic particles in the PPO matrix, and EDX measurements showed the embedded particles contained Al and Si elements, which confirmed the hydrolysis and condensation of TEOS with aluminium hydroxonitrate. DSC analysis showed a decrease in the glass transition of the EPMM membranes with increasing of TEOS loading. The fractional free volume of the EPMM membranes was predicted through the measurement of the heat capacity jump at the glass transition temperature. The integrity of the EPMM membranes was confirmed in gas separation test with air, in which the ideal selectivity for O_2/N_2 was observed to be as high as 4.56.

RÉSUMÉ

L'objectif de cette étude est d'améliorer la compatibilité des nanoparticules dans les matériaux composites. Ceci a été réalisé en concevant une méthode de fabrication dans laquelle un précurseur inorganique contenu dans une émulsion aqueuse/organique est mélangé à une solution polymérique contenant un deuxième précurseur inorganique. La polymérisation inorganique s'est produite dans le domaine aqueux au sein de la solution polymérique. La synthèse in situ du précurseur a été accomplie afin d'augmenter la compatibilité à l'échelle nanométrique entre la matière inorganique et le polymère. Cette technique a produit des matériaux que nous avons appelés: « emulsion polymerized mixed matrix » (EPMM).

une série de membranes inorganiques-organiques a base de PPO poly (oxyde 2,6-dimethyl-1,4-phenylène) ont été préparées en utilisant cette méthode. L'orthosilicate tétraéthylique (TEOS) a été dissous dans une solution de PPO et de trichloroethylène. Une émulsion comprenant une solution aqueuse d'hydroxonitrate d'aluminium dispersé dans du trichloroethylène a été ajoutée à cette solution. La dimension des gouttelettes organiques dans les émulsions aqueuses/organiques se situe entre 254 et 344 nm.

La micrographie à balayage électronique (SEM), la diffraction par rayons X (EDX), l'analyse thermogravimétrique (TGA), la calorimétrie balayage différentiel (DSC) des mesures de perméation de gaz et de séparation ont étés effectuées pour caractériser les membranes d'EPMM. La SEM a indiqué la présence de particules inorganiques dans ces membranes, et les mesures d'EDX ont révélé la présence d'aluminium et de silice dans ces particules. Les résultats indiquent l'hydrolyse et la condensation du TEOS et de l'hydroxonitrate d'aluminium. L'analyse de DSC a montré une diminution de la transition de verre des membranes d'EPMM avec l'augmentation de la charge de TEOS. Le volume libre partiel des membranes d'EPMM a été déterminé par la mesure du saut de capacité de chaleur à la température de transition de verre. L'intégrité des membranes d'EPMM a été confirmée dans plusieurs essais de séparation de gaz avec de l'air, où on a observé une sélectivité idéale pour l'O_2/N_2 de 4.56.

ACKNOWLEDGMENTS

I wish to express my gratitude to professors A. Tremblay and B. Kruczek for their guidance, advice and supervision of this project. The financial support of National Science and Engineering Research Council of Canada is also appreciated.

I would like to thank to my parents, my sister and brother for their moral support and encouragement. Special thanks to my best friend Mr. George Popek for inspiring me to complete this work.

I am grateful to Messrs L. Tremblay, Gerald Nina and Franco Ziroldo for technical assistance during the course of this work.

Finally, I would like to thank to Siamak Lashkari, Roza Tizva , and all my friends in the membrane group at University of Ottawa.

TABLE OF CONTENTS

LIST OF TABLES

LIST OF FIGURES

NOMENCLATURE

ABBRIVATION

DLS	Dynamic Light Scattering
DSC	Differential Scanning Calorimetry
EDX	Energy Dispersive X-ray Spectroscopy
EPMM	Emulsion Polymerized Mixed Matrix
EPMM2	Emulsion polymerized mixed matrix with 5% TEOS loading
EPMM3	Emulsion polymerized mixed matrix with 10% TEOS loading
EtOH	Ethanol
GC	Gas Chromatography
HLB	Hydrophilelipophile Balance
MDDSC	Modulated Differential Scanning Calorimetry
PPO	Poly(2,6 dimethyl -1, 4phenylene oxide)
SDS	Sodium dodecyl sulfate
SEM	Scanning Electron Microscopy
Span 83	Sorbitan sesquioleate
St.Dev	Standaed Deviation
STP	Standard Temperature and Pressure conditions
TCE	Tricholoroethylene
TEOS	Tetraethylorthosilicate
TGA	Thermogravimetric Analysis
W/O	Water in oil
W/O/W	Water in-oil-in water

SYMBOLS

a	constant in Mark-Houwink equation (2-19).....	
A	permeation area of the membrane.....	[cm^3]
b	hole affinity constant	[$cmHg^{-1}$]
c	concentration	[$g\ dL^{-1}$]
c_D	concentration of gas in the Henry sites of polymer	[cm^3(STP) cm^{-3}]
c_H	concentration of gas in Langmuir sites of polymer.....	[cm^3(STP) cm^{-3}]
c'_H	hole saturation constant.....	[cm^3(STP) cm^{-3}]
d	d-spacing	[Å]
$d_{3,2}$	mean droplet size.....	[nm]
D	diffusivity coefficient	[cm^2s^{-1}]
D_D	diffusivity coefficient in Henry sorption sites.....	[cm^2s^{-1}]
D_H	diffusivity coefficient in Langmuir sorption sites	[cm^2s^{-1}]
ΔC_P	specific heat capacity.....	[$J\ g^{-1}\ ^oC^{-1}$]
E	energy.....	[J]
E_g	internal latent heat of vaporization at glass transition temperature	[$J\ mol^{-1}$]
E_V	energy density.....	[$kJ\ cm^{-3}$]

f	factional free volume.....	
f_g	fractional free volume at glass transition temperature.....	
h	thickness of film (Eq 2-30).....	[cm]
h	degree of hydrolysis.....	
J	flux	[cm^3(STP)cm^{-2} s^{-1}]
K	constant in Mark-Houwink equation (2-19).....	
l	Membrane thickness.....	[cm]
M	molecular weight.....	[g mol^{-1}]
N_h	number of moles of hole.....	
N_o	number of moles of molecules.....	
p	pressure.....	[cm Hg=1.3kPa]
P	permeability.....	[Barrer]
P_c	permeability of continuous phase.....	[Barrer]
P_d	permeability of dispersed phase.....	[Barrer]
Δp	pressure gradient across the membrane.....	[cm Hg]
r	wafer radius.....	[cm]
R	universal gas constant	[J $mol^{-1}K^{-1}$]
S	solubility coefficient	[cm^3(STP)cm^{-3} $cmHg^{-1}$]
T	absolute temperature.....	[K]
T_c	critical temperature.....	[K]
T_d	decomposition temperature.....	[°C]
T_g	glass transition temperature	[°C]
T_m	melting point	[°C]
v	molar volume.....	[m^3mol^{-1}]
v_h	molar free volume.....	[m^3mol^{-1}]
v_o	molar volume occupied by macromolecules	[m^3mol^{-1}]
V_e	emulsion volume.....	[cm^3]
x	mole fraction in feed streams.....	
y	mole fraction in permeat streams.....	

GREEK SYMBOLS

α	separation factor.....	
α^*	Ideal selectivity = permeability ratio = permselectivity..	
ε_h	energy of free volume macrocavity formation.....	[J mol^{-1}]
Φ	volume fraction	
γ	activity coefficient.....	
λ_x	wave length of X-rays.....	[Å]
$[\eta]$	intrinsic viscosity	[dL g^{-1}]
μ	Viscosity.....	[g $cm^{-1}s^{-1}$]
ω	Rotational speed.....	[rpm]

CHAPTER 1

INTRODUCTION

1.1 Motivation

Membrane gas separation has emerged as an alternative gas separation technology more than three decades ago. The intensive research in this field has lead to several commercial applications of gas separation membranes, which include the production of high purity nitrogen from air, the recovery of hydrogen from mixtures with larger molecules such as methane, nitrogen and carbon monoxide, and the purification of natural gas by the removal of carbon dioxide.

Despite the fact that membranes have made many inroads in the field of gas separation, their market share in comparison with other competing technologies such as cryogenic distillation, absorption and pressure swing adsorption is rather limited. Moreover, the number of commercial applications of gas separation membranes is quite low in comparison with application of reverse osmosis, ultrafiltration and microfiltration membranes. To overcome this definite underachievement of gas separation membranes the research efforts in this field are focused on the development of new membrane materials having improved permeability and selectivity for gases, as well as, good thermal and chemical stability. Nanoporous-inorganic particles such as zeolites and molecular sieves, which are incorporated in organic polymers, are at the center of research efforts focused on the development of new membrane materials.

The major challenge in the development of inorganic/organic materials for gas separation is to prevent the formation of nonselective voids at the inorganic/polymer interface. If the inorganic phase is not adequately dispersed or the polymer does not effectively wet the inorganic material surface, then the selectivity of the final membrane is drastically reduced (Mahajan and Koros, 2000). Therefore, the interfacial force between the inorganic and organic phases of the materials plays a major role in controlling the microstructure and properties of these materials.

In the present project, in order to enhance the compatibility between the inorganic and organic phases of materials, we have developed a novel method, in which a zeolite precursor contained in a well dispersed stable emulsion is allowed to grow in a continuous phase of the polymer solution. The aqueous phase for growing zeolites acts as a micro-reactor. Moreover, the size of the final inorganic particles is controlled by the droplet size of the emulsion. By minimizing the droplet size in the emulsion it is possible to improve the contact between the inorganic and organic phases. This prevents the aggregation of inorganic particles, and maximizes the loading of the inorganic phase.

While there is an infinite number of possible combinations of organic and inorganic phases, in this project the inorganic particles were formed by the copolymerization of tetraethylorthosilicate and aluminum hydroxonitrate in a buffered aqueous phase dispersed in a dilute solution of poly (2,6-dimethyl-1,4-phenylene oxide). These emulsions were used for the preparation of homogeneous membranes using a spin coating technique. The gas transport properties of the membranes were tested using a constant pressure testing system equipped with a gas chromatograph. The membranes were also characterized using

thermogravimetric analysis (TGA), differential scanning calorimetry (DSC), X-ray diffraction (XRD) and scanning electron microscopy (SEM) techniques.

1.2 Organization of the thesis

This thesis is divided into seven chapters. Chapter 2 provides a comprehensive literature review on gas transport mechanisms through the membranes, membrane structure, aluminum silicate chemistry, emulsion preparation, and application of spin coating in thin film preparation. Chapter 3 presents the general objectives of this project as well as the specific tasks. Chapter 4 provides a detailed description of the experimental procedures for polymer modification, membrane preparation, and membrane characterization.

Chapters 5 and 6, present the results and discussion of the experimental work. Chapter 5 focuses on preparation of different emulsions for membrane formation and their characterization. Chapter 6 presents the results of membrane characterization and performance. Chapter 7 includes the conclusion of the work and the recommendations for improving the current approach as well as suggestions for the future work.

Details on some experimental recipes, calculation of the actual inorganic loading, and raw data from modulated DSC are presented in the Appendices.

CHAPTER 2

LITERATURE REVIEW

This project is aimed at the development of a novel method for the incorporation of inorganic materials into polymer matrices, as well as, the study of the potential of these modified materials for manufacturing gas separation membranes.

2.1 Gas Permeation and Separation through Membranes

The most important property of membranes is their ability to permeate species at different rates leading to the partial separation of the permeating species. The membrane permeability coefficient provides the overall measure of the ease of transporting a permeant *i* through the membrane. It is evaluated from the steady state flux (J_i) through the membrane: (Crank, 1975)

$$P_i = \frac{J_i}{\Delta p_i / l} \qquad (2\text{-}1)$$

Where Δp_i is the difference between the partial pressures of component *i* in the feed and permeate streams, and l is the membrane thickness. It follows from Eq. (2-1) that the permeability coefficient is simply a pressure and thickness normalized flux. The common unit of the permeability coefficient is Barrer:

$$1 \text{ Barrer} = 10^{-10} \text{ cm}^3 \text{ (STP) cm / (cm}^2 \text{ s·cmHg)} \qquad (2\text{-}2)$$

The ability of a membrane to separate gases is characterized by the separation factor (α), which for a pair of gases i and j is defined by:

$$\alpha_{ij} = \frac{y_i / y_j}{x_i / x_j} \tag{2-3}$$

where y and x refer to the mole fractions in the permeate and feed streams, respectively. The ideal selectivity for a pair of gases i and j is defined by the ratio of the respective permeability coefficients:

$$\alpha_{ij}^{*} = \frac{P_i}{P_j} \tag{2-4}$$

When the downstream pressure is negligible compared to the feed pressure the separation factor defined by Eq. (2-3) is equal to the ideal separation factor defined by Eq. (2-4). When the downstream pressure cannot be ignored, the actual separation and the ideal separation factors are related through:

$$\alpha_{ij} = \alpha_{ij}^{*}\left(\frac{x_i(\alpha_{ij} - 1) + 1 - r\alpha_{ij}}{x_i(\alpha_{ij} - 1) + 1 - r} \right) \tag{2-5}$$

where r is the ratio of the downstream pressure to the upstream pressure. To distinguish between ideal selectivity obtained from a gas separation test and that from pure gas permeation test the latter is referred to as permeability ratio.

The actual mechanism of gas separation membrane depends on the membrane structure. Generally membranes are categorized as porous or non porous.

2.1.1 Porous membranes

There are four different mechanisms by which a gas mixture can be separated in a porous membrane. These are: (1) Knudsen diffusion, (2) molecular sieving, (3) surface

diffusion, and (4) capillary condensation (Rao, and Sircar, 1993). In Knudsen diffusion the components are separated on the basis of the difference in their molecular weights, and the rate of transport is inversely proportional to the square root from the molecular weight of the permeating species. Consequently, the separation factors associated with this mechanism are generally not sufficient for practical applications. For Knudsen diffusion to occur, the pore size must be much smaller than the mean free path of gas molecules. The separation factors obtained with porous membranes exhibiting this separation mechanism are generally not sufficient for practical applications.

In molecular sieving, the separation occurs on the basis of size/shape exclusion. Consequently, molecular sieve membranes require pore sizes comparable to the molecular size of the separating species, and the resulting separation factors are generally higher than those found in Knudson flow.

In surface diffusion, the molecules are separated on the basis of their selective adsorption followed by the surface flow and the required pore size must be between that for the molecular sieving and Knudsen diffusion. In separation by pore condensation the molecules are separated on the basis of their condensability. The pressure required for capillary condensation is related to the pore size through Kelvin equation, and the pore size for separation by capillary condensation is also in the range between the pore sizes for molecular sieving and Knudsen diffusion, however, it is generally greater than that for surface diffusion. The membranes separating the species on the basis of surface diffusion and capillary condensation are often referred to as inverse selectivity membranes, because they allow a preferential transport of larger molecules over the smaller molecules through the membrane.

2.1.2 Nonporous membranes

Gas transport in nonporous membranes can be explained by the solution diffusion model, in which the permeant first dissolves in the membrane material, and then diffuses from the upstream to the downstream face of the membrane. The permeants are separated based on the differences in their solubilities in the membrane and the differences in the rates of their diffusion through the membrane. In general all membranes made from rubbery polymers and most membranes made from glassy polymers are considered nonporous membranes; currently most gas separation membranes are made from polymers.

The transport equations for any membrane process, including gas separation, can be described using a thermodynamic approach (Wijmans and Baker, 1995). The overall driving force, which produces the movement of a permeant, is the chemical potential gradient of the permeant. By restricting the process to the driving forces generated by concentration and pressure, a differential change in the chemical potential (μ_i) is written as:

$$d\mu_i = RTd\ln(\gamma_i c_i) + v_i dp \tag{2-6}$$

where: γ_i and c_i are the activity coefficient and the concentration of component i in the membrane, p is the pressure, v_i is the molar volume of component i, R is the ideal gas constant and T is the absolute temperature, μ_i is chemical potential. The transport of a component i across a membrane is then described by the following equation:

$$J_i = -L_i \frac{d\mu_i}{dx} \tag{2-7}$$

where: $d\mu_i/dx$ is the chemical potential gradient of component i, and L_i is a coefficient of proportionality.

The solution-diffusion model assumes that the pressure in the membrane is uniform, and the chemical potential gradient arises from the concentration gradient (Wijmans and Baker, 1995). Consequently, in the absence of the pressure gradient, a differential change in the chemical potential simplifies to:

$$d\mu_i = RTd\ln(\gamma_i c_i) \tag{2-8}$$

Assuming an ideal solution, Eq. (2-7) in the solution diffusion model becomes Fick's first law (Zolandz and Fleming, 1992):

$$J_i = -D_i(c_i)\frac{dc_i}{dx} \tag{2-9}$$

In the solution diffusion model the permeability coefficient is considered to be a material property, which can be written as a product of a thermodynamic factor called the solubility coefficient (S_i), and a kinetic parameter called diffusion coefficient (D_i) (Koros and Fleming, 1993):

$$P_i = S_i D_i \tag{2-10}$$

The solubility coefficient is thermodynamic in nature and is affected by polymer-penetrant interactions. In addition, in case of glassy polymers, S_i is also affected by excess interchain gaps. The diffusion coefficient, which is kinetic in nature, is largely determined by polymer-penetrant dynamics. It strongly depends on the fractional free volume of the membrane and the kinetic diameter of the penetrant.

The ideal separation factor defined by Eq. (2-4) can be broken into:

$$\alpha_{ij}^{*} = \left(\frac{S_i}{S_j}\right)\left(\frac{D_i}{D_j}\right) \tag{2-11}$$

The selectivity of the membranes in which gas transport is governed by the solution diffusion model can be seen as a product of solubility selectivity and the mobility selectivity.

Using a thermodynamic approach Wijmans and Baker (1995) showed that the permeability coefficient can be expressed by:

$$P_i^G = \frac{D_i \gamma_i}{\gamma_{i(m)} P_i^{sat}} \qquad (2\text{-}12)$$

Where: P_i^G permeability coefficient, D_i is diffusivity coefficient, γ_i is activity coefficient of component i, $\gamma_{i(m)}$ activity coefficient of component on the membrane. The above equation shows that high permeability coefficients are associated with permeants having a large diffusion coefficient, a low saturated vapor pressure. Moreover, Eq. (2-12) indicates that the permeability coefficient can indeed be considered as a material property since it is relatively independent of the composition and pressure of the feed and permeate gases. However, it must be treated with a caution, because the effects such as plasticization influence the diffusion coefficient and the activity coefficient, and thus the permeability coefficient. The effect of the molecular weight on the permeability coefficient can be rationalized by Eq. (2-12). Although both the permeant's saturation vapor pressure and the diffusion coefficient decrease as the molecular weight increases, they have the opposite effect on the permeability coefficient. A reduction in diffusivity causes the permeability coefficient to decrease, whereas a reduction in the vapor pressure leads to an increase in the permeability coefficient. In glassy polymers, the effect of the diffusion coefficient on the permeability outweighs other effects, and thus the permeability coefficient decreases as the molecular weight increases. In rubbery polymers, for molecular weight up to 100, the permeant's saturation vapor pressure is dominant term, and the permeability coefficient increases with increasing molecular weight. Above molecular weight of 100, the permeant's diffusivity coefficient gradually

become dominant, and the permeability coefficient decreases with increasing molecular weight (Baker and Wijmans, 1994).

The difference between the separation characteristics of membranes made from glassy and rubbery polymers arises from their different sorption behavior. Gas solubility in rubbery polymers is well described by Henry's law. On the other hand, gas solubility in glassy polymers is governed by so-called dual mode sorption. The total sorption in glassy polymers is the sum of two populations. The first population (c_D) arises from uptake into environment similar to that of rubbery polymers. The second population (c_H) is due to uptake into the unrelaxed volume present in glassy polymers, which are referred to as Langmuir sites. Mathematically the dual sorption model for a single component is described as (Barrer et al., 1958):

$$c = c_D + c_H = k_D p + \frac{c_H' b p}{1 + b p} \tag{2-13}$$

Where k_D is the Henry's law constant, p is the penetrant pressure, c_H' and b are the hole saturation and hole affinity constants, respectively.

The transport model for a single component corresponding to the dual-mode sorption expresses the local flux in terms of a two part contribution (Paul and Koros, 1976):

$$J = -D_D \frac{dc_D}{dx} - D_H \frac{dc_H}{dx} \tag{2-14}$$

Where D_D and D_H refer to the diffusivity coefficient of the penetrants in Henry's and Langmuir sorption sites, respectively. Typically, D_D is much larger than D_H, and both coefficients follow Arrhenius expressions with the activation energy for D_H being larger than for D_D. For the special case in which the downstream side of the membrane is at vacuum, the

appropriate expression for permeability of a pure component in a glassy polymer is given by (Koros and Paul, 1978b):

$$P = k_D D_D \left(1 + \frac{FK}{1+bp}\right) \tag{2-15}$$

Where $F = D_H/D_D$ and $K = c_H' b/k_D$.

The dual-mode sorption concept can be extended into multicomponent systems (Zolandz and Fleming, 1992). For a binary mixture of gases *i* and *j* in which gas *i* is the primary component of the mixture, equations (2-13) and (2-15) become (Koros, 1980):

$$c_i = k_{Di} p_i + \frac{c_{Hi}' b_i p_i}{1 + b_i p_i + b_j p_j} \tag{2-16}$$

$$P_i = k_{Di} D_{Di} \left(1 + \frac{F_i K_i}{1 + b_i p_i + b_j p_j}\right) \tag{2-17}$$

2.2 Materials for Gas Separation Membranes

Although almost all industrial gas separation processes use polymeric membranes, there is a growing interest in other membrane material such as metals and ceramics. In addition, in the last decade, mixed matrix and hybrid membranes have gained a lot of attention. In this project we have attempted to produce hybrid-type membranes based on poly(2,6-dimethtyl 1,4-phenylene oxide) (PPO). A comprehensive review on PPO and its properties as well as on ceramic, mixed matrix and hybrid material is provided in the following subsections.

2.2.1 PPO and its properties

Poly (2,6-dimethyl-1,4-phenylene oxide), which is known as PPO, is a linear amorphous thermoplastic with a free phenolic hydroxyl on the head group of each polymer chain. In 1956, it was discovered that 2,6-dimethylphenol could be oxidatively polymerized to a high molecular weight linear PPO at room temperature with oxygen in the presence of an amine complex of a copper(I) salt as catalyst (Hay et al., 1959). The stoichiometry of polymerization of 2,6-dimethylphenol is as shown in Figure 2.1.

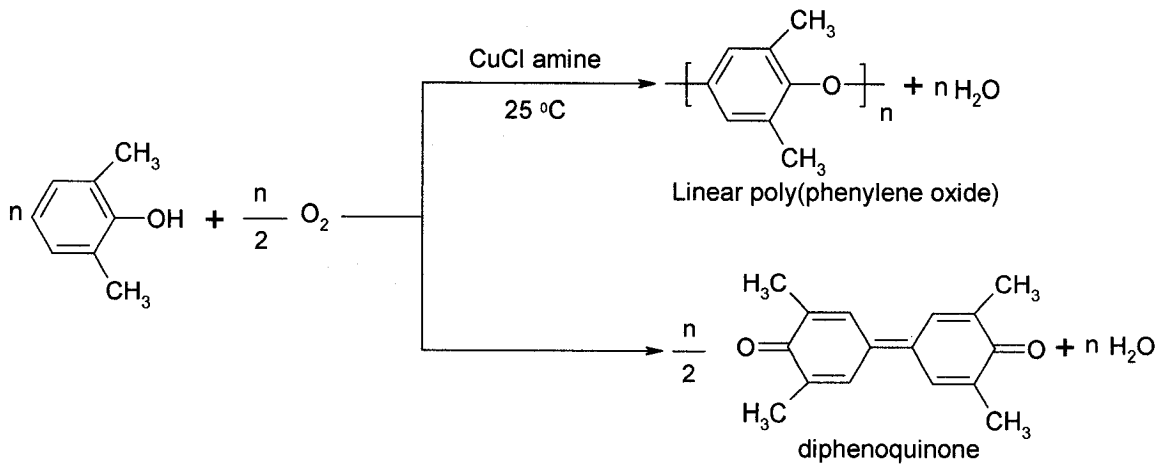

Figure 2.1 The stoichiometry of polymerization of 2,6-dimethylphenol

Small amounts of the diphenoquinone are also produced in this reaction. Diphenoquinone is a dominating product at higher temperatures.

The PPO suitable for injection molding or extrusion has a weight–average molecular weight $\overline{M}_w$ of about 40,000 and a number-average molecular weight $\overline{M}_n$ of about 18,000 (Aycock, 1974). A relationship between the intrinsic viscosity $[\eta]$ and $\overline{M}_n$ for PPO is (Hay, 1967):

$$[\eta] = 3.8 \times 10^{-4} \left(\overline{M}_n\right)^{0.73} \qquad (2\text{-}18)$$

Alternatively, the intrinsic viscosity is correlated with viscosity average molecular weight through Mark-Houwink equation:

$$[\eta] = K\left(\overline{M}_v\right)^a \tag{2-19}$$

Table 2-1 illustrates the constants for Eq. (2-19) reported by Barrales and Pepper (1966).

Table2-1 Mark Houwink constants for PPO

Solvent	K	a
Toluene	2.85×10^{-2}	0.68 ± 0.02
Chlorbenzene	3.78×10^{-2}	0.66 ± 0.02
Choloroform	4.83×10^{-2}	0.64 ± 0.02

PPO is soluble in toluene, benzene, and halogenated hydrocarbons. The solubility parameter of PPO is between 9.5 and 10.21 $(J/m^3)^{1/2}$. It is slightly soluble in aliphatic hydrocarbons, acetone, most alcohols, and tetrahydrofuran (Krause et al., 1978).

PPO is a glassy polymer with a glass transition temperature ranging from 206-225°C depending on the molecular weight. The stability of the ether linkage in the PPO structure is the factor that contributes to its good chemical and thermal stability, and good mechanical properties (Aycock, 1974). The thermal properties of PPO are given in Table 2-2 below.

Table-2.2 Thermal properties of PPO.

Molecular Weight, $\overline{M}_w$	Glass transition temperature T_g, °C	Crystal melting temperature T_m, °C	Decomposition temperature T_d °C	Heat of fusion J/g	References
40,000	224.85	266.85	456.85	16.4	Karasz and O Reily (1965)
39,000	213	275	450	-	Aguilar and Paul (1993)
34,000	212	-	-	-	Toi et al. (1982)
	221	-	-	-	Hay and Dana (1989)
	206.85	261.85	-	-	Wrasidlo (1972)

The T_g of PPO increases with the molecular weight. The relatively high T_g of PPO is attributed to strong interactions between the polymeric chains (Shultz, 1970). A unique feature of PPO is the very small difference between its T_g and its melting temperature (T_m). A linear correlation exists between the T_m and T_g in numerous polymers:

$$T_m = aT_g \tag{2-20}$$

Where a for most polymers varies from 1.5-2.0 (Krevelen, 1990) the value of a for PPO is 1.1 (Wrasidlo, 1972). PPO has a lower thermoxidative stability compared to other aryl polymers and decomposes rapidly in oxidative environments (Aguilar 1993).

PPO has one of the highest permeabilities to gases among glassy polymers, which is attributed to the absence of polar groups in its polymer backbone. Lack of polar groups results in weaker inter-chain interactions and a higher degree of chain mobility and flexibility. The ether linkages suppress chain packing and create a very open arrangement of polymer chains. The rotation of phenyl rings about the ether linkage in the glassy state is relatively unhindered but not completely free (Brooks et al., 1992).

Toi et al. (1982) measured the sorption and transport of CO_2, CH_4, Ar, and N_2 in PPO. The extent of sorption and rate of permeation of these gases were quite large for a PPO, with $\overline{M}_w$=34,000 and T_g of 220°C compared to other glassy polymers with rigid chain backbones. They showed that the sorption and permeation data for each gas was well described by the dual sorption model. Very large solubilities for these gases were observed for PPO. This can be a result of the high glass transition temperature of this polymer which leads to a large Langmuir sorption capacity.

The effect of the molecular weight parameters on gas transport properties of PPO was investigated by Polotskaya et al. (1996). It was found the oxygen and nitrogen permeabilities

of PPO improve with increasing polymer molecular weight; however, at a fixed temperature the value of permselectivity is virtually independent of its molecular weight. Moreover, they have shown that the density of PPO homogeneous membranes decreases at higher molecular weights. This is due to an increase in the free volume of the polymer matrix, which causes an increase in permeability. Their argument was consistent with the interpretation of Kesting and Fritzsche (1993), in which free volume increases with increasing the molecular weight. On the other hand, at low molecular weight, the polymer chains are more mobile because of less steric hindrance. As the molecular weight increases, the concentration of chain ends decreases and in turn, polymer free volume decreases (Ghosal and Freeman, 1993). Meares (1965) has argued that decreasing the M_W leads to an increase in free volume, which is in agreement with the hypothesis of Ghosal and Freeman.

Many research efforts have been made on the modification of PPO in order to improve its selectivity and permeability. Chemical characteristics of PPO repeat unit allows it to be modified by various electrophobic substitution including bromination, carboxylation, solfonylation and acrylation (Mahajan, 1991).

The incorporation of inorganic materials in to the PPO matrix is another course of action for improving the gas transport properties of PPO. In contrast to many studies on the chemical modification of PPO the only attempt to incorporate inorganic particles into the PPO matrix was reported by Zhang (2005); however gas separation properties of such modified PPO were not reported.

2.2.2 Ceramic membranes

One of the major limitations of polymeric membranes is their thermal stability. Consequently, parallel to the intensive research on the development of polymeric membranes many membrane laboratories focus their efforts on ceramic membranes.

In general ceramic membranes, for example zeolite membranes, are prepared by the sol-gel method. Sols of very small particles are usually prepared by hydrolysis and condensation of the corresponding alkoxides (Caro et al., 1999). Ceramic membranes are multilayer composite structures formed by coating sols (dip coating, slip-casting or spin coating) on a porous support.

The pore size of the ceramic membranes is mainly determined by the degree of branching of the inorganic polymer. Very narrow pores require a low degree of branching. Such polymeric SiO_2 sols of low branching are prepared by acidic hydrolysis of the corresponding Si alkoxides (Elfernik et al., 1996).

2.2.3 Mixed- matrix membranes

Mixed-matrix membranes are membranes prepared from materials consisting of zeolite or molecular sieves dispersed in a polymer matrix. These membranes are expected to combine the selectivity of zeolite membranes with the low cost and ease of manufacture of polymer membranes (Baker, 2004).

Mixed-matrix membrane performance can be modeled by the Maxwell's equation

$$P = P_c\left[\frac{P_d + 2P_c - 2\Phi(P_c - P_d)}{P_d + 2P_c + \Phi(P_c - P_d)}\right] \qquad (2\text{-}21)$$

Where P is the overall permeability of the mixed-matrix membrane, Φ is the volume fraction of the dispersed zeolite phase, P_c is the permeability of the continuous polymer

phase and P_d is the permeability of the dispersed (e.g., zeolite phase). The concept of mixed matrix membranes is illustrated in Figure 2.2 below

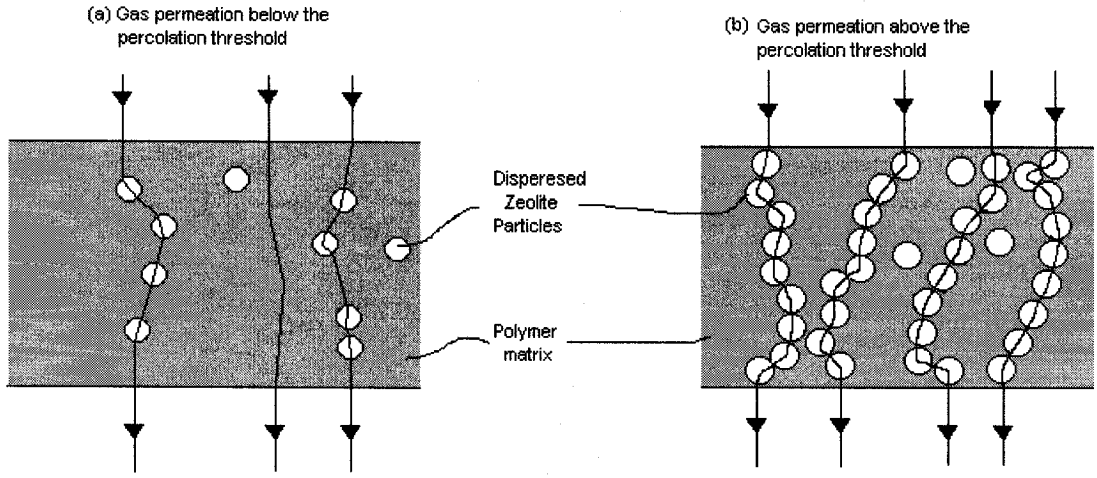

Figure 2.2 Gas permeation through mixed-matrix membranes containing different amount of dispersed zeolite particles (Baker, 2004).

At low loadings of the dispersed zeolite (Fig 2.2 (a)), the average zeolite particle is in contact with one or two other particles, and they are well dispersed in the polymer matrix. Therefore, permeation occurs by a combination of diffusion through the polymer phase and the zeolite phase, and Eq. (2-21) is applicable. At higher zeolite loadings, the particles form some small islands, and as the zeolite loading increases these islands grow and connect to form extended pathways. At a certain critical value of the loading, continuous channels form within membrane and almost all zeolite particles participate in the formation of these channels. This critical value is called the percolation threshold. At this point, the Maxwell equation is no longer valid to predict the overall membrane permeability. Figure 2.2 (b) illustrates this concept. The percolation threshold is achieved at particle loadings of 25- 30 vol% (Baker, 2004).

At very high zeolite loadings the zeolite phase becomes a continuous phase while the polymer phase becomes a dispersed phase Eq. (2-21) becomes applicable.

Mixed matrix membranes were thoroughly investigated by Mahajan and Koros (2000), and Smolder et al. (1993). Mahajan and Koros focused on zeolite with a small aperture, for example zeolite 4Å, in order to improve the oxygen separation over nitrogen in polyimides and polyvinyl acetate. At first, they investigated the zeolite 4Å -Matrimide system and observed that the permeability was much higher than that of pure Matrimide, instead of being lower as predicted by the Maxwell equation. They noted the presence of voids between the interface of the zeolite and polymer, which ultimately resulted in gas by passing around the zeolite. These voids were due to the inability of polymer chains to wet the zeolite surface, because of rigidity of the polymer. Their next attempt was a poly vinyl acetate-zeolite 4Å system, and the results showed a considerable improvement in the selectivity of polyvinyl acetate at low zeolite loadings, probably because of high flexibility and low T_g of polyvinyl acetate, which allow for a better contact between the zeolite and the polymer chain. Smolder et al. (1993) studied the effect of the introduction of carbon molecular sieves and zeolites into polydimethylsiloxane (PDMS) on the gas separation properties of the modified polymer. They showed that zeolites, such as silicate-1, 13X, and KY, improve to a large extent the separation properties of poorly selective rubbery polymers towards a mixture of CO_2/CH_4, whereas carbon molecular sieves do not lead to any significant improvement of the gas separation properties of the rubbery polymers. They also showed that using silicate-1 with pore size between 5.3-5.6 Å results in an improvement of the O_2/N_2 separation properties of the rubbery polymers.

2.2.4 Hybrid Membranes

In the last two decades, molecular level combination of organic polymers and inorganic materials has been extensively studied, because it exhibits a wide range of multifunction properties. The sol-gel method is a common method for preparation of hybrid membranes. This method offers several advantages over other techniques. The micro- and macrostructure of the host polymer matrix can be controlled through the optimization of several synthetic parameters, such as pH, concentration, water-to-alkoxide ratio (Brinker and Scherer, 1990). The presence of well dispersed silica networks in polymer matrix provides a good mechanical resistance, thermal stability, and amorphous character. Therefore, to promote the fine dispersion of the inorganic component in polymers, the simplest method is to grow the inorganic phase by a sol-gel process in polymer solution. For the preparation of the inorganic phase, tetraethoxy silane (TEOS) or tetramethoxysilane (TMOS) is added to a solution containing the organic polymer and hydrolysis and condensation is induced by the acid catalysis. Joly et al. (1996) used this procedure to produce a silica/polyimide hybrid membrane. Jiang et al. (2006) used TEOS hydrolysis sol-gel reaction to incorporate silica in Nafion polymer.

The incorporation of inorganic materials in polymer matrix through the sol-gel method leads to phase separation, if there is no compatibility between the inorganic phase and the polymer chains. The compatibility of phases in hybrid materials is enhanced by formation of hydrogen bonding between the two phases. Polymers such as polyvinyl acetate, polyvinyl pyroliddone, and poly (N,N-dimethyl acrylamide) are able to form hydrogen bonds with silanols on the silicate network resulting in transparent homogeneous hybrid films. Moreover, the presence of the OH groups in the organic polymer chain helps to retard phase separation during the film formation (Landry et al., 1996). For example, Kim and Lee (2001)

managed to produce the organic/inorganic hybrids of poly (amide-6-b-ethylene oxide) (PEBAX) and silica through situ polymerization of TEOS. In their work, the gas transport properties of these hybrid membranes were also studied. Another route for forming hydrogen bonding in hybrid materials is to functionalize polymer backbone with trialkoxysilyl, $Si(OR)_3$, groups. These functionalized groups can then undergo hydrolysis and condensation via a sol-gel process with or without a coupling agent such as TEOS. This procedure was applied by Zhang et al. (2005) to synthesize a hybrid material based on poly (2,6-dimethyl-1,4-phenylene oxide).

2.3 Material development

The compatibility between inorganic particles and a polymer matrix plays a key role in mixed matrix and hybrid membranes. In the former, if polymer chains do not wet the surface of the inorganic particles or inorganic particles cannot be well dispersed in the polymer matrix; there will be voids in the inorganic/organic interface. In the latter, a lack of compatibility between the inorganic phase and polymer chains leads to phase separation during the incorporation of inorganic phase through the sol-gel process.

In this research we attempted to develop a new category of membranes, which will be referred to as emulsion polymerized mixed matrix membranes (EPMM). To prepare these membranes we explore a new method, in which an inorganic precursor contained in a stable W/O emulsion is allowed to polymerize in a continuous phase of polymer solution.

Silica alkoxides are well known as a source of an inorganic phase for the preparation of hybrid membranes. In this research, tetraethylorthosilicate (TEOS), which is used as an

inorganic source, is added to a W/O emulsion containing a continuous polymeric phase, and then its hydrolysis and condensation is induced by aluminum hydroxonitrate.

To better understand the method of formation of EPMM membrane it is necessary to review aluminum silicate chemistry and well as basic concepts relevant to formation of stable emulsions.

2.3.1 Aluminum silicate chemistry

This part deals with the representations of the aluminumsilicate synthesis procedure and ingredients needed in the process. Sodium metasilicate, silica gel, silica sol, and TEOS can be used as sources of silica. Alumium hydroxide, aluminum nitrate, and aluminum sulfate are considered when choosing a source of aluminum (Szostak, 1998). In the present research, aluminum nitrate and TEOS were chosen as sources of aluminum and silica respectively. Although the main focus of this part is on the copolymerization of TEOS and aluminum hydroxonitrate, we begin our discussion of hydrolysis and condensation of both aluminum and TEOS.

2.3.1.1 Hydrolysis and Condensation of Al (III)

Al^{3+}, with an ionic radius of 0.5Å has a coordination number of water $N=6$ and exists as the unhydrolyzed species $\left[Al(H_2O)_6\right]^{3+}$ below pH 3. With increasing pH, $\left[Al(H_2O)_6\right]^{3+}$ can be hydrolyzed as follows:

$$\left[Al(H_2O)_6\right]^{3+} + hH_2O \rightarrow \left[Al(OH)_h(H_2O)_{6-h}\right]^{(3-h)+} + hH_3O^+ \qquad (2\text{-}22)$$

$$hH_3O^+ + hOH^- \rightarrow 2hH_2O \qquad (2\text{-}23)$$

Where h is defined as the molar ratio of hydrolysis, which is equivalent to equivalent to $[OH]_{tot}/[Al(III)]_{tot}$ ratio according to the reactions (2-22, 2-23). Subsequent condensation results in polynuclear hydroxides. Distribution of polynuclear hydroxides is very sensitive to the precise conditions of the hydrolysis procedure such as time, temperature and base concentration. Baes and Mesmer (1976) reported the production of two small polynuclear species, $\left[Al_2(OH)_2(H_2O)_4\right]^{4+}$ and $\left[Al_3(OH)_4(H_2O)_9\right]^{5+}$ at low base concentration, and the production of large polynuclear species $\left[AlO_4Al_{12}(OH)_{24}(H_2O)_{12}\right]^{7+}$, at higher base concentration.

In this study, we focus on the structure of $\left[AlO_4Al_{12}(OH)_{24}(H_2O)_{12}\right]^{7+}$, which has a Kegging structure. For convenience, $\left[AlO_4Al_{12}(OH)_{24}(H_2O)_{12}\right]^{7+}$ is abbreviated as Al_{13}^{7+}. The Kegging structure of Al_{13}^{7+} is composed of a tetrahedral $AlO_{4/4}^{+}$ center surrounded by 12 octahedral $AlO_{1/4}(OH)_{4/2}(H_2O)^{0.5+}$ units. Each of the octahedra carries one terminal water ligand. Hence, it can be concluded that $Al_{13}O_4(OH)_{24}(H_2O)_{12}^{7+}$ is a polyprotic acid with 12 identical functional groups. The dissolved Al_{13}^{7+} species are detectable by ^{27}Al *NMR* spectroscopy, because it has a symmetric structure (Furrer et al., 1992). Figure 2.3 represents a Kegging Al_{13}^{7+} structure.

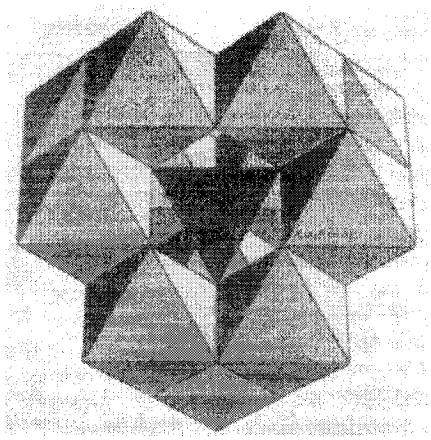

Figure 2.3 Structure of the Keggin Al_{13}^{7+} complex: A tetrahedral $AlO_{4/4}^{+}$ center is surrounded by 12 $AlO_{1/4}(OH)_{4/2}(H_2O)^{0.5+}$ groups (Brinker and Scherer, 1990).

The Al_{13}^{7+} species is thermodynamically unstable with respect to a transformation to Al^{3+}, however, it is rapidly formed, even at room temperature, by partial neutralization of acidic Al(III) solutions (Wehrli et al., 1990). It was found that solutions of Al_{13}^{7+} are stable almost up to a year, if the neutralization ratio, h, does not exceed the value of 2.5. Bottero et al., (1980) showed that if h is increased above 2.5, the dissolved Al_{13}^{7+} species tends to aggregate and precipitate, and precipitated Al_{13}^{7+} is transformed into amorphous aluminum hydroxides at h =3.

Hydrolysis of Al^{3+} with sodium carbonate was studied by Akitt and Farthing (1981). They reported that hydrolysis of Al^{3+} with sodium carbonate produces solutions whose compositions depend upon the degree of hydrolysis achieved and contain varying proportions of $\left[Al(H_2O)_6\right]^{3+}$, $\left[(H_2O)_4Al(OH)_2Al(H_2O)_4\right]^{4+}$, and $Al_{13}O_4(OH)_{24}(H_2O)_{12}^{7+}$. In fact, the fundamental hydrolysis of Al^{3+} seems to involve only these three species. They also studied the effect of experimental conditions on the course of aging and the decomposition of Al_{13}^{7+}. Their findings can be summarized as follows:

At 27°C and h= 2.5, Al_{13}^{7+} has a half-life of about 2 years, whereas at 77°C and h= 2.5, Al_{13}^{7+} is lost 1800 times more rapidly. At 27°C and a hydrolysis degree between 1 and 2.4, Al_{13}^{7+} decomposes more rapidly than when the hydrolysis degree is 2.5. At 77°C and hydrolysis degree of 2.4, the rate of decomposition of Al_{13}^{7+} increases 30 times. Since the degree of hydrolysis is below 1, there is sufficient acidity in the system to cause the decomposition of Al_{13}^{7+} by acid attack. As hydrolysis proceeds, Al_{13}^{7+} is formed more abundantly. In order to form Al_{13}^{7+} at all hydrolysis degrees, sodium carbonate solution must be added. As soon as the base is added, a precipitate forms. The precipitate has to be dissolved as rapidly as possible; otherwise it changes into an insoluble material.

In summary, the stable complex ion Al_{13}^{7+}, which has a Kegging structure type, seems to be formed at a high degree of hydrolysis. However, it depends on the experimental conditions, the aluminum concentration, and the base concentration.

2.3.1.2 Hydrolysis and condensation of Tetraethylorthosilicate

The traditional method for preparing tetraethyloxysilane or tetraethylorthosilicate (TEOS) is by reacting tetrachlorosilane with alcohol.

$$SiCl_4 + EtOH \rightarrow Si(OEt)_4 + 4HCl \qquad (2\text{-}24)$$

Tetraethyloxysilane polymerization is most often conducted by employing a mineral acid or base as a catalyst. Three reactions involved in hydrolysis and condensation of TEOS are as follows:

Hydrolysis

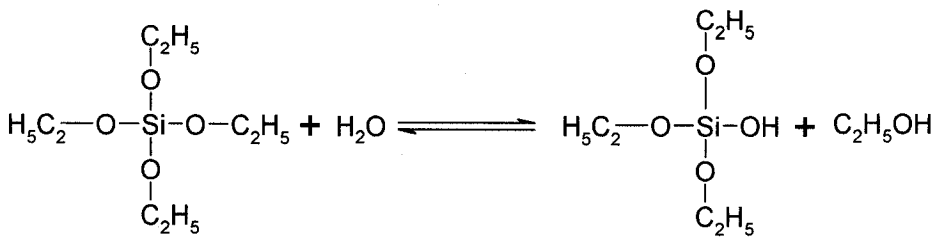

The hydrolysis replaces alkoxide groups (OR) with hydroxyl groups. In other words, a hydrolysis is caused by the nucleophilic attack of the oxygen contained in water on the silicon atom.

Alcohol condensation

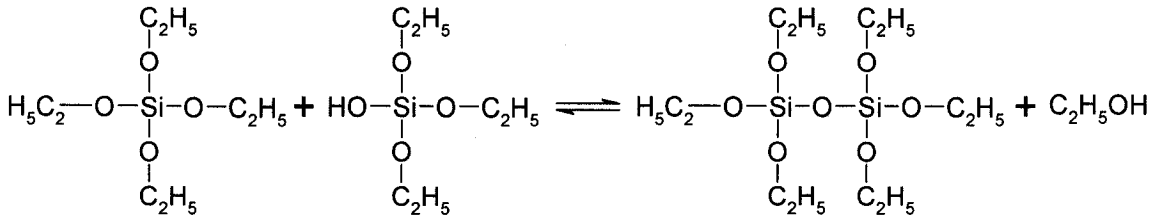

Water condensation:

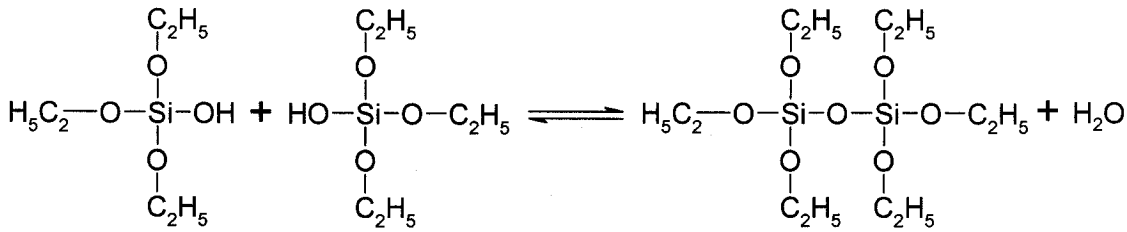

According to the alcohol and water condensation reactions, which involve the silonal groups, silanol groups produce siloxane bonds (Si-O-Si) and alcohol or water as by products. Under most conditions, condensation starts before hydrolysis is complete. Hydrolysis can be facilitated in the presence of homogenizing agents such as alcohols, THF, acetone, etc. However, the addition of these solvents may promote depolymerization reactions according to reverse equations of alcohol and water condensation. The hydrolysis reaction is

accelerated when catalysts are employed. The rate and extent of the hydrolysis reaction is most influenced by the strength and concentration of the acid or base catalyst.

Under acidic conditions, an alkoxide group is protonated in a rapid first step. Electron density is withdrawn from the water can attack protonated TEOS and impart a partial positive charge. The positive charge of protonated alkoxide is reduced, and it makes alcohol a better leaving group. The acid-catalayzed hydrolysis of TEOS is shown

In the following equation:

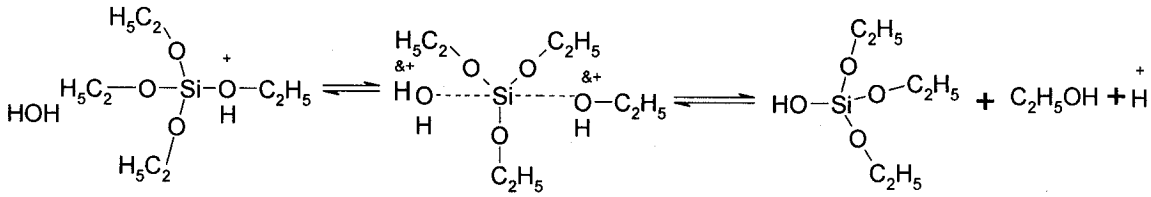

The acid-catalyzed condensation involves a protonated silanol species. Protonation of silanol makes silicon more electrophilic and more susceptible to nucleophilic attack.

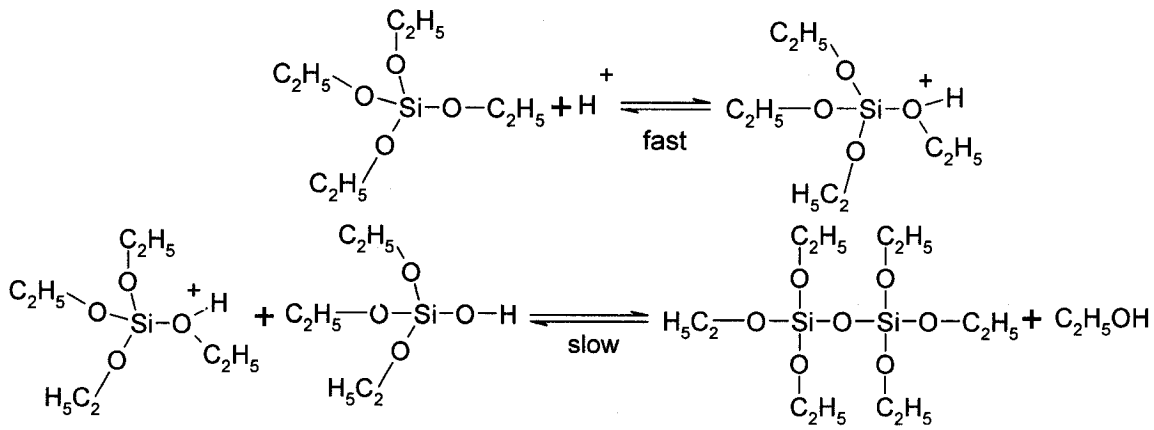

It should be mentioned that in acid-catalyzed hydrolysis and condensation, the condensation starts before silicon alkoxide is completely hydrolyzed; therefore, a transparent gel with a low degree of polymerization and crosslinking will be obtained.

Under basic conditions, it is likely that water dissociates to produce nucleophilic hydroxyl anions in a rapid first step. The hydroxyl anion then attacks the silicon atom.

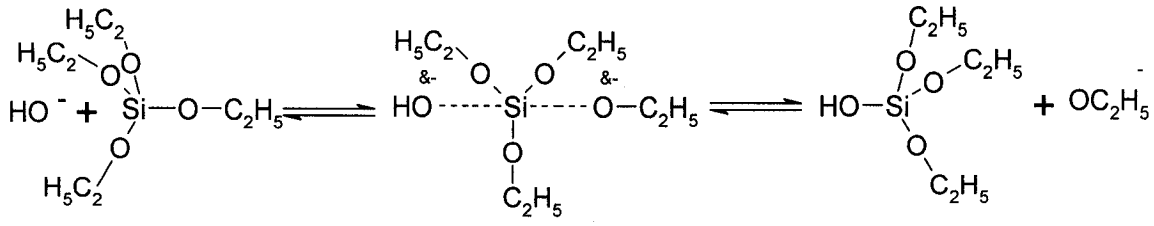

Base-catalyzed condensation:

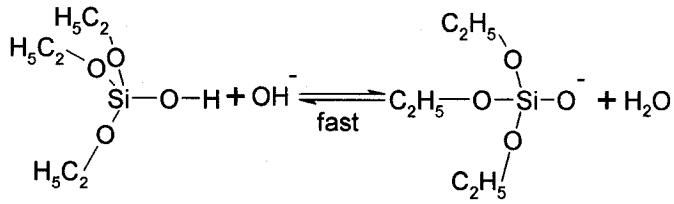

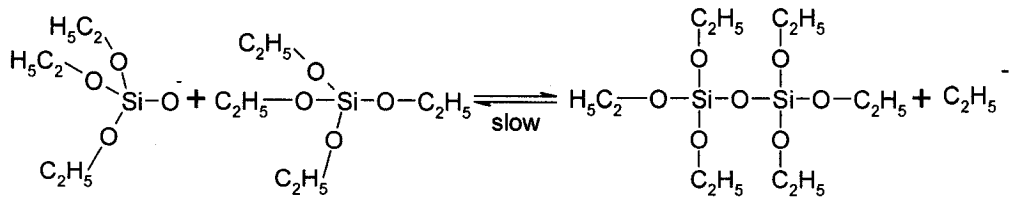

In base-catalyzed hydrolysis and condensation, condensation starts after silicon alkoxide is completely hydrolyzed; therefore, an opaque gel with a high degree of polymerization and cross linking will be obtained (Brinker and Schere, 1990).

2.3.1.3 Hydrolysis and condensation of TEOS in the presence of aluminum hydroxonitrates:

The polymerization of tetraethylorthosilicate (TEOS) in the presence of an aqueous solution of aluminum hydroxonitrate was investigated by Eliseev et al. (1999). Their works revealed that the hydrolysis of TEOS in the presence of aluminum hydroxonitrate with high a degree of hydrolysis ($h > 1.9$) occurs very rapidly and resulting gels are opaque, whereas the hydrolysis of TEOS in the presence of aluminum hydroxonitrate with a low degree of hydrolysis ($h < 1.9$) is much longer (3-4 days) and obtained gels are transparent. The enhanced rate of gelation in the presence of aluminum hydroxonitrate with a

high degree of hydrolysis ($h>1.9$) indicates that aluminum-containing species take part in the polycondensation of TEOS and $^{27}Al\ NMR$ data proved that tetrahedrally coordinated aluminum is incorporated into the silica network. In addition, the spectrophotometric study of gelation kinetics demonstrates that the copolymerization of TEOS and aluminum hydroxonitrate is of the first-order with respect to aluminum.

As was mentioned in the acid-catalyzed hydrolysis of TEOS, the nucleophilic attack of water molecules on TEOS is the limiting step. However, during the hydrolysis of TEOS in the presence of aluminum hydroxocomplex, the nucleophilic agent can be either the H_2O molecule or the OH^- group coordinated in aluminum cation. The partial charge model shows that the partial charge on the OH group directly coordinated to the aluminum can be lower than that in the free H_2O molecule and hence it can possess stronger nulceophilic activity (Livage et al., 1994).

The OH^- group coordinated in the aluminum cation can attack on the TEOS molecule:

$$Si(OEt)_4 + [Al(OH)_x(H_2O)_y]^{m+} \rightarrow EtO\text{-}[Si(OEt)_2]\text{-}O\text{-}[Al(OH)_{x-1}(H_2O)_y] + EtOH$$

$^{27}Al\ NMR$ data of the gel suggests that all aluminum incorporated into the gel matrix is tetrahedrally coordinated (Eliseev et al., 1999). The only well-characterized aluminum hydroxocomplex containing tetrahedrally coordinated metal atoms is tridecanuclear complex $Al_{13}O_4(OH)_{24}(H_2O)_{12}^{7+}$ which has a Kegging structure. Therefore, it can be concluded that $Al_{13}O_4(OH)_{24}(H_2O)_{12}^{7+}$ is responsible for the enhanced rate of polycondensation of TEOS in the presence of aluminum hydroxonitrate with high degree of hydrolysis ($h>1.9$). Indeed, the value of the partial charge on OH groups in $Al_{13}O_4(OH)_{24}(H_2O)_{12}^{7+}$ is -0.051. Because of high

nucleophilic strength of the OH groups in this species, $Al_{13}O_4(OH)_{24}(H_2O)_{12}^{7+}$ can attack a TEOS molecule readily and form Al-O-Si bonds in tetrahedrally coordinated species (Swaddle et al., 1994).

2.3.2 Emulsification

An emulsion is defined as a heterogeneous system, which consists of at least one immiscible liquid dispersed in another in the form of a droplet (Becher, 1965). The stability of emulsions can be enhanced by surfactants. Surfactants are characterized by the following features:

- *Amphipatic structure*: Surfactant molecules are composed of groups of opposing solubility tendencies, typically an oil-soluble hydrocarbon chain and a water-soluble ionic group.
- *Solubility*: A surfactant is soluble in at least one phase of a liquid system.
- *Adsorption at interfaces*: At equilibrium, the concentration of a surfactant at the interface is greater than its concentration in the emulsion
- *Micelles formation*: When the concentration of the surfactant in the soluble phase exceeds a limiting value, the so-called critical micelle concentration, surfactant molecules (ions) aggregate.

Nonionic surfactants, which are interest in this research, are often characterized in terms of their hydrophilelipophile balance (HLB) number. For simple alcohol ethoxylates, the HLB number may be calculated from the following equation:

$$HLB=E/5 \qquad (2\text{-}25)$$

Where: E is the weight percentage of ethylene oxide in the molecule.

In equivolume mixtures of two immiscible liquids, the HLB number of surfactants determines the type of the emulsion, i.e., W/O or O/W (Abismail et al., 1999).

From a thermodynamic point of view, surfactants reduce the surface free energy by lowering the interfacial tension that allows the interfacial area to increase. However, additional shear forces or energy might be needed to break large droplets into smaller ones. The required energy may be provided by mechanical agitation or/and ultrasound homogenizer.

The action of an ultrasound homogenizer in producing emulsion and preventing agglomeration of droplets as well as its chemical effects in polymerization and depolymerization reactions was investigated by Wood

Energy density is a common parameter that is used to compare the efficiency of emulsification of different devices. The energy density (E_V) is defined as the amount of energy dissipated in the unit volume of emulsion (Behrend and Schubert, 1999):

$$E_V = \frac{E}{V_e} \tag{2-26}$$

There are several mechanisms for droplet formation under the influence of ultrasounds. However, it is generally recognized that all non-chemical and chemical effects of ultrasound are due to a cavitation mechanism. This mechanism consists in the following steps: formation, growth, and implosive collapse of the bubbles in a liquid. This is illustrated in Fig. 2.4. The top figure (Fig 2.4 (a)) shows a typical sinusoidal variation of acoustic pressure resulting from passing ultrasound waves through a liquid. In the expansion period of the cycle, the molecules of the liquid are being pulled away from each other. If the ultrasound energy is sufficiently high, the negative pressure may exceed the local tensile strength of the liquid resulting in cavitation. The size of the cavity oscillates over many expansion and

compression cycles. In the expansion stage of the cycle the size of the bubble increases, whereas in the compression stage it decreases When ultrasound energy is high, the expansion of the bubble is larger then its shrinkage in each cycle. Therefore, over many cycles, the bubble will grow, as shown in Fig 2.4(b). When the growing bubble reaches a critical size, which for a given system depends on the energy of ultrasound, the external force exerted on the bubble by a surrounding liquid breaks the bubble (Kenneth, 1994).

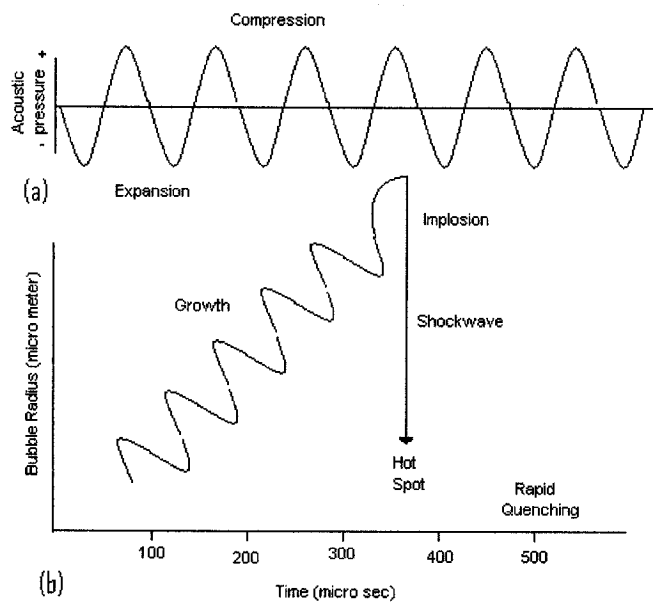

Figure 2.4 The cavity growth at low intensity (Kenneth, 1994)

In ultrasound emulsification processes, the cavitation succeeded by a mechanical oscillation at ultrasonic frequencies causes a breakdown in the continuity of the liquid phase in its weak spot in the negative pressure phase. A weak spot is where the symmetry of the intermolecular cohesive bonds of liquid is disrupted (Neduzhii, 1961).

Lauterborn et al. (1997) showed that the implosion of cavities generates intensive shock waves in the surrounding liquid. This may cause the droplet disruption in the vicinity

of a collapsing cavity. In spite of the large number of studies devoted to the cavitations, the exact process of droplet disruption due to cavitations is not yet clear (Behrend, 1999).

2.3.2.1 Double emulsion

Double emulsions may be either of water-in-oil-in-water type (W/O/W) (oil globules containing smaller aqueous droplets dispersed in the aqueous phase) or of the oil-in-water-in-oil (O/W/O) (aqueous globules containing smaller oily droplets dispersed in the oil phase). This study focuses on water in-oil-in water (W/O/W) emulsions.

Figure 2.5 shows a schematic diagram of a W/O/W emulsion. Small water droplets are trapped within large oil droplets that in turn are dispersed in a continuous water phase.

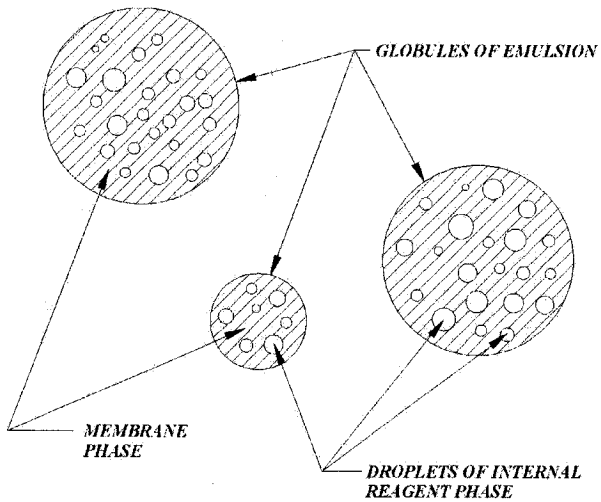

Figure 2.5 The schematic diagram of an emulsion liquid membrane (Winston and Sirkar, 1992).

The preparation of multiple W/O/W emulsions is a two step process, which requires at least two emulsifiers. The first step requires a low HLB surfactant to stabilize the primary W/O emulsion and the second step requires a high HLB surfactant to stabilize the secondary O/W emulsion. The low-HLP surfactant is dominantly hydrophobic and is added to the oil phase. The high-HLB surfactant is dominantly hydrophilic and is added to the outer

continuous aqueous phase. The concentration ratio of these two surfactants is important to obtain stable and high yields of W/O/W emulsions. There are two interfaces in W/O/W emulsions. The primary interface, lying between the inner aqueous phase and the oil phase, contains the low-HLB surfactant. In contrast, both the high and low HLB surfactants are present at the secondary interface, i.e., between the multiple droplets and the outer continues aqueous phase (Shinoda, 1980).

2.3.2.2 Concepts of coalescence and diffusion-driven destruction

There are two types of instabilities, which cause the coalescence of double emulsions. These are: i) coalescence of small inner droplets with the secondary interface; ii) coalescence between small inner droplets within the oil globule. The first type of instability is due to the rupture of the secondary interface, which leads to a complete delivering of the small inner droplets towards the external phase. The second type of instability leads to an increase of the average diameter of the internal droplets and a decrease of in their number. However, it does not lead to delivery of the internal aqueous droplets to the external aqueous phase.

The coalescence of small inner droplets with the secondary interface, which leads to conversion of double W/O/W emulsion into a single O/W emulsion, is affected by several parameters. The most important one is the concentration of hydrophilic surfactant within the continuous phase and the internal droplets (Ficheux et al., 1998). When the hydrophilic surfactant in the continuous aqueous phase exceeds its critical micelle concentration, the resultant micelles may solubilize the hydrophobic surfactant that was originally present in the oil phase and carry it into the outer continuous aqueous phase. This would lead to a decrease in the concentration of hydrophobic surfactant in the oil phase and eventually to a rupture of

the oil layer and a loss of the internal aqueous droplets. To maintain a sufficient amount of the hydrophobic surfactant in the oil phase, a high concentration of hydrophobic surfactant is preferred (Hou and Papadopoulos, 1997).

2.3.2.3 Swelling of globules in W/O/W emulsions

In W/O/W the oil phase acts as a membrane separating these two aqueous phases. Polar molecules dissolved in the aqueous phases can pass through the oil layer by diffusion if there is a concentration gradient. These polar molecules are often transported via micelles of hydrophobic surfactant present in the oil phase. The existence of concentration gradient leads also to a difference in the osmotic pressures in the two aqueous phases which drives water from the phase having higher osmotic pressure to the one having lower osmotic pressure. When the external aqueous phase has a higher osmotic pressure the diffusion water through the oil phase leads swelling of the internal aqueous droplets. On the other hand, when the internal aqueous phase has a higher osmotic pressure the diffusion water through the oil phase leads to shrinkage of the internal aqueous droplets. In both cases this may adversely affect the stability of the double emulsion. In addition, a change in the volume fraction of the primary emulsion alters the rheological properties of double emulsion (Jiao and Burgess, 2003).

2.4 Spin Coating Process:

Spin coating is a technology, which allows the formation of uniform films on flat substrates. Spin coating is used in various applications, such as coating of photo resist on silicon wafers, sensors, protective coatings, paint coatings, optical coatings and membranes.

In this project spin coating is used to prepare uniform films from different materials that are subsequently tested in gas permeation and separation experiments.

The spin-coating process is carried out by depositing a liquid solution (in our case a polymer solution) on a wafer, and then rapidly accelerating the wafer to the final spin speed, maintaining the constant spin speed for a certain period of time, followed by deceleration of the wafer to rest. This may be followed by a baking step to remove residual solvent and/or to cure the polymeric precursor to its desired final form (Bornside et al., 1987). Therefore, the spin coating process can be divided into the following three steps: i) deposition and spin up; ii) 2- spin off; iii) film drying.

The spin coating is governed by the continuity, momentum, and convective diffusion equations (Bird et al., 2002):

$$\frac{d\rho}{dt} = -(\nabla.\rho\upsilon) \tag{2-27}$$

$$\frac{\partial}{\partial t}\rho\upsilon = -[\nabla.\rho\upsilon\upsilon] - \nabla p - [\nabla.\tau] + \rho g \tag{2-28}$$

$$\frac{Dw_s}{Dt} = \nabla.(D\nabla w_s) \tag{2-29}$$

where υ is the velocity vector of the liquid, p is the liquid pressure, g is the gravitational force vector, τ is the stress tensor, and w_s is the weight fraction of solvent. It should be mentioned that whereas $(\nabla.\rho\upsilon)$ represents the rate of the loss of the mass per unit volume by fluid flow, the quantity $[\nabla.\rho\upsilon\upsilon]$ represents the rate of loss momentum per unit volume by fluid flow.

2.4.1 Deposition and spin up

A liquid solution may be deposited in several different manners, ranging from pouring the entire solution at the center of the wafer, to delivering the solution over the rotating wafer. In all cases, the amount of the deposited solution should be in a large excess in order to cover completely the surface of the wafer. Next, the wafer is accelerated to its final rotational speed. The majority of the liquid solution is lost from the wafer when the wafer is accelerated due to the centrifugal forces. As long as the deposited amount of the solution is in a large excess, the final film thickness is independent of the manner of deposition, the actual amount of the deposited solution, and the acceleration rate of the wafer to its final spin speed. However, if the wafer is accelerated extremely slowly or if an insufficient amount of liquid is used, the final film thickness may depend on these parameters (Bornside et al., 1989).

2.4.2 Spin off

During this stage, the film is thinned owing to a combination of convection and solvent evaporation. The centrifugal forces, which drive the radial flow of the solution to the edge of the wafer, are hindered only by the viscous resistance. The latter is enhanced by solvent evaporation. In addition, solvent evaporation leads to film thinning. The first models for predicting the final thickness of the film ignored completely the evaporation of solvent.

Emslie et al., (1957) were the first to describe the spin-coating process theoretically. In addition to neglecting the evaporation of solvent, they assumed that the viscosity of the liquid is independent of the shear rate (i.e., the liquid behaves as a Newtonian fluid), the wafer is horizontal, the liquid flow is one dimensional in radial direction, shear resistance is

significant only in horizontal planes, and the Coriolis forces are negligible. Consequently, the continuity and momentum equations simplified to:

$$r\frac{\partial h}{\partial t} = -\frac{\partial (rq)}{\partial r} \tag{2-30}$$

$$-\mu\frac{\partial^2 \upsilon_r}{\partial z^2} = \rho\omega^2 r \tag{2-31}$$

where: h is the thickness of the film, q is the radial flow per unit length of circumference, μ is the viscosity, ρ is fluid density, ω is the rotational speed, and $v_\theta = r\omega$. Noting that $\upsilon_r(z=0)=0$ and $\partial\upsilon_r/\partial z(z=h)=0$, the integration of the momentum equation leads to:

$$\upsilon = \frac{1}{\mu}\left(-\frac{1}{2}\rho\omega^2 r z^2 + \rho\omega^2 r h z\right) \tag{2-32}$$

Consequently q becomes:

$$q = \int_0^h \upsilon dz = \frac{\rho\omega^2 r h^3}{3\mu} \tag{2-33}$$

Substituting Eq. (2-42) into the continuity equation leads to:

$$\frac{\partial h}{\partial t} = \frac{\rho\omega^2}{3\mu r}\frac{\partial (r^2 h^3)}{\partial r} \tag{2-34}$$

Solving the above equation allowed Emilsile et al. (1957) to determine the thickness profile

Acrivos et al., (1960) extended the Emilsile et al, model by considering the solution to behave as a non Newtonian fluid by Power law:

$$\tau = K\left(\partial \upsilon/\partial z\right)\left[\partial \upsilon/\partial z\right]^{n-1} \tag{2-35}$$

Where: K and n are the characteristic parameters of the fluid. With this the momentum equation becomes:

$$\partial\left[K\left(\partial \upsilon/\partial z\right)\left[\partial \upsilon/\partial z\right]^{n-1}\right]/\partial z = -\rho\omega^2 r \tag{2-36}$$

Mayerhofer (1978) was the first one to propose a mathematical model, which incorporated evaporation of the solvent. Assuming that the evaporation rate of the solvent (e) is uniform and proportional to $\omega^{1/2}$, they showed that the final thickness of the film depends on ω, the initial viscosity of the solution (μ_0) and e according to:

$$h \propto \omega^{-2/3}\mu_0^{1/3}\, e^{1/3} \tag{2-37}$$

They found an excellent agreement between the model and the experimental results obtained on positives photoresists.

Several researchers (Mayerhofer 1978, Bronside et al. 1989, Peurrung et al., 1991) separated the spin coating process into two mechanisms: centrifugally driven fluid flow and solvent evaporation. They assumed that the rate of film thinning is dominated first by the

centrifugal force and then by the solvent evaporation. This approach is called the split model. During the first stage, only fluid flow occurs, while in the second stage, mass transfer occurs.

Yonkoksi and Soane (1992) objected the assumption in the split model that evaporation of solvent can be neglected in the fluid flow stage. They showed that solvent evaporation plays an important role during the flow-dominated stage, because the viscosity strongly depends on the solvent concentration profile. Therefore, solvent evaporation mechanism cannot be completely separated from the fluid flow stage. They showed that the spin coating process can be described by two characteristic parameters; a characteristic film thickness that includes the initial solvent content as well as the spinning conditions, and a Sherwood number that contains a mass transfer coefficient depending on the rotational speed and the initial diffusion coefficient. Their model showed that if the spin coating time is long enough, the fluid flow mechanism becomes negligible and the solvent evaporation is the dominant mechanism for film thinning, which is in agreement with the split model. However, when spin time is very short so that the solvent evaporation is not the dominant mechanism for thinning, the split model shows significant errors.

2.4.3 Film drying

In this final stage of spin coating, fluid flow is stopped and further shrinkage of film occurs only by solvent evaporation. In the previous step, the solvent concentration profiles depend on fluid convection. However, as the velocity drops to zero, this dependency becomes unimportant. It is the point where the spin off stage ends and the film drying stage begins.

2.4.4 The morphology of the spin-coated-film

Keddle et al., (1994) investigated the glass transition temperature (T_g) of thin polystyrene films spin-coated on a Si substrate and observed a reduction in the T_g of polystyrene with a decrease in the thickness of the spin coated films. Mayes (1994) suggested that a higher chain segment mobility in the surface layer than in the bulk results in a larger free volume in the surface. In turn, the greater the free volume the lower the T_g. Consequently, as the film thickness decreases the contribution of a lower T_g surface increases lowering the overall T_g of the film. On the other hand, when the interactions between the film and the substrate are high the free volume at the film-substrate interface decreases leading to an increase in the T_g. Therefore, the effect of film thickness on the T_g of coated polymer films strongly depends on the interactions between the polymer and the substrate. This was confirmed by Forrest et al. (1996) who observed that the largest reduction with the film thickness occurs in case of free standing films, that is, those having two surfaces with increased segmental chain mobility.

The influence of polymer-solvent interactions on the thickness and topography of spin-coated polymer film was investigated by Spangler et al., (1990). The volatility of the solvent seems to have a great impact on the topography of the films. It was found that when two solvents with similar volatilities are used to prepare a solution, only the good solvent can produce a uniform film. A poor solvent may cause irregularities in the surface, because the conformation of the polymer chain in the solution is not able to scatter the waves produced during spin coating. These irregularities are described as "orange peel" and "cloudiness".

On the other hand, when two films are made using two good solvents having different volatilities a low volatility solvent produces a more uniform film than a high volatility one.

During spin coating, a highly volatile solvent causes a rapid increase in the viscosity of the solution, which prevents the liquid flow, and this may lead to nonuniformity of the final film.

CHAPTER 3

RESEARCH OBJECTIVES

3.1 Scope of Research

The present research is a study of a novel method to prepare modified PPO membranes. The performance relationship of both PPO and modified PPO in relation to separation of oxygen over nitrogen in air as well as the permeation of oxygen and nitrogen as single gases are studied. In particular, PPO membranes were modified via the in situ polymerization of aluminum silicate into the PPO matrix.

3.2 General Research Objectives

- To develop PPO-based nanomaterials.
- To investigate the effect of inorganic loading on the properties of the synthesized material.
- To prepare macroporous free homogenous and composite membranes from synthesized materials and to measure their oxygen and nitrogen permeability and investigate their air separation potential.
- Set up a gas separation experimental apparatus for direct measure of nitrogen and oxygen as single gas, and air as gas mixture.

3.3 Specific Research Objectives and Tasks

The following tasks were accomplished in order to achieve the objectives:.

1. Study double emulsions in the preparation of the nanosized particles.
2. Preparation of heterogeneous solutions based on stable emulsion systems.
3. Study of aluminum nitrate hydrolysis in order to form Al in a Kegging structure.
4. Preparation of composite membranes.
5. Study the effect of ultrasound energy density on the membrane preparation.
6. Preparation of dense membranes from PPO and modified PPO (EPMM) membranes using spin coating.
7. Characterization of dense membranes;
   - 7.1 X-ray diffraction analysis,
   - 7.2 Differential scanning calirometery analysis,
   - 7.3 TG analysis,
   - 7.4 SEM and EDX analysis,
   - 7.5 Gas permeation experiments,
   - 7.6 Gas separation experiments.

CHAPTER 4

METHODOLOGY AND EXPERIMENTAL

This chapter includes experimental methods, instruments employed and materials used in this research.

4.1 Preparation of precursor solutions for nanoparticle production

This section describes the preparation of W/O emulsions for making membranes and the preparation of W/O/W emulsions.

4.1.1 W/O emulsion preparation

A W/O emulsion was prepared in a two-step procedure: In the first step, a primary emulsion was prepared by dispersing the aqueous solution containing aluminum nitrate, as described below, into 5 cm^3 of PPO solution containing a surfactant and sonicating using an ultrasonic homogenizer for a given time. In the second step, the primary emulsion was added to the 5 cm^3 of PPO solution containing TEOS and stirred with the ultrasonic homogenizer for a given time, depending on the TEOS loading. Figure 4.1 illustrates a schematic diagram of a W/O emulsion preparation. An ultrasonic dismembrator described in section 4.1.3 was used to produce all emulsions.

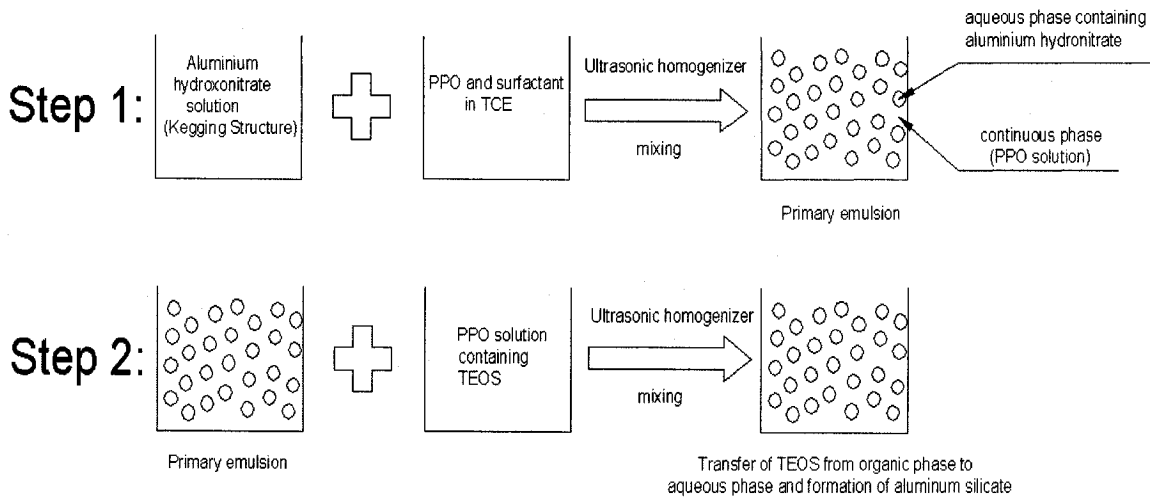

Figure 4.1 The schematic diagram of W/O emulsion preparation.

Preparation of aluminum hydroxonitrate solution

The initial solutions of aluminum nitrate were prepared by dissolving solid aluminum nitrate in distilled-deionized water. Varying concentrations of sodium carbonate from 0.089 to 0.127 g/cm^3 were prepared by dissolving solid sodium carbonate in distilled-deionized water. The initial solutions of aluminum nitrate were treated with the prepared sodium carbonate solutions. As soon as the sodium carbonate was added, a precipitate formed. At low sodium carbonate concentrations, the precipitate rapidly dissolved, while at high sodium carbonate concentrations, the precipitate was insoluble. The concentration of aluminum nitrate in the all-resultant solutions was 1 M.

The pH of the solution was measured by a pH analyzer 350.

The quantities of aluminum nitrate, sodium carbonate and water used in the preparation of aluminum hydroxonitrate solution are indicated in Table 4.1. The final solutions were kept for a certain time at ambient temperature in order to achieve hydrolytic equilibrium.

Table 4.1 The quantities of aluminum nitrate, sodium carbonate and water in aluminum hydroxonitrate solutions.

Ingredients	Sample-1	Sample-2	Sample-3	Sample-4	Sample-5
Water (cm^3)	56	56	56	56	56
$Al(NO_3)_3\ 9H_2O$ (g)	21	21	21	21	21
Na_2CO_3(g)	5	5.5	6	6.5	7.1
pH	3.167	3.346	3.655	aggregation	aggregation

The following experiment was conducted to ensure that the degree of hydrolysis of aluminum hydroxonitrate is higher than 1.9 and that the aluminum is in tetrahedral form:

The gelation time of TEOS in the aluminum hydroxonitrate solution-EtOH medium was measured in each experiment. The volume ratio of TEOS: EtOH: aluminum hydroxonitrate solution was 1:3:1. Since the aluminum hydroxonitrate solution and TEOS were immiscible, EtOH had to be used as a mutual solvent.

4.1.2 W/O/W emulsion preparation

W/O/W emulsions were prepared by using a two-step procedure, at first; the primary W/O emulsion was prepared by adding the internal phase to the organic phase at an equal volume ratio and mixing with an ultrasonic homogenizer. In the second step, the primary emulsion was stirred in an external phase with a magnetic stirrer. Figure 2.5 illustrates a schematic diagram of a double emulsion solution.

W/O primary emulsion

The primary W/O emulsion was prepared by adding the aqueous internal phase to the organic phase and mixing with an ultrasonic homogenizer for 40 sec.

Internal aqueous phase

The internal aqueous phase was an aluminum nitrate solution prepared via the following procedure; 22.5 g aluminum nitrate and 0.225 g sodium carbonate were dissolved in 60 cm^3 of water. The pH of the internal phase was 1.340.

Organic phase

The organic phase was kerosene which contained a surfactant. Sorbitan sesquioleate (Span 83) with a HLB of 3.7 was used as the surfactant.

Double emulsion

The external water phase was slowly added to the primary emulsion and stirred with a magnetic stirrer.

External aqueous phase

External phase was a solution of distilled water, EtOH, and tetraethylorthosilicate (TEOS) and sodium dodecyl sulfate with a HLB=40. In order to satisfy the stoechiometic requirements for the formation of aluminum silicate the molar ratio of aluminum nitrate in the internal phase to TEOS in the external phase was kept at 1:1. Because water and TEOS were immiscible, we had to use a mutual solvent as a homogenizing agent. Two different homogenizing agent, EtOH and isaopropanol, were tested. The ternary –phase diagram of TEOS, H_2O and Synasol (95%EtOH, 5% water) used in calculation of volume ratio of EtOH to water is shown in Figure 4.2. A ternary–phase diagram of TEOS, H_2O and isopropanol

was presented in Appendix A along with the quantities of ingredients used in the preparation of double emulsion.

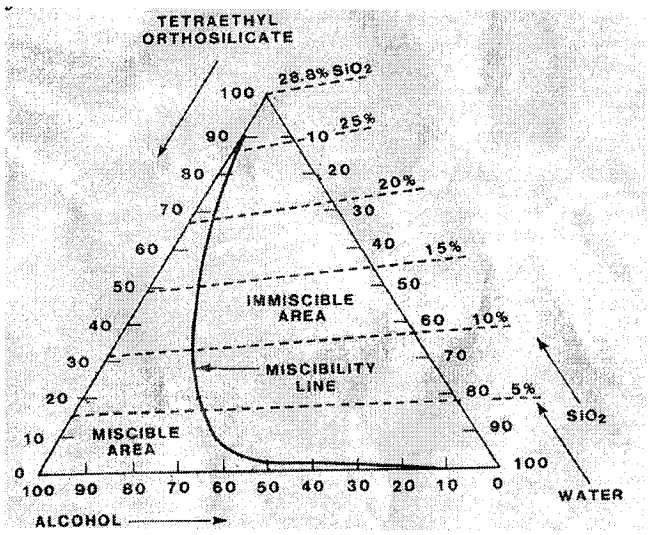

Figure 4.2 The ternary –phase diagram of TEOS, H_2O and Synasol (95% EtOH, 5% water) (Brinker and Scherer, 1990).

4.1.3 Equipment

Ultrasonic Homogenizer

An ultrasonic dismembrator (Fischer Scientific, Model 550, Pittsburgh, PA, USA) equipped with a standard horn with a length of 12.7 cm and diameter of 3.8 cm, a generator, and a convertor or transducer operating at 20 kHz was used throughout this work.

Microscope

We used an Olympus Microscope equipped with a Polaroid Digital Microscope camera and a computer to take photomicrograph. The microscope consists of an eyepiece with a 10X magnification and objective lenses with 2X, 20X, and 100 X magnifications. The

magnification of the image transmitted to the computer was determined by a micro-scale ruler.

Particle Size Analyzer

Dynamic light scattering is a technique for measuring the size of particles and droplet suspensions which are in sub-micron region. In dynamic light scattering, the speed at which the particles are diffusing due to Brownian motion is measured. Particles in a dispersion which are in a constant or random Brownian motion causes the intensity of the scattered light fluctuates as function of time. Translational diffusion coefficient of particles can be obtained by measuring fluctuation rate of scattered light. Consequently, the diameter of the particle is calculated from the translational diffusion coefficient by applying the Stokes-Einstein equation, the diameter that is measured in dynamic light scattering is referred as a hydrodynamic diameter. The hydrodynamic is the diameter of a sphere that has same transitional diffusion coefficient as the particle has. In this study, we measured droplet size with using a dynamic light scattering instrument (MALVERN Zetasizer, UK) which it allows the size of dispersed droplet in range to 0.6 nm to 6 μm be determined. The following correlation was employed to estimate the tricholoroethylene viscosity.

$$\log \mu_{liq} = A + B/T + CT + DT^2 \qquad (4\text{-}1)$$

$A = -5.5389$, $B = 7.8313 \times 10^2$, $C = 1.2849 \times 10^{-2}$, $D = 1.3292 \times 10^{-5}$,
$T = Temperatur\, e\ (K)$

The mean droplet size, expressed as the Sauter diameter, was calculated from the DLS measurements using the following equation (REF):

$$d_{32} = \frac{\sum_{i=1}^{N} n_i d_i^3}{\sum_{i=1}^{N} n_i d_i^2} \tag{4-2}$$

Where: d_{32} is Sauter diameter, n_i is number of droplets, and d_i is droplet size.

4.2 Membrane making

Multi-layered membranes were made by spin coating layers of PPO solution and the W/O emulsion onto a silicone wafer. The emulsion polymerized mixed matrix (EPMM) membranes were produced by spin coating the W/O emulsion onto a silicone wafer. The methods and equipment used to produce these membranes and characterization techniques are described below.

4.2.1 Spin coating machine

A 100 series CEE Model Spinner was used to spin-coat the casting solutions. The 100 Series Spinner utilizes a single-board microcomputer as its main controlling element and a vacuum to keep the wafer on the spin chuck. The spinner incorporates a stainless steel spin bowl and a plastic lid, which covers the spin bowl. The spinner is programmed by using the front panel. There are ten user programs available, each capable of storing ten program steps. Each step consists of a rotation speed value, an acceleration value (rpm/second), and a step duration time value (seconds). This machine is designed to process round substrates up to eight inches in diameter and square plates up to six square inches. In this study, round substrates with a four-inch diameter were used as wafers.

4.2.2 Multi-layered membrane preparation

The multi-layered membranes, which were made in the present work, consist of three layers. They were prepared through the following procedure:

W/O emulsion solution preparation

The W/O emulsion solution was prepared as follows: 0.2 cm^3 of aluminum nitrate solution prepared via section 4.1.1 was added to the 5 cm^3 of 10% PPO solution including 0.1g of Span 83(surfactant) and mixed by an ultrasound homogenizer for 40 sec. The resultant solution was added to 5 cm^3 of 10 % PPO solution including 0.2 cm^3 of TEOS, and mixed by a magnetic stirrer for 2 hours.

Membrane preparation

The first layer was made by depositing 10cm^3 of 5%PPO solution on the wafer and spun at 100 rpm for 240 sec; it was then kept at ambient temperature for 2 hours.

The second layer was made by delivering 10cm^3 of W/O emulsion prepared via above procedure on the rotating wafer at 600 rpm for 100 sec; the film was heated in vacuum oven (purged with nitrogen) at 120°C for 48 hours. The third layer was coated by depositing 10cm^3 of 5% PPO solution on the rotating film at 150 rpm for 240 sec.

4.2.3 EPMM membrane preparation at high pH (EPMM1)

In this step, we attempted to make a macroporous free homogenous membrane. For convenience, this membrane was EPMM1. The W/O emulsion used in make of EPMM1 membrane was prepared via a procedure is similar to that reported for the multi-layered membrane except the surfactant. N-octanol was used as a surfactant. 0.02cm^3 of 5 N sodium hydroxide was added to the W/O emulsion and then mixed by ultrasonic homogenizer for 40

sec. The resultant solution was deposited on the wafer and spun at 50 rpm for 300 sec. The film was kept at ambient temperature for 2 hours, the film was then washed out in the boiling water for 4 hours, and finally it was heated in vacuum oven (purged by nitrogen) at 120°C for 48 hours.

4.2.4 EPMM membrane preparation at intermediate pH (EPMM2 and EPMM3)

EPMM membranes with two different TEOS loadings were made in order to investigate the effect of the inorganic loadings on the PPO properties. The following procedure was applied in order to make the EPMM2 and EPMM3 membranes.

W/O emulsion solution preparation

A W/O emulsion was prepared via the procedure reported in the 4.1.1 Table 4-2 indicates quantities of the ingredients used in preparation primary and secondary W/O emulsions along with ultrasonic energy density applied for the preparation of the EPMM2 membrane.

Table 4-2 Quantities of the ingredients used and the power dissipated in preparation primary and secondary W/O emulsion of the EPMM2 membrane.

Aluminum hydroxonitrate solution (cm^3)	TEOS (cm^3)	N-octanol (cm^3)	10% PPO solution (cm^3)	Molar ratio of aluminum nitrate to TEOS	Molar ratio of water to TEOS	Volume ratio of N-octanol to water
0.0172	0.05	0.0104	10	0.07167	4.0	0.60465
Ultrasound energy in the primary emulsion (kJ/ cm^3)				Ultrasound energy in the secondary emulsion (kJ/ cm^3)		
$\frac{600W \times 0.50 \times 30}{5} = 1.8$				$\frac{600W \times 0.30 \times 420}{10} = 7.56$		

The quantities of the ingredients used in the preparation of the EPMM3 membrane are tabulated in Table 4-3. To promote the transfer of TEOS from the organic phase to the internal phase, three different amount of power were applied.

Table 4-3 Quantities of the ingredients used and the power dissipated in preparation primary and secondary W/O emulsion of the EPPM3 membrane.

Aluminum hydroxonitrate solution (cm^3)	TEOS (cm^3)	N-octanol (cm^3)	10% PPO solution (cm^3)	Molar ratio of aluminum nitrate to TEOS	Molar ratio of water to TEOS	Volume ratio of N-octanol to water
0.0346	0.1071	0.0209	10	0.07167	4.00	0.60465
Ultrasound energy density in the primary emulsion (kJ/ cm^3)						
$\frac{600W \times 0.50 \times 60}{5} = 3.60$						
Ultrasound energy in the secondary emulsion (kJ/ cm^3)						
1) $\frac{600W \times 0.30 \times 785}{1000} = 14.13$ 2) $\frac{600W \times 0.30 \times 1200}{10} = 21.60$ 3) $\frac{600W \times 0.30 \times 1800}{10} = 32.4$						

Membrane preparation:

Ten cm^3 of the W/O emulsion was placed on the wafer and spun at 600 rpm for 200 sec. This formed a smooth film on the surface of the wafer. The coated wafer was kept at room temperature for 2 hours. The coated wafer was then heated at 120°C in the vacuum oven (purged with nitrogen) for 2 hours. A second layer was applied over the first by delivering another ten cm^3 of the W/O emulsion over the rotating wafer at 600 rpm for 200 sec after which the wafer was kept at room temperature for 2 hours. The second coating was applied over the wafer while it was rotating to prevent the dissolution of the original coating. This dissolution occurred when fresh solution was allowed to rest on the surface of the coated wafer for even a few seconds. Addition of the second coating while the wafer was

spinning produced a film of uniform thickness across the diameter of the wafer. The film was then peeled off the wafer by soaking it in distilled water for 5 minutes.

Post treatment

The unreacted TEOS was washed out from the free-standing membrane in boiling water for 4 hours. The solubility of TEOS in water is 36.91 g/L at 25 °C. Finally, the membrane was dried in a vacuum oven that was initially purged with nitrogen. It was kept at 120°C under 12 mm Hg for 48 hours.

4.3 Membrane characterization

4.3.1 Membrane thickness measurement

The membrane thickness was measured by using a micrometer. Twenty readings were taken from the entire area of the membrane and the average and standard deviation of the thickness were then calculated.

4.3.2 X-ray diffraction analysis

An X-Ray Diffractometer (SCINTAG, Model 2000, Cupertino, CA, USA) was used to provide information on the degree of crystallinity as well as phase purity. The most significant information obtained from X-ray powder diffraction was; the uniqueness of structure, the presence of a single phase or a mixture of phases, the incorporation of other elements into structural framework sites and the level of crystallinity.

The X-ray powder diffraction pattern of the zeolite is generally taken between the value of 2° and 40° 2θ. It is within this range that the most intense peaks characteristic of the zeolite structure occur. The peaks at values higher than 40° 2θ are of low intensity, and may not be

observable (Szostak, 1998). Hence, the range between 2° 2θ and 40°2θ with a step size of 2θ equal to 0.02° is examined for most routine X-ray screening of zeolite phases.

The d-spacing (d) can be obtained by using Bragg equation:

$$d = \frac{\lambda_X}{2\sin\theta} \tag{4-3}$$

Where λ_X is a wavelength of X-rays. A copper cathode generated a monochromatic beam of X-rays of wavelength λ_X equal to 1.54. Å.

4.3.3 Thermal gravimetric analysis

A TGA2950 thermo-analysis instrument (TA Instruments, New Castle, DE, USA) was used to investigate the degradation process and thermal stability of the membranes. The TGA measurements were carried out under nitrogen with a scanning rate 10°C/min from 25°C to 800°C.

4.3.4 Differential scanning calorimetry

Differential scanning calorimetry (DSC) was performed using a QA series TA 1000 differential scanning calorimetric analyzer (TA Instruments, New Castle, DE, USA). In order to obtain precise and accurate thermal properties of the membranes, both conventional and modulated (MDDSC) were used. The principles of MDDSC, as well as the differences between MDDDC and conventional will be discussed in Appendix B. For the conventional DSC, the heating rate was 10°C/min, and nitrogen flow was $50\,\mathrm{ml/min}$. For MDDSC, the modulated heating rate was ± 1.00 °C every 60 second.

4.3.5 SEM-EDX analysis

The membrane cross section was investigated using a Hittachi S3200 N scanning electron microscope (SEM) (Hittachi, Pleasanton, CA, USA) instrument equipped with an Oxford link ISIS energy dispersive X-ray (EDX) spectrometer.

4.3.6 Gas permeation and separation test

Gas transport properties of membranes were determined in both gas mixture and single gas permeation test. Gas permeation experiments were performed in a constant pressure testing system equipped to a Gas Chromatography (GC) unit. A complete set of permeation experiments for a given membrane consisted of tests with air as a gas mixture and pure gases in the following order: O_2 and N_2

In the single gas permeation tests, gas permeates through the membrane were measured at three different pressure gradients in the following order: 120, 90 and 60 psi. In the gas mixture, the gas transport properties of the membranes were determined at a pressure gradient of 66 psi.

Constant pressure system

Figure 4.3 illustrates a schematic diagram of the constant pressure equipped to the GC. The system consisted of two permeation test cells inside of which a membrane was placed. Gas at a certain pressure was fed to the cells; the retentate flow was set to 110cm^3/min and permeate discharged to atmosphere. The volumetric permeate flow rate was measured by a bubble flow meter. Bubble flow meters with volumes of 500 and 100 micro

liters were used. In addition, oxygen and nitrogen concentrations in the permeate side were determined by using a Gas Chromatography unit.

Figure 4.4 shows a cross-flow test cell having surface area of 20 cm^2. The cell was sealed by a metal ring. In addition, a Viton Oring was placed in the lower part of the cell in order to improve cell sealing. A filter paper was put on the porous surface of the cell to avoid damage to the membrane. A Viton Oring was used to seal the upper part of the cell.

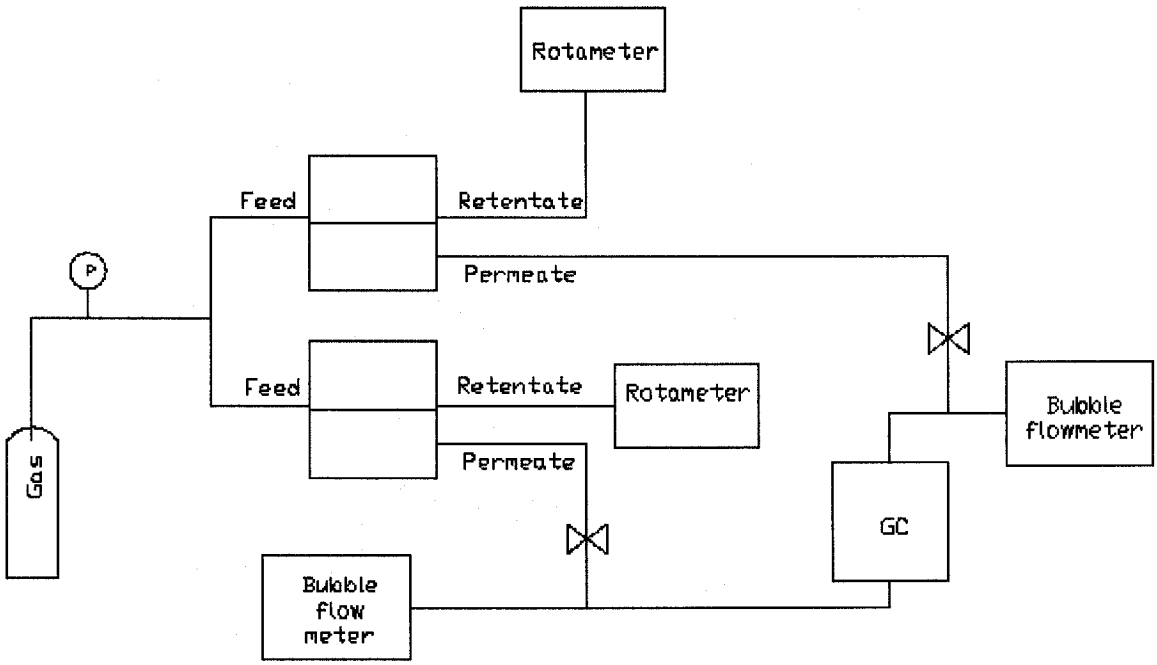

Figure4.3 Constant pressure system equipped with a GC.

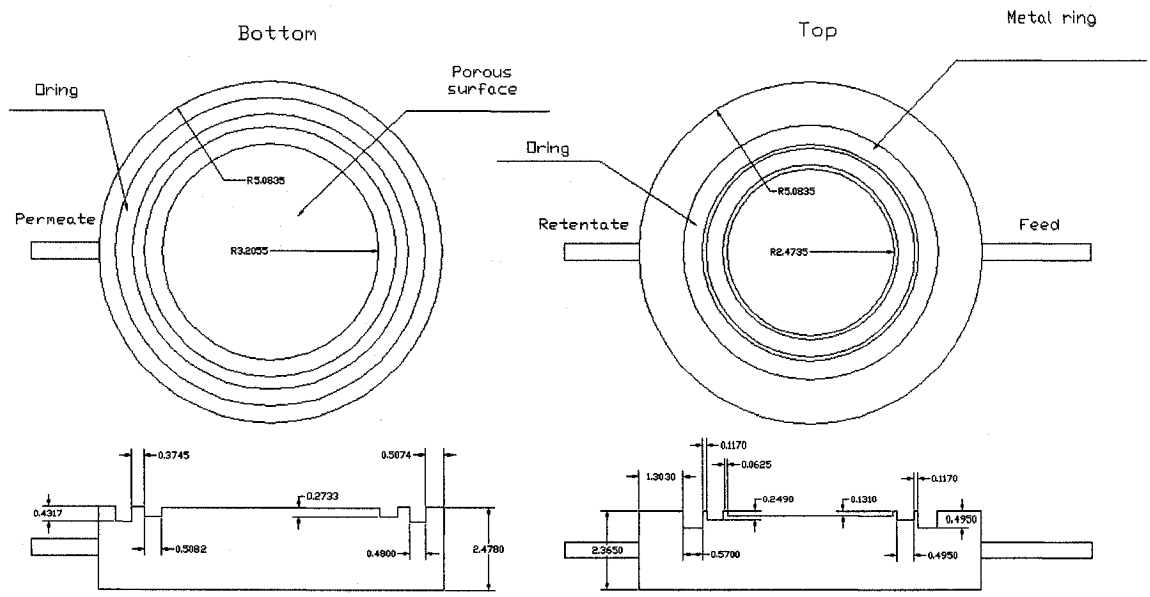

Figure4.4 Diagram of the cross-flow cell (dimensions in cm).

Gas Chromatography (GC) unit

A 5700 HP Gas chromatography HP, with a thermal conductivity detector and a 5A molecular sieve column was used to measure concentrations of oxygen and nitrogen in the permeate gas stream. To precondition of the column, it was heated at 300°C for approximately 4 hours. The operating conditions of the GC were as follows: flow rate of the carrier gas (helium): 30 cm^3/min, detector temperature: 150°C, column temperature: room temperature.

To obtain quantitative results from the GC, a response value has to be applied to the area obtained for the nitrogen and oxygen peaks. For the GC with thermal conductivity detector, these response values are independent of temperature, carrier gas, flow rate and concentration. The thermal response values of oxygen and nitrogen are tabulated in Table 4-4.

Table 4-4 Response values for thermal conductivity detector

Compound	M_W	Thermal Response
Nitrogen	28	42
Oxygen	32	40

The normalized response value was obtained by dividing area under the curve by the relative thermal response value of that component. The mole percent of the component was obtained by using these normalized values (Dietz, 1967).

4.4 Materials

An alphabetic list of chemicals and gases utilized in this work along with their supplier is presented in Table 4-5.

Table 4-5 Material used during the course of this research

Chemicals	**Specification**	**Source**
Aluminum nitrate nonahydrous		Sigma-Aldrich
Air	Industrial Grade	Praxair
Ethanol	99.5%	Sigma-Aldrich
Isopropanol		Fischer Scientific
kerozene		Fischer Scientific
Nitrogen	Industrial Grade	Praxair
N-octanol	99%	Sigma-Aldrich
Oxygen	Industrial Grade	Praxair
PPO	Powder, $[\eta] = 1.78\, dL/g @ 25\ ^{\circ}C$	GE
SDS	sodium dodecyl sulfate	Sigma-Aldrich
Silicon wafer		
Sodium hydroxide		Sigma-Aldrich
Sodium carbonate anhydrous	Granular ACS Reagent	Sigma-Aldrich
Span 83	Sorbitan sesquioleate	Sigma-Aldrich
Trichloroethylene (TCE)	99.5% Reagent	Sigma-Aldrich
Tetraethylorthosilicate	Reagent Grade 98%	Sigma-Aldrich

CHAPTER 5

RESULT AND DISCUSSION –

Emulsion Characterization

This chapter describes the microscopic observations made in the investigation of W/O/W emulsion stability and the characterization of W/O emulsions used in the preparation of EPMM membranes.

5.1 W/O/W double emulsion

Figure 5.1 illustrates a stable primary W/O emulsion. The diameter of the internal phase in the primary emulsion is less than 4.5μm. The stability of this primary emulsion indicates the performance of the Span 83 in the preparation of a stable W/O emulsion.

Figure 5.2 shows a stable W/O/W double emulsion in which the size of the globules is approximately 33 μm, while an unstable W/O/W emulsion is shown in Figure 5.3. As mentioned in the literature review, a stable double emulsion requires two surfactants with high and low HLB. The concentration of these surfactants also plays a key role on the stability of the W/O/W emulsions. The stability of W/O/W emulsion shown in Figure 5.2 not only indicates the performance of these surfactants, Span 83 and SDS, but also confirms that a stable W/O/W emulsion was obtained at the concentrations used in this work. In spite of the fact that the W/O/W emulsion observed in Figure 5.3 contains both surfactants, Span 83 and SDS, it is unstable. The only difference between the stable W/O/W emulsion observed in

Fig 5.2 and the unstable W/O/W emulsion in Figure 5.3 is related to the difference in the components of the external phase. The external phase of the unstable W/O/W emulsion includes TEOS and EtOH. The insolubility of TEOS in water requires the use of a mutual solvent, such as EtOH or Isopropanol, in the external phase. We observed that the W/O/W emulsion systems that included isopropanol in their external phase also show instability similar to that of previous W/O/W system.

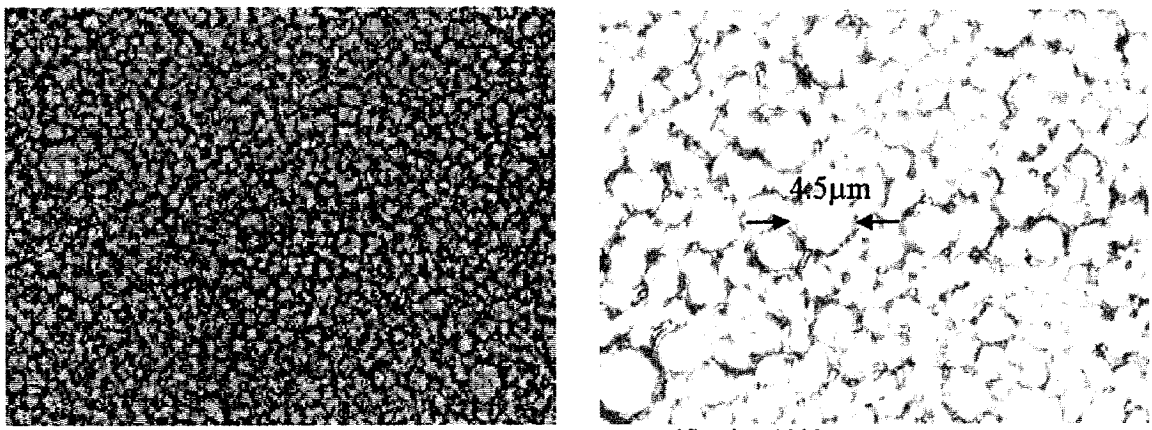

(a) Magnification 200 **(b)** Magnification 1000

Figure 5.1 Microscopic pictures of a primary emulsion. This primary emulsion consists of the 50% internal aqueous phase and 20% Span 83 in kerosene.

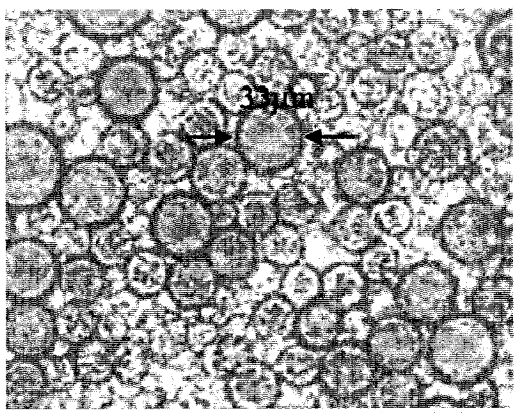

Fig 5.2 Microscopic picture of a stable W/O/W double emulsion, magnification 200, this double emulsion is composed of 20% primary emulsion in aqueous external phase including 0.1%SDS.

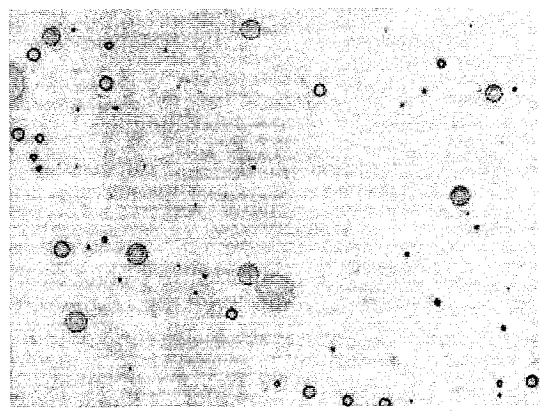

Fig 5.3 Microscopic picture of a poor W/O/W double emulsion, magnification 200, this double emulsion is composed of 20% primary emulsion in aqueous external phase including 2.2% TEOS, 50% EtOH, and 0.1% SDS.

5.2 Characterization of the W/O emulsion of EPMM

The important parameters for a W/O emulsion used in preparation of EPMM membranes are: the degree of hydrolysis of the aluminum hydroxonitrate inside the internal aqueous phase of W/O emulsion, and the size of the aqueous droplets.

5.2.1 Determination of the degree of the aluminum hydroxonitrate hydrolysis

Hydrolysis and condensation polymerization rate of TEOS in the presence of aluminum hydroxonitrare increases drastically in the systems where the degree of hydrolysis of the aluminum nitrate is higher than 1.9 and the aluminum is in a tetrahedral form. The rapid hydrolysis (short gelation time, 10 to 20 min) of TEOS in the presence of aluminum hydroxonitrate indicates a high degree of aluminum hydroxonitrate hydrolysis, where $h>1.9$, whereas slow hydrolysis (long gelation time, nearly 3-4 days) of TEOS shows a low degree of aluminum hydroxonitrate hydrolysis, where $h<1.9$. More over, the resulting gels at high degree of aluminum hydroxonitrate hydrolysis are opaque, while the resulting gels having a low degree of aluminum hydroxonitrate hydrolysis are transparent (Eliseev et al., 1999). In the present research, a gelation time of 4 to 7 min was observed for the copolymerization of TEOS in the presence of aluminum hydroxonitrate, and resulting gels were opaque as shown in the Fig 5.4. This indicates that the degree of aluminum hydroxonitrate hydrolysis is higher than 1.9. The measurement of the gelation time was performed for each experimental run in order to assure a high degree of aluminum hydroxonitrate hydrolysis.

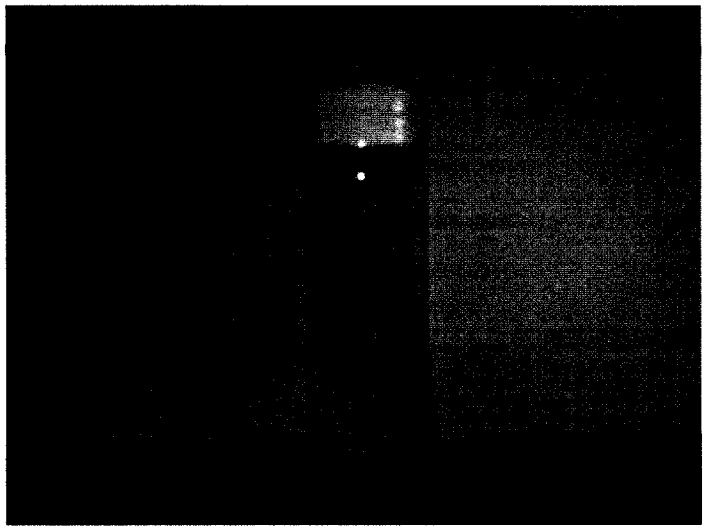

Figure 5.4 The gel obtained from hydrolysis TEOS in the presence of aluminum hydroxonitrate.

5.2.2 Measurement of aqueous droplet size

Table 5-1 shows the mean diameter, obtained from DLS measurements, of the internal aqueous droplets in the W/O emulsions of EPMM2 and EPMM3 membranes along with the energy density applied in the first step of the W/O preparation.

Table 5-1 Mean diameter of the internal aqueous droplet along energy density applied for preparation of W/O emulsion.

W/O emulsions	Internal aqueuse phase volume content %	mean diameter (nm)	St.Dev	Energy density kJ/cm^3
EPMM2	0.34	245	10.2	1.8
EPMM3	0.69	344	16.1	3.6

It can be observed from this table that the doubling of the energy density in preparing the emulsion, containing twice the amount of aqueous phase, did not maintain the size of the emulsion at the value of 245 nm (observed in the W/O emulsion used in the preparation of

the EPMM2 membrane). This limitation can be due to high viscosity of the continuous phase (10% PPO solution).

At higher aqueous phase content the possibility of the coalescence of aqueous droplets increases. In the high viscous continuous phase, the influence of the coalescence will be more significant, because small droplets, after disruption, are slowly separated, which leads to long contact times between droplets and consequently their coalescence (Behrend and Schubert, 2000).

CHAPTER 6

RESULT AND DISCUSSION –

Membrane Characterization

This chapter is concerned with characterization of EPMM membranes prepared according to the procedures described in Chapter 4. The results of membrane characterization are divided into four sections:

In section 6.1, the X-ray diffraction spectra of the membranes are presented and the effect of the inorganic loading is discussed. In section 6.2, the thermal properties of the membranes are studied using thermogravimetric analysis and differential scanning calorimetry. This section also includes the study on specific heat capacity changes of the membranes at the glass transition temperature, and the determination of fractional free volume of the membranes. In section 6.3, scanning electron microscopy and energy dispersive X-ray analysis are conducted to investigate the morphology and atom composition of the membranes. In section 6.4, the gas transport properties of the membranes are determined by using a constant pressure system equipped with a gas chromatography unit.

6.1 Wide-Angle X-ray Diffraction Analysis

The structural changes induced by the incorporation of aluminum silicate domains into PPO were characterized using wide-angle X-ray diffraction. In general, X-ray diffraction provides information about the morphological properties and the degree of crystallinity of the

membranes. The *d*-spacing and peak intensity parameters can be extracted from an X-ray diffraction spectrum.

6.1.1 X-ray diffraction analysis of PPO, multi-layered and EPMM1 membranes

The wide-angle X-ray pattern obtained from the multi-layered membrane, which is prepared via the procedure described in the section 4.2.2, is compared with those of the PPO membrane. Figure 6.1 illustrates the X-ray diffraction spectra of the PPO and the multi-layered membranes. It should be mentioned that the crystallinity of PPO powder is somewhat lower than that of polymer films. Different conditions for preparation of films with different surface/ volume ratios can be responsible for this behavior (Alentiev et al., 1997). The X-ray spectrum of the PPO membrane shows a major peak occurring at $2\theta = 14.28^{\circ}$ (d_2), which corresponds to a *d*-spacing of 6.2Å. This *d*-spacing value is in agreement with 6.1Å reported by Story and Koros (1992). In addition, a broad peak is present at $2\theta = 28.6^{\circ}$ (d_3), which corresponds to a *d*-spacing of 3.1Å. The X-ray spectrum of PPO in Figure 6.1 is typical for semicrystalline polymers (Wenig et al., 1976).

The X-ray diffraction spectrum of the multi-layered membrane shows that the location of the major peak of does not change in comparison with that of the PPO membrane. A sharp peak at $2\theta = 29.41^{\circ}$ (d_3) corresponding to *d*-spacing of 3.0Å is attributed to the presence of sodium nitrate in the multi-layered membrane. Consequently, on the basis of the X-ray diffraction patterns the multi-layered and PPO membranes have similar structures.

Figure 6.2 illustrates the X-ray diffraction spectra of the PPO and EPMM1 membranes. As seen in the spectrum of the EPMM1 membrane, a new peak appears at $2\theta = 7.99^{\circ}$ (d_1), which corresponds to *d*-spacing of 11.05Å. The major peak for the EPMM1

membrane occurs at $2\theta = 13.29°$ (d_2), which in comparison with the major peak of the PPO membrane, is shifted towards a lower 2θ value, while the peak width becomes narrower. The third peak (d_3), which appears as a shoulder in the diffraction spectrum, becomes more pronounced and is shifted towards the lower 2θ values in the EPMM1 membrane (2θ = 22.05°), corresponding to *d*-spacing of 4.03Å. The fourth peak at $2\theta = 29.41°$(d_4) similarly to the multi-layered membrane arises from the presence of sodium nitrate.

Table 6-1 summarizes the X-ray diffraction analysis of the PPO and the multi-layered membrane. The spectra are compared in terms of peak location, peak intensity normalized based on the membrane thickness. These significant changes in the EPMM1 membrane structure could also be due to the reaction of TEOS with Na(OH) added in the casting solution. Based on the literature data, the condensation polymerization of TEOS at high pH leads to the macroporous structure (Caro et al., 2000), which is not appropriate for the gas separation process as seen later in the gas separation experiments.

Table 6-1 Wide-angle diffraction analysis data for PPO, the EPMM1, and the multi-layered membranes.

Membrane	d_1	d_2	d_3	d_4
PPO				
2θ		14.28	28.6	
d-spacing		6.2	3.1	
Intensity (a.u)		70763	23587	
EPMM1 membrane				
2θ	7.99	13.29	22.05	29.41
d-spacing	11.05	6.65	4.03	3.0
Intensity (a.u)	14540	395681	15698	
Multi-layered membrane				
2θ		14.28	28.6	29.41
d-spacing		6.2	3.1	3.03
Intensity (a.u)		54380	13904	35476

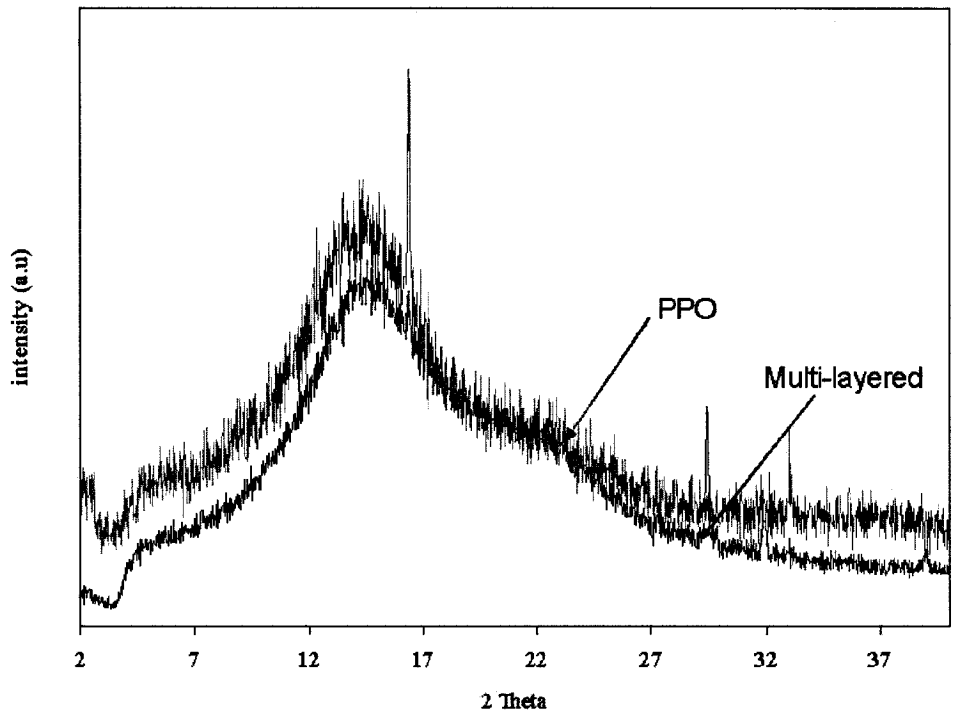

Figure 6.1 Normalized X-ray diffraction spectra of PPO and the multi-layered membranes.

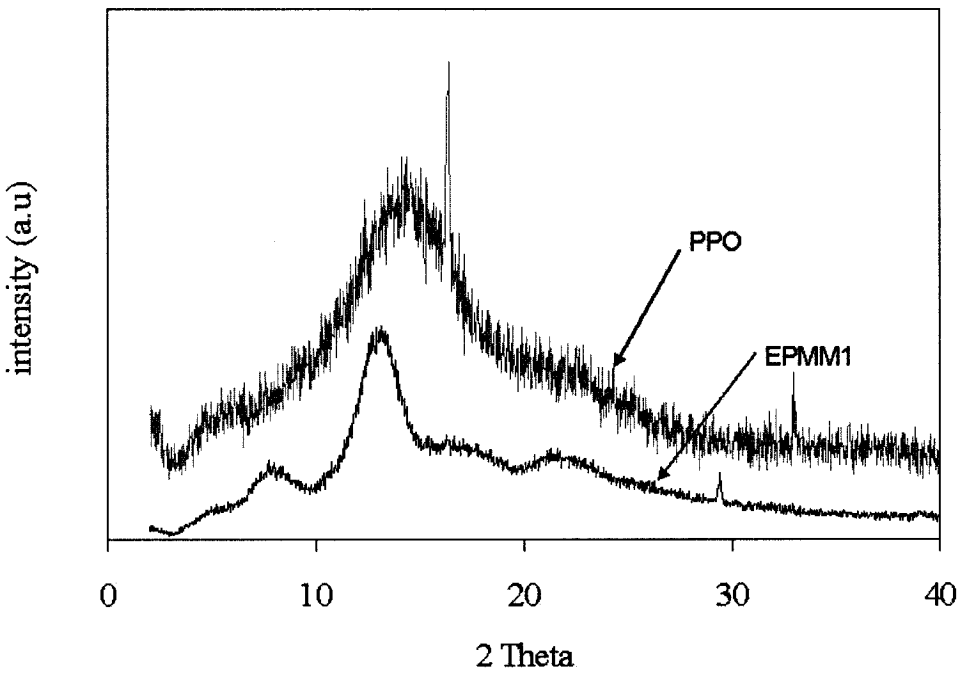

Figure 6.2 Normalized X-ray diffraction spectra of PPO and the EPMM1 membranes.

6.1.2 X-ray diffraction PPO EPMM2 and EPMM3 membranes

The wide-angle X-ray patterns obtained from the EPMM2 and EPMM3 membranes are compared with those of the PPO membrane and aluminum silicate. Figure 6.3 illustrates the wide-angle X-ray spectra of PPO membrane, aluminum silicate, EPMM2 and EPMM3 membranes.

The X-ray spectrum of the aluminum silicate powder shows that the aluminum silicate powder prepared at low temperature has an amorphous domain, which is entirely consistent with the result reported by (Huang et al., 1997). Although the X-ray measurements of EPMM2 and EPMM3 membranes show that the locations of the peaks are not changed by the incorporation of aluminum silicate, the normalized intensities of EPMM2 and EPMM3 membrane peaks are reduced by 44.22% and 51.70%, respectively. The sharp peak (d_4), which was observed at $2\theta = 29.41^{\circ}$ in the both EPMM1 and multi-layered membranes, fades away in the EPMM2 and EPMM3 membranes, since sodium nitrate has been washed out during post treatment of EPMM1 and EPMM2 membranes preparation. This step was not carried out in the preparation of EPMM1 and multi-layered membranes.

The X-ray spectra of EPMM2 and EPMM3 are typical of being amorphous, despite the existence of aluminum silicate content. This agrees with the results of the synthesis of modified PPO reported by Zhang et al. (2005). Zhang et al. prepared (PPO)-based organic-inorganic hybrid materials through the sol-gel process of polymer precursors PPO-S(OCH_3). The XRD study of this material shows that it is amorphous despite the presence of inorganic material.

Wu et al. (2004) showed that all the hybrid materials prepared through sol- gel process are amorphous. This is consistent with the X-RD results obtained by Kim and Lee

(2001), in which the crystallinity of poly (amide-6-b-ethylene oxide) decreases with increasing inorganic (TEOS) content. Kim et al., (2004) also reported that X-ray diffraction peaks of poly (vinyl alcohol)/SiO_2 hybrid membrane become somewhat broadened by addition of silica. On the other hand, Jiang et al. (2005) observed that the X-ray diffraction spectrum of silica/Nafion membrane produced at 120°C becomes narrower as silica is added, which indicates that this membrane has a higher crystallinity than pure Nafion.

Table 6-2 summarizes the X-ray diffraction analysis of the PPO, the EPMM2 and EPMM3 membranes.

Table 6-2 Summary of X-ray spectra analysis of PPO, EPMM2 and EPMM3 membranes.

Membrane	d_1	d_2
Blank PPO		
2θ	14.28	28.6
d-spacing	6.2	3.12
Intensity (a.u)	46.125	15.25
EPMM2		
2θ	14.28	28.44
d-spacing	6.2	3.13
Intensity (a.u)	27.077	10.615
EPMM3		
2θ	14.28	28.8
d-spacing	6.2	3.1
Intensity (a.u)	22.63	7.56

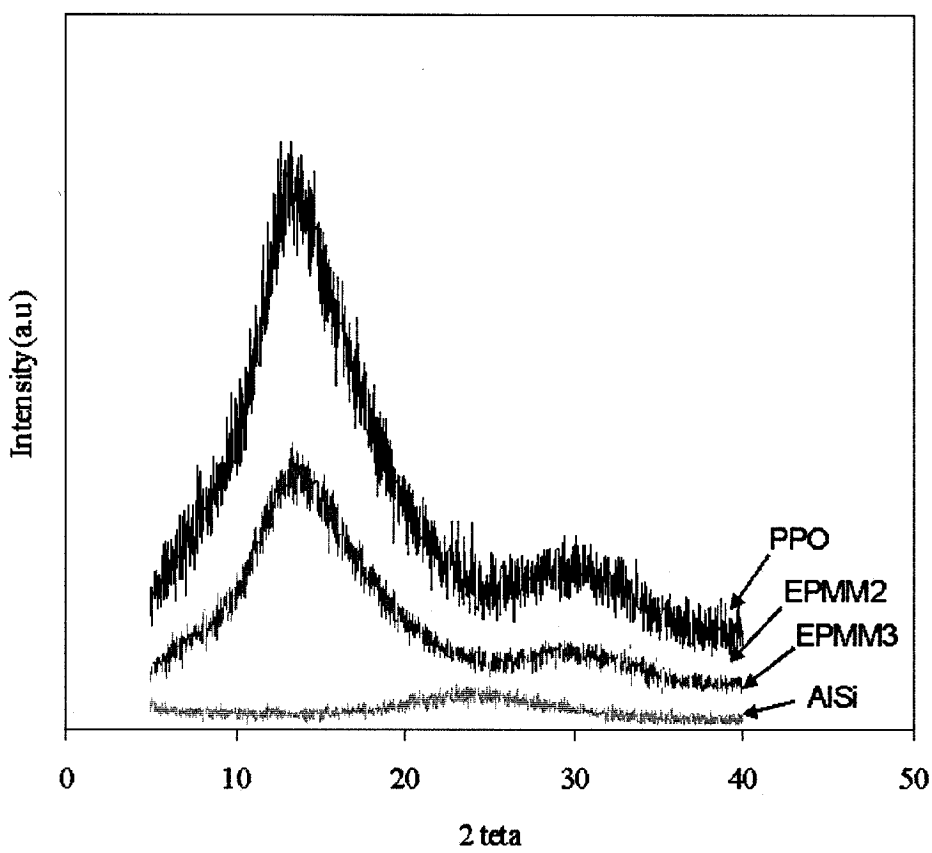

Figure 6.3 Normalized X-ray diffraction spectra of PPO, EPMM2, EPMM3 and aluminum silicate membranes.

6.2 Thermal analysis

Thermogravimetric analysis (TGA) and differential scanning calorimetry (DSC) were carried out on the membranes to determine the decomposition temperature, the glass transition temperature and specific heat capacity, as well as the ratio of inorganic components inside the membrane.

6.2.1 Thermal gravimetric analysis

Figure 6.4 presents the results of the TG analysis of the PPO membrane. Two curves shown in the TG spectrum represent the weight loss and the derivative of the percentage of the weight loss with respect to the temperature (DTG). It is evident from Figure 6.4 that the PPO membrane decomposes in a single step. The weight loss occurs between the temperatures of 400°C and 690°C; however, the DTG curve shows two major peaks around 436°C and 525°C. The average temperature, 480°C, is considered to be the decomposition temperature of PPO. The decomposition temperature of PPO is comparable to the value of 456°C reported by Karasz and Reilly (1965) and the value of 464°C reported by Tran (2004).

Figure 6.5 shows the thermogravimetric analysis results of the EPMM3 membrane. Unlike PPO, the sample shown in Figure 6.5 indicates some weight loss at temperatures well below the actual point of decomposition of the polymer. This first weight loss is 7.79% of the original weight of the membrane, which occurs between 100°C and 250°C, could be associated with the loss of water incorporated in the aluminum hydroxonitrate (Chakraborty, 2004), and the removal of the residual N-octanol. The second weight loss occurring between 354°C and 567°C is attributed to the actual decomposition of the polymer, and the corresponding highest DTG occurs at 495°C.

An improvement in the thermal stability of hybrid membranes was observed by many researchers (Kusakabe, 1998; Kim et al., 2004; Zhang et al., 2005). It is generally believed that the introduction of an inorganic component into the polymer improves their thermal stability of the membrane (Wen et al., 1996). The investigation of Kim et al. (2004) on the thermal behavior of the poly (vinylalchohol)/SiO_2 hybrid membrane demonstrates that the introduction of silica into the poly (vinylalchohol) chains enhances the thermal stability of this hybrid membrane. This is in agreement with the work of Zhang (2005), in which they showed that the brominated PPO/SiO_2 materials have much higher thermal stability than PPO. For PPO the initial decomposition temperature is 470°C at a heating rate of 10°C/min, which is the result of splitting of the main chains.

In the EPMM3 membrane, the residual weight after the polymer decomposition indicates the amount of inorganic components. At 700°C, the residual weight percentage for the EPMM3 was 2.12 wt% whereas the residual weight percentage for the PPO membrane was 0.45, which is attributed to PPO impurities. From the residual weight percentage of the EPMM3 membrane, we can conclude that the conversion with respect to SiO_2 is around 71.63% (Appendix C), and this means that 71.63% of the initial TEOS was incorporated into the PPO matrix and the rest of the TEOS was most likely removed during membrane soaking in boiling water.

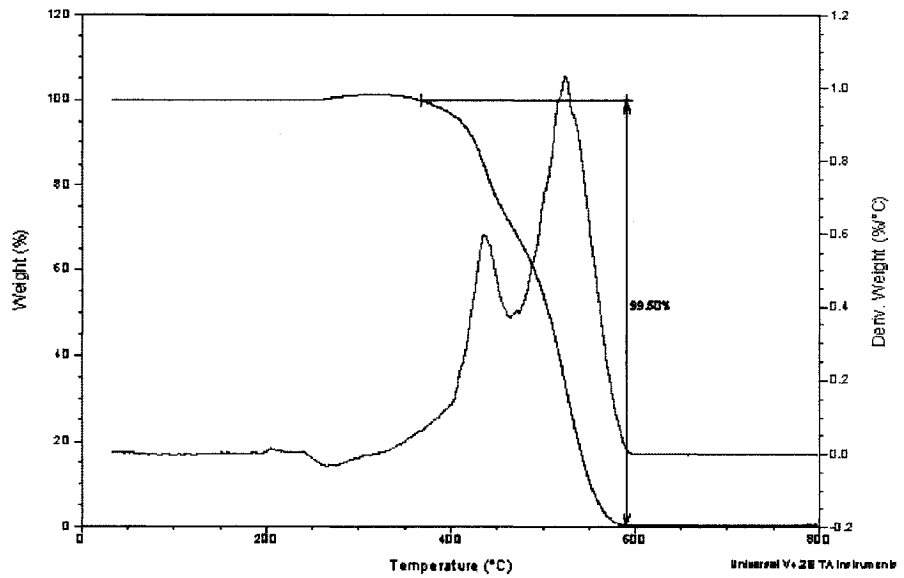

Figure 6.4 Thermal gravimetric analysis of PPO membrane.

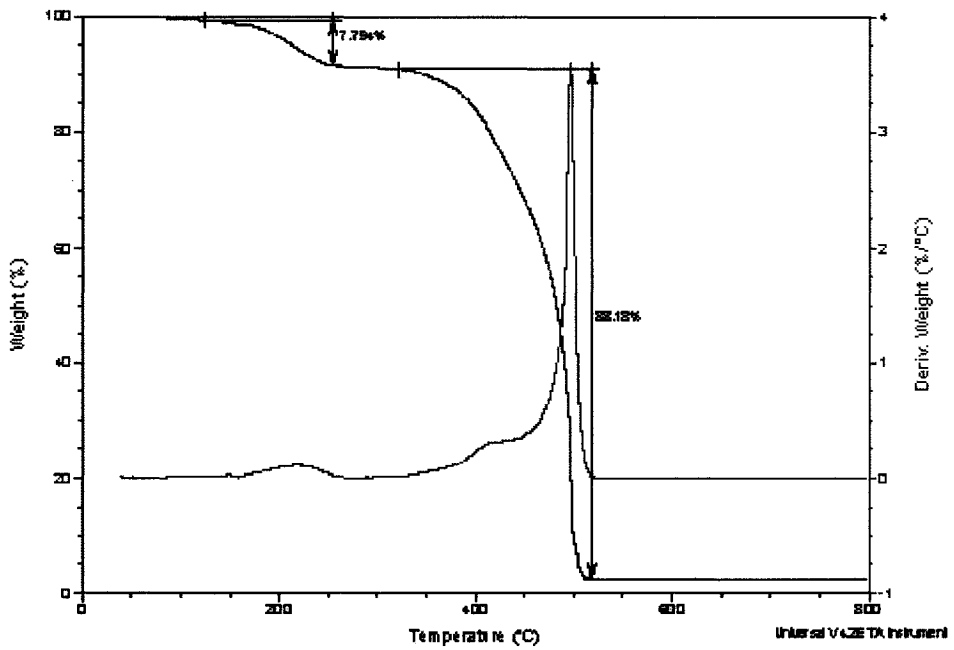

Figure 6.5 Thermal gravimetric analysis of EPMM3 membrane.

6.2.2 DSC (Differential scanning calorimetry) analysis

Differential scanning calorimetry of the PPO, EPMM1 membrane, EPMM2 and EPMM3 membranes was carried out using conventional DSC and modulated DSC. For convenience, the modulated DSC spectra of EPPM1, EPPM2, and EPMM3 are presented in Appendix B.

Figure 6.6 represents the conventional DSC spectrum of a PPO membrane. The sample was heated up to 250°C and was then cooled down to 50°C. This cycle was repeated two times to show the repeatability of the experiment. In the heating ramp, at low temperatures, it can be seen that the heat flow increases linearly with temperature. At approximately 214°C there is a drastic change in the slope of heat flow. The next step change in the heat flow rate was at 217°C. The glass transition temperature is generally considered to be the temperature in the middle of the range where a jump in the heat flow rate takes place (Hay 1969). In the cooling ramp, the first shift occurred at approximately 216°C and next one was at 208°C. Therefore, the T_g of the PPO membrane estimated based on the first heating ramp was 216°C, which is close to the T_g of 214°C obtained in the first cooling ramp. The data is quite repeatable as the second heating and cooling ramps indicate glass transition temperatures of 218°C and 214°C, respectively.

A glass transition temperature of 225°C for a powdered PPO with $\overline{M}_W$ =40,000 was observed by Karasz and Reily (1965), which is slightly higher than that obtained in this study. This difference between the glass transition temperatures could be due to the difference between the heating rates applied in this study (10°C/min) and that of the study performed by Karasz and Reily (40°C/min). Toi et al., (1982), and Aguilar and Paul (1983)

found glass transition temperatures of 212°C and 213°C, respectively, which are comparable to that obtained in this project.

Figure 6.7 represents the modulated DSC spectra of the PPO membrane. There are three spectra, which indicate modulated and reversible heat flows, and the reversible heat capacity. It is evident in Figure 6.7 that there is a dramatic shift in the three spectra around the glass transition temperature. According to the reversible heat flow spectrum of the PPO membrane, the T_g of this sample is around 216.5°C, which is consistent with the results obtained by the conventional DSC.

Figure 6.8 illustrates the conventional DSC spectrum of EPMM1 membrane. Unlike the PPO membrane, the first heating ramp shows some endothermic peaks. The first broad endothermic peak can be attributed to the decomposition of free water, while the second endothermic peak is likely be due to the decomposition of incorporated water in aluminum silicate, and the decomposition of sodium nitrate and the surfactant. As is shown in Figure 6.8, the heat flow pattern of the second heating ramp is similar to those of the first and second cooling ramps. The glass transition temperature obtained from the second heating ramp of 196°C which matches with the T_g values observed in the first and second cooling ramps. The modulated DSC of the EPMM1 membrane is demonstrated in Appendix B, Figure B.1. The glass transition temperature, 200°C, obtained from the modulated DSC is slightly higher than the T_g value observed in the convectional DSC.

Figure 6.9 illustrates the conventional DSC spectra of the EPMM2 membrane, the sample was heated up to 250°C with a heating rate of 10°C/min. It was then cooled down to 50°C with a cooling rate of 10°C/min. In order to show the consistency of the result, the heating ramp and cooling ramp were repeated two times. The heat flow pattern observed in

the first heating ramp is different than that of the second heating ramp. The first heating ramp shows a lower T_g value in comparison with T_g value of second heating ramp. This can be due to the presence of residual solvent in the membrane (Kesting and Fritzche, 1993). This residual solvent consists of the water trapped in the inorganic structure, and the residual N-octanol used in fabricating the membrane. The glass transition temperature of 204°C obtained from the second heating ramp is comparable with T_g values observed in the first and second cooling ramps. The modulated DSC spectra of the EPMM2 membrane shown in Appendix B, Figure B.2, illustrate that reversible heat flow and modulated heat flow have a significant shift around the glass transition temperature. The glass transition temperature estimated from the reversible heat flow is around 196°C, which is slightly lower than that obtained from the conventional DSC.

Figure 6.10 represents the conventional DSC spectra of the EPMM3. The first run of conventional DSC shows some endothermic peaks, which most likely result from the evaporation of water, N-octanol and the decomposition of nitrates, and could contribute to the 7.79% weight loss observed in the TGA spectrum of this polymer in Figure 6.5. The first heating ramp presents a lower T_g which will confirm the presence of residual solvent. On the other hand, unlike unmodified PPO, the T_g of the EPMM3 membrane observed in the second heating ramp of 182.5°C is similar to the T_g values observed in the first and second cooling ramps. The modulated DSC spectra of the EPMM3 membrane are shown in Appendix B, Figure B.3. The glass transition temperature of the membrane calculated from reversible heat flow rate is 182°C and is in agreement with the value of 183°C glass transition temperature obtained from the conventional DSC.

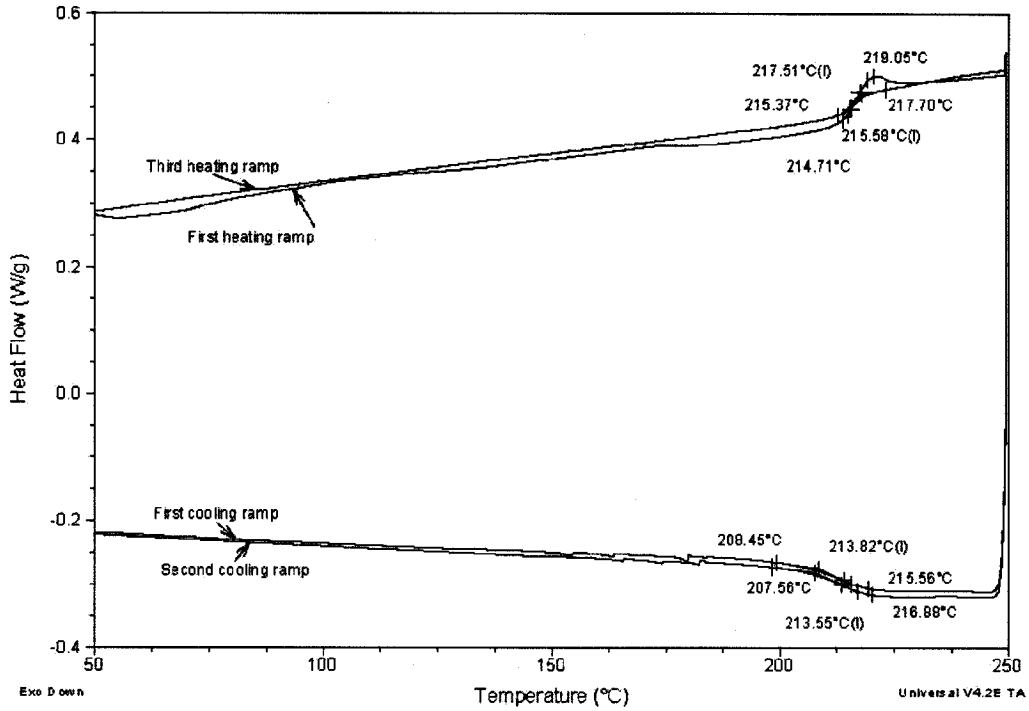

Figure 6.6 Conventional DSC analysis of PPO membrane.

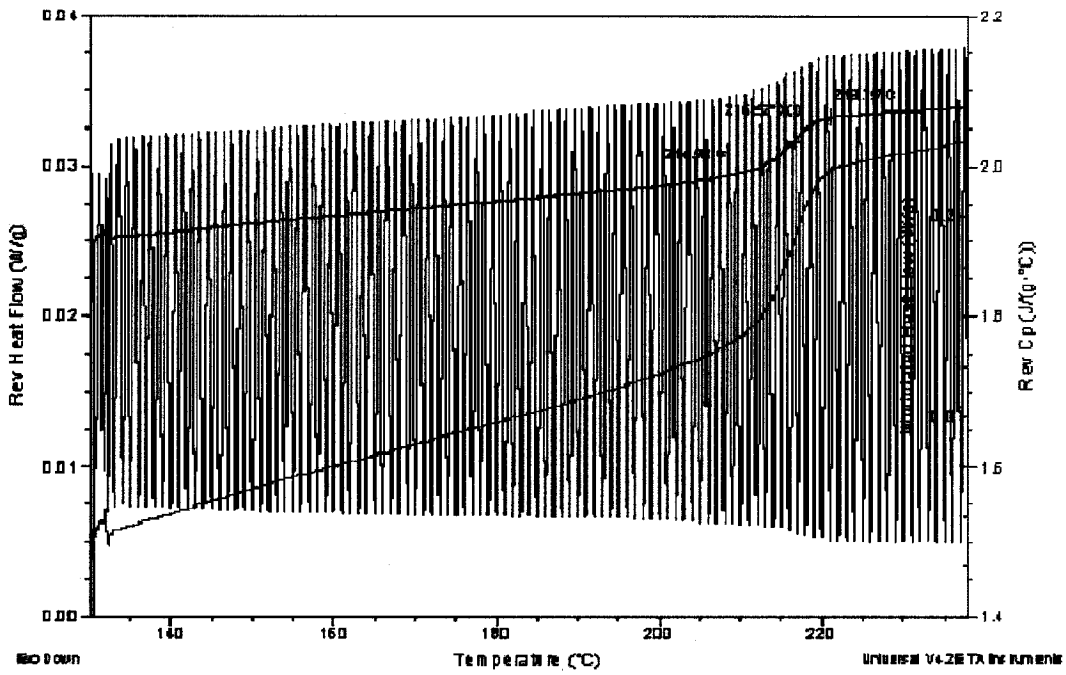

Figure 6.7 Modulated DSC analysis of the PPO membrane.

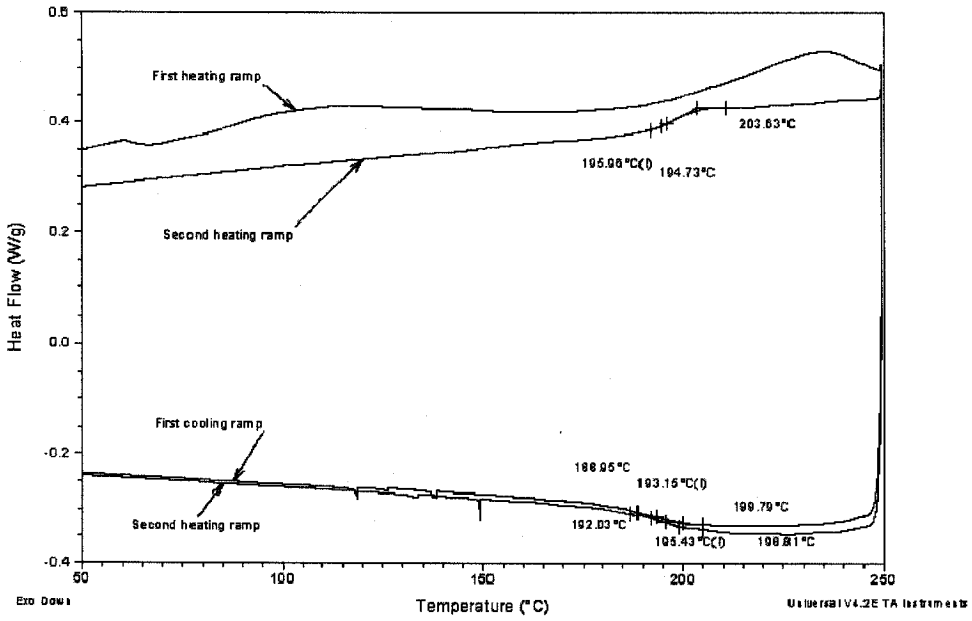

Figure 6.8 Conventional DSC analysis of EPMM1 membrane.

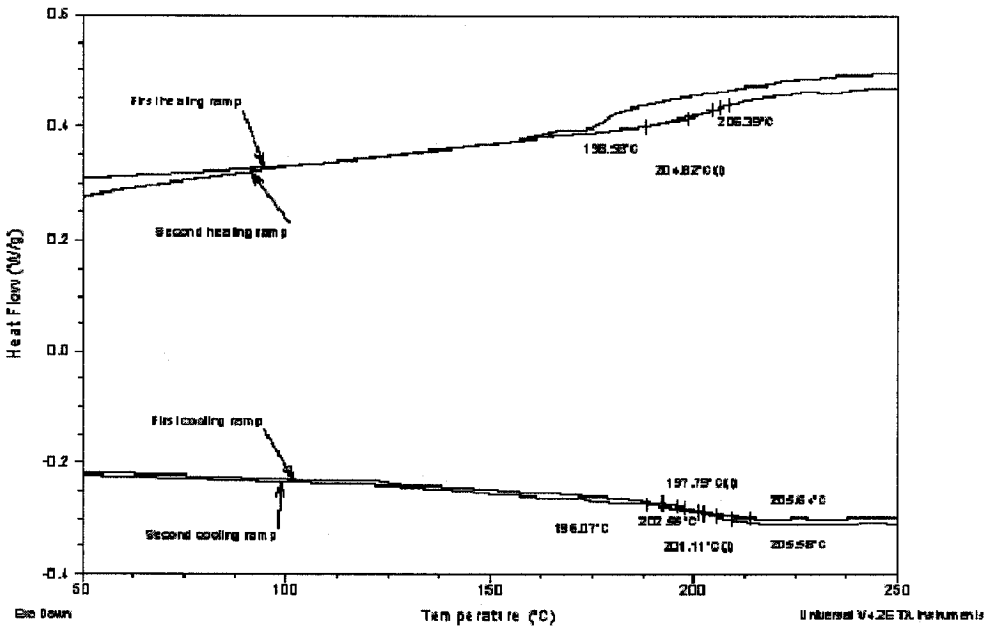

Figure 6.9 Conventional DSC analysis of EPMM2 membrane.

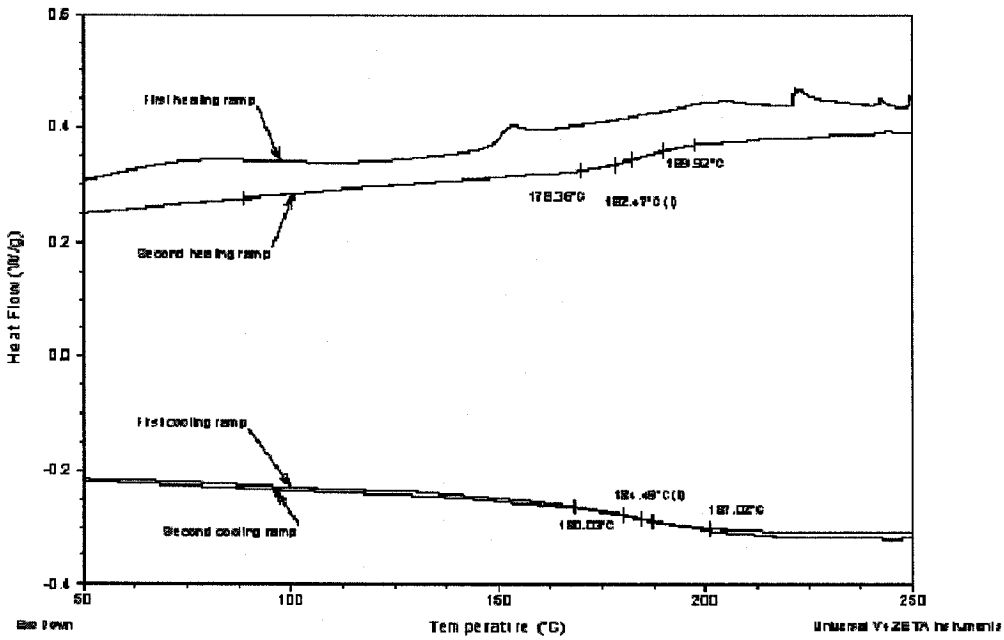

Figure 6.10 Conventional DSC analysis of the EPMM3 membrane.

In order to facilitate a comparison between the T_g of PPO and those of the EPMM2 and EPMM3 membranes, the second heat ramp of the convectional DSC spectra of the membranes was plotted on the same Figure. As is shown in Figure 6.11, the glass transition temperature of the PPO-based mixed-matrix membranes is reduced with an increase in the TEOS loading. This is an evidence of the reduction in rigidity of the polymer chain. The DSC analysis of the PVA-based hybrid membranes was shown to increase with TEOS content. This leads to an increase in the glass transition temperature of the resulting membrane (Srikant et al., 2004).

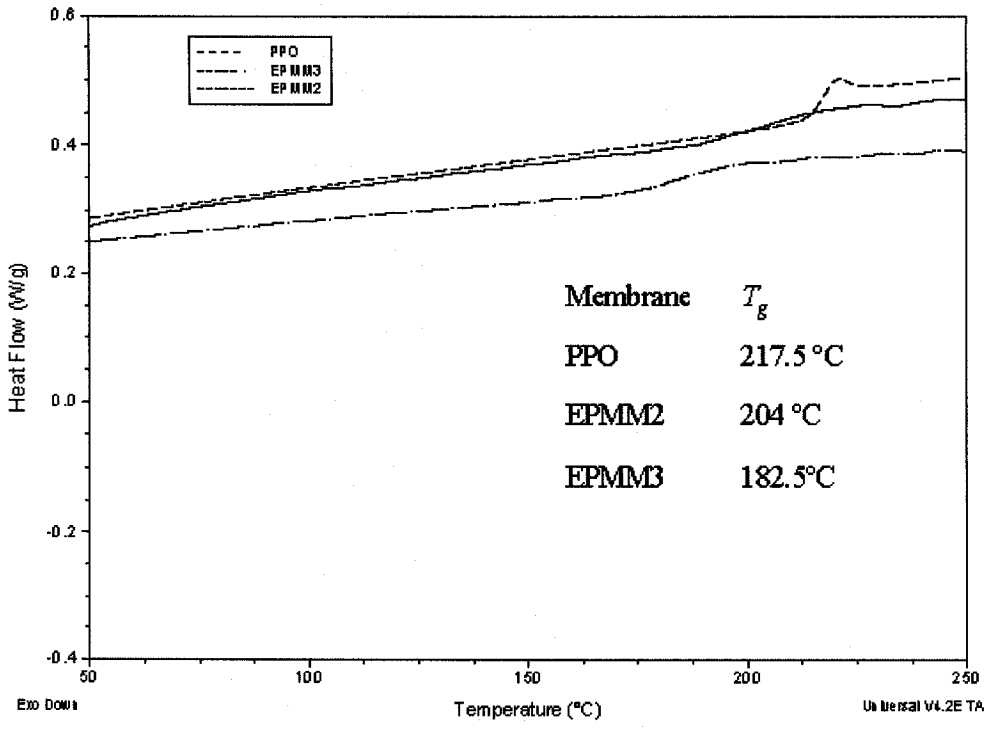

Figure 6.11 The second heat ramps of PPO and the EPMM membranes.

6.2.3 The change in specific heat capacity of the membranes during the glass transition temperature

Specific heat capacity jump, ΔC_P, at the glass transition temperature, T_g, of the PPO membrane, EPMM1 membrane, and EPMM2 and EPMM3 was measured. In order to calculate the specific heat capacity jump at glass transition temperature, the reversible specific heat capacity gradient of each given membrane vs. temperature was plotted.

Figure 6.12 exhibits the reversible specific heat capacity gradient of the PPO membrane. At temperatures below the glass transition temperature, the reversible specific heat capacity gradient (dC_P/dT) is constant, while at a temperature around the glass transition temperature, dC_P/dT changes drastically. A discontinuity in the reversible

specific heat capacity spectrum of PPO was observed at around the T_g. A ΔC_p of $0.26\,J/g°C$ was obtained for this PPO membrane, which is close to the value of $0.238\ J/g^\circ C$ reported by (Wrasidlo, 1974). However, a ΔC_p of $0.162\,J/g\,K$ for a powdered PPO of $\overline{M}_W = 40,000$ was observed by Karasz and O'Reily (1965).

The reversible specific heat capacity gradient of the EPMM1 membrane is illustrated in Figure 6.13. Unlike the PPO membrane, the graph shows a broad peak around the glass transition temperature, which means that the increase in the specific heat capacity of EPMM1 membrane at T_g is lower than that of PPO membrane. A ΔC_p of $0.15\,J/g°C$ at T_g was observed for this membrane.

Figure 6.14 and 6.15 represent the reversible specific heat capacity gradient of the EPMM2 and EPMM3 membranes, respectively. Like the EPMM1 membrane, dC_p/dT of the EPMM2 membrane shows a broad peak around the glass transition temperature, while it is nearly constant at temperatures below and above the glass transition temperature. A specific heat capacity jump of $0.177\,J/g°C$ was observed for this membrane. As is seen in the Figure 6.15, the dC_p/dT of the EPMM3 membrane does not follow the patterns of the EPMM1 and EPMM2 membranes. The inability to measure the specific heat capacity jump at T_g for this membrane is due to the presence of more than one dominant peak around the glass transition temperature.

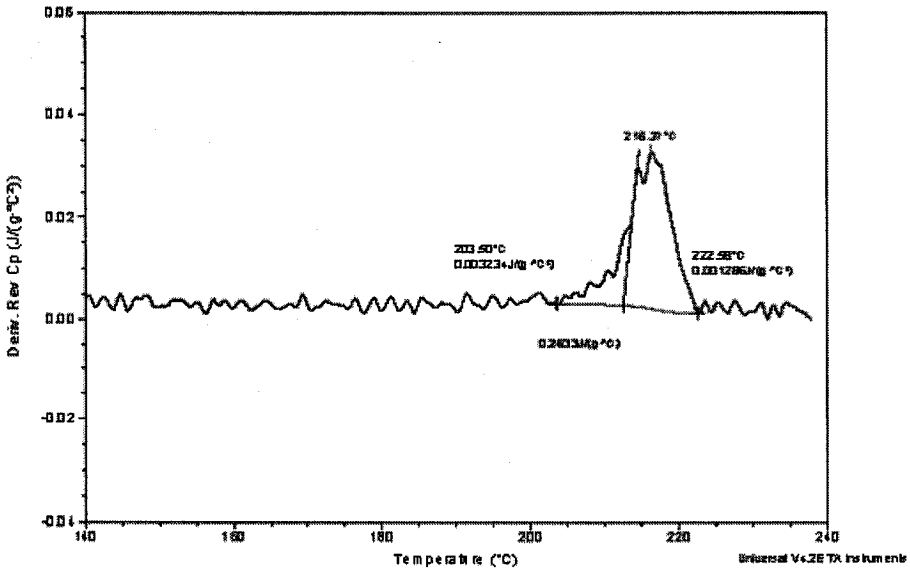

Figure 6.12 The reversible specific heat capacity gradient of PPO membrane.

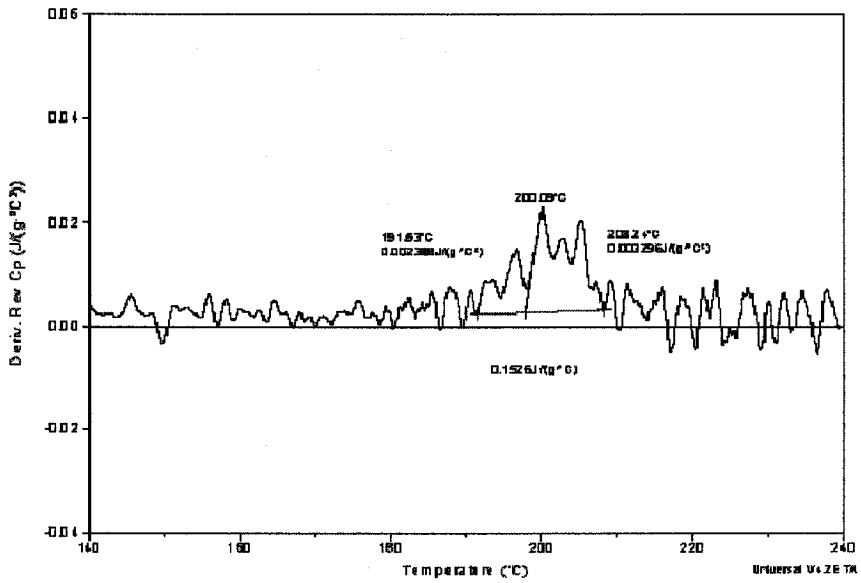

Figure 6.13 The reversible specific heat capacity gradient of the EPMM1 membrane.

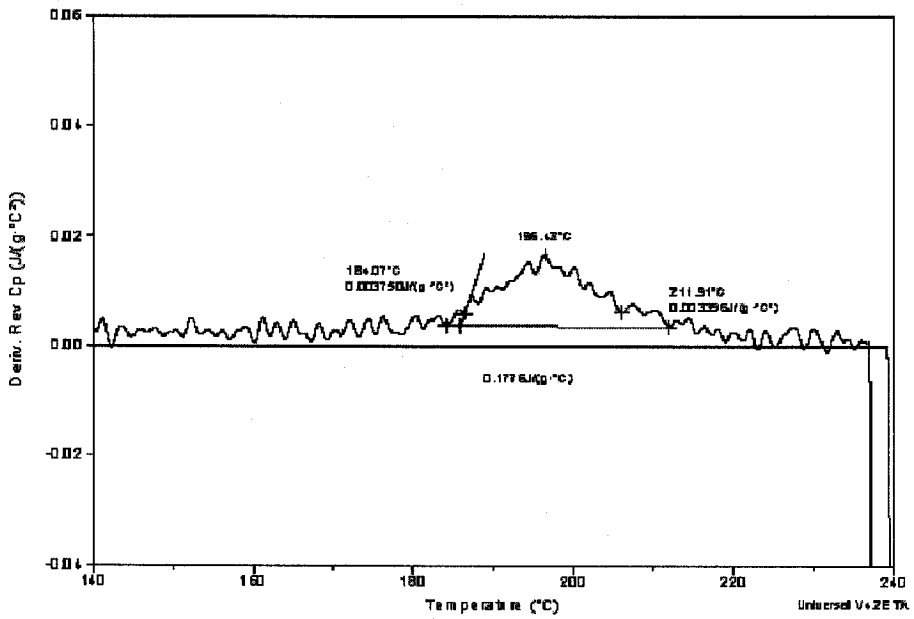

Figure 6.14 The reversible specific heat capacity gradient of the EPMM2 membrane.

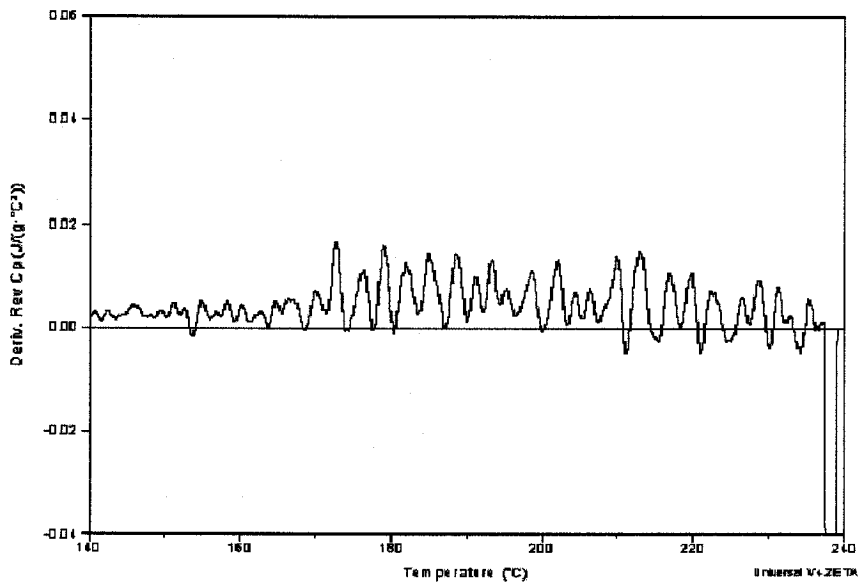

Figure 6.15 The reversible specific heat capacity gradient of EPMM3 membrane.

6.2.4 Correlation between the specific heat capacity jump and fractional free volume

The fractional free volume of a membrane is usually determined by Bondi's group contribution method or density measurements. In this research, a new approach to calculate the fractional free volume of membranes was established based on measurements of the specific heat capacity jump of a membrane at the glass transition temperature. This was obtained by combining Wunderlich's (1960) and Hirai and Eyring (1958) equations to obtain equation (6-4) that relates the specific heat capacity jump at the glass transition temperature and the fractional free volume of the polymer material.

A mathematical correlation was proposed by Wunderlich (1960) in order to estimate the specific heat capacity jump, ΔC_p, at the glass transition temperature.

$$\Delta C_p = \frac{E_g}{T_g}\left(\frac{\varepsilon_h}{RT_g}\right)e^{-\varepsilon_h/RT_g} \tag{6-1}$$

Where E_g is internal latent heat of vaporization at the glass transition per mole of molecules (or mole of repeat units), ε_h is the energy of free volume microcavity formation, T_g glass transition temperature, R is universal gas constant.

In the derivation of equation (6-1), the theoretical basis of the hole theory in liquids was used as well as the formulations developed by Hirai and Eyring (1958) in their "Theory of Bulk Viscosity". Hirai and Eyring described the equilibrium between holes and phonons associated to the liquid lattice. Each hole was characterized by its molar volume and energy of free volume formation. Hirai and Eyring in the "Theory of Bulk Viscosity" came up to the following equation:

$$\frac{N_h}{N_0} = \frac{\upsilon_0}{\upsilon_h}e^{-(\varepsilon_h + p\upsilon_h)/RT} \tag{6-2}$$

Where R is the universal gas constant; υ_h is the molar free volume; υ_0 is the molar volume occupied by macromolecules; N_0 is the number of moles of molecules, p is pressure. T is absolute temperature.

At ordinary pressure $p\upsilon_h/RT$ term is negligible. Therefore, the equation (6-2) is simplified as

$$\frac{N_h}{N_0} = \frac{\upsilon_0}{\upsilon_h} e^{-\varepsilon_h/RT} \tag{6-3}$$

A mathematical correlation between specific heat capacity jump and fractional free volume is obtained by combing equation (6-1) and equation (6-3)

$$\Delta C_p = \frac{E_g}{T_g} \times \ln\left(\frac{1-f_g}{f_g}\right) \times \left(\frac{f_g}{1-f_g}\right) \tag{6-4}$$

where f_g is fractional free volume at glass transition temperature.

Therefore, the fractional free volume at glass transition temperature can be calculated basing the specific heat capacity jump at glass transition temperature. By using the calculated fractional free volume at T_g, molar hole energy, ε_h, is obtained according to the following equation

$$\varepsilon_h = -RT_g\left(\ln\left(\frac{f_g}{1-f_g}\right)\right) \tag{6-5}$$

In general, when a polymer reaches its fractional free volume at glass transition temperature, it can be considered a glass, and one expects that the fractional free volume stays constant with lowering temperature. However, the fractional free volume still falls over an extended period of time due to aging phenomena (kesting and Fritzche, 1993). In this study, a fractional free volume of 0.201 was obtained for PPO membrane at glass transition

temperature, which agrees with the value of 0.1988 reported by Aguilar Vega and Paul (1993). They calculated the fractional free volume based on the group contribution method developed by Bondi. A fractional free volume of 0.186 was also reported for a PPO with T_g of 210 °C, which is estimated from group contribution method. Tables 6-3 and 6-4 show the fractional free volumes estimated from specific heat capacity jump at glass transition temperature, along with fractional free volume obtained from other method for poly (phenyl oxide), poly (2,6-dimethyl-1,4-phenylene oxide) and poly (2,6-diphenyl-1,4-phenylene oxide).

Table 6-3 The fractional free volume at the glass transition temperature for PPO as calculated using Equation (6-4)

Polymers	T_g (°C)	Fractional free volume at T_g (f_g)
Poly (phenyl oxide)	90	0.1327
Poly (2,6-dimethyl-1,4-phenylene oxide)	216	0.201
Poly (2,6-diphenyl-1,4-phenylene oxide).	220	0.1221

Table 6-4 The fractional free volume for PPO as calculated using group contribution method

Reference: Aguilar-Vega and Paul (1993)	T_g (°C)	Fractional free volume (f)
Poly (phenyl oxide)	90	0.1562
Poly (2,6-dimethyl-1,4-phenylene oxide)	213	0.1988
Poly (2,6-diphenyl-1,4-phenylene oxide).	229	0.1882
Reference: Ghosal and Freeman (1993)	T_g (°C)	Fractional free volume (f)
Poly (2,6-dimethyl-1,4-phenylene oxide)	210	0.186

Quantities of f_g, T_g, ε_h/RT_g, and ε_h for the membranes are tabulated in Table 6-5. As is seen, the fractional free volume at the glass transition temperature for the EPMM1 and EPMM2 membranes is lower than that of PPO membranes.

Table 6-5 The quantities of f_g, T_g, ε_h/RT_g, and ε_h for the membranes.

Samples	T_g(K)	f_g	ε_h/RT_g	ε(cal/mol)
PPO membrane	489.15	0.201	1.8733	5218.897
EPMM2 membrane	496.55	0.100	2.186	8534.697
EPMM1 membrane	474.05	0.073	2.536	9997.551

6.3 Morphological study of the membranes

The control of morphology and phase separation is very critical factor in order to achieve highly homogeneous organic and inorganic materials. Therefore, scanning electron microscopy and energy dispersive X-ray analysis were conducted to investigate the distribution of aluminum silicate and atom composition on the surface and cross section of the EPMM3 membrane.

Figure 6.16 demonstrates the surface morphology of the EPMM3 membrane. As a comparison, the SEM result of the unmodified PPO is shown in Figure 6.17. A comparison of the SEM image of the EPMM3 membrane and that of PPO membrane shows that a few aluminum silicate particles could be found to disperse in the polymer matrix, although they are not very clear.

The SEM images taken of cross section of the EPMM3 membrane are shown in the Figures 6.18 and 6.19. Figure 6.18 shows a SEM image with low magnification, 250, showing the inorganic particles that were observed. In Figure 6.19 the SEM image of

aluminum silicate with high magnification, 2500, shows size of aluminum silicate particles through the EPMM3 membrane cross section.

Some researchers have tried to enhance the connectivity between the inorganic network and organic phase by the use of compatibilizers, which diffuse to the interface between the two immiscible phases and reduce interfacial tension. Others have polymerized metal alkoxides in organic polymer matrices. In the latter, polymers with an appropriate backbone structure should be chosen so that they can induce physical or chemical interactions with the growing metal alkoxide network. For example, Zhang et al. (2005) showed that one route for forming covalent bonding between PPO and 3-aminopropyl-trimethoxysilane is to functionalize PPO with trialkoxysilyl groups before polymerization of 3-aminopropyl-trimethoxysilane in PPO solution. This method of synthesis of PPO-inorganic hybrid materials requires a preliminary step in which the bromination of PPO is involved. Their SEM results showed a uniform distribution of silica in PPO structure at low inorganic loading, while the SEM results obtained from the present study show that the compatibility of the PPO and inorganic can be obtained by using compatibilizers such as N-octanol.

The energy dispersive X-ray analysis was also conducted to investigate the atom composition on the surface and the cross section of the EPMM3 membrane. Although in Figure 6.16, energy dispersive X-ray spectrum of the EPMM3 membrane surface indicates a strong peak for carbon, the aluminum and silica peaks are observed as well. An Al/Si intensity ratio of 0.257 was obtained from the EDX spectrum of the EPPM3 membrane.
The energy dispersive X-ray spectra of the cross section of the EPMM3 membrane are shown in Figures 6.18 and 6.19. The EDX mapping results represent that the intensity ratio of Al/Si is ranging between 0.208 and 0.54.

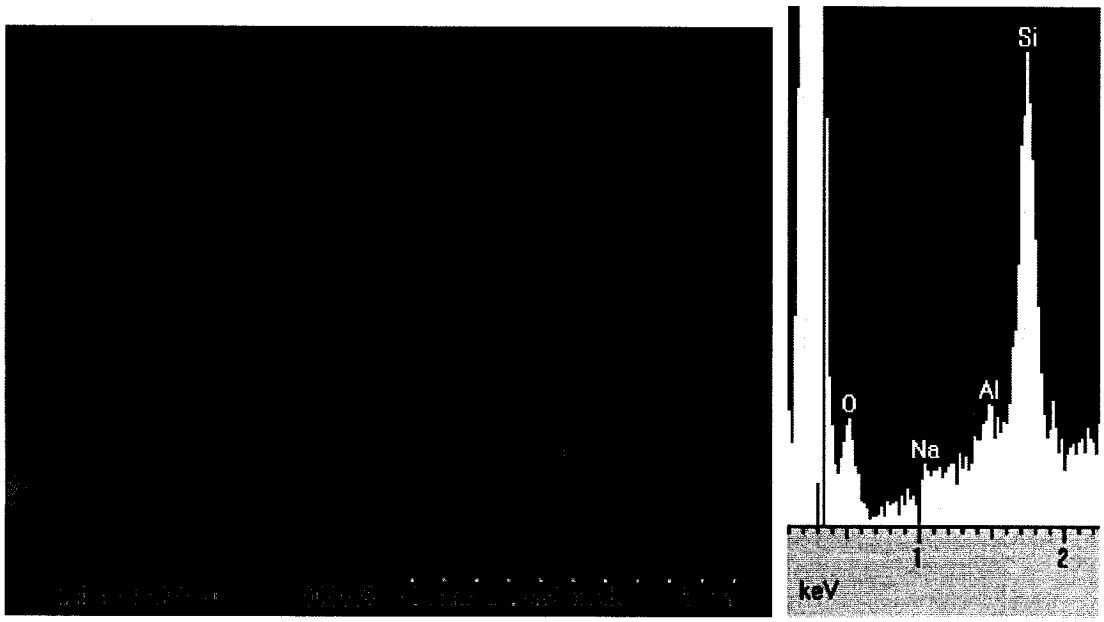

(a) **(b)**

Figure 6.16 SEM image and EDX spectrum of the surface of EPPM3 membrane: (a) SEM image; (b) EDX spectrum of the surface.

Figure 6.17 SEM image of the surface of the PPO membrane surface.

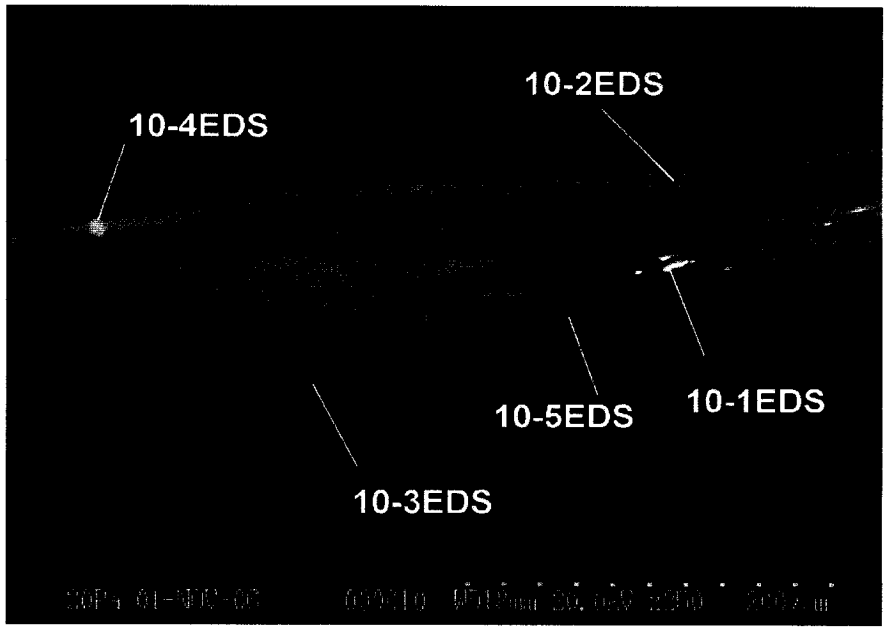

(a)

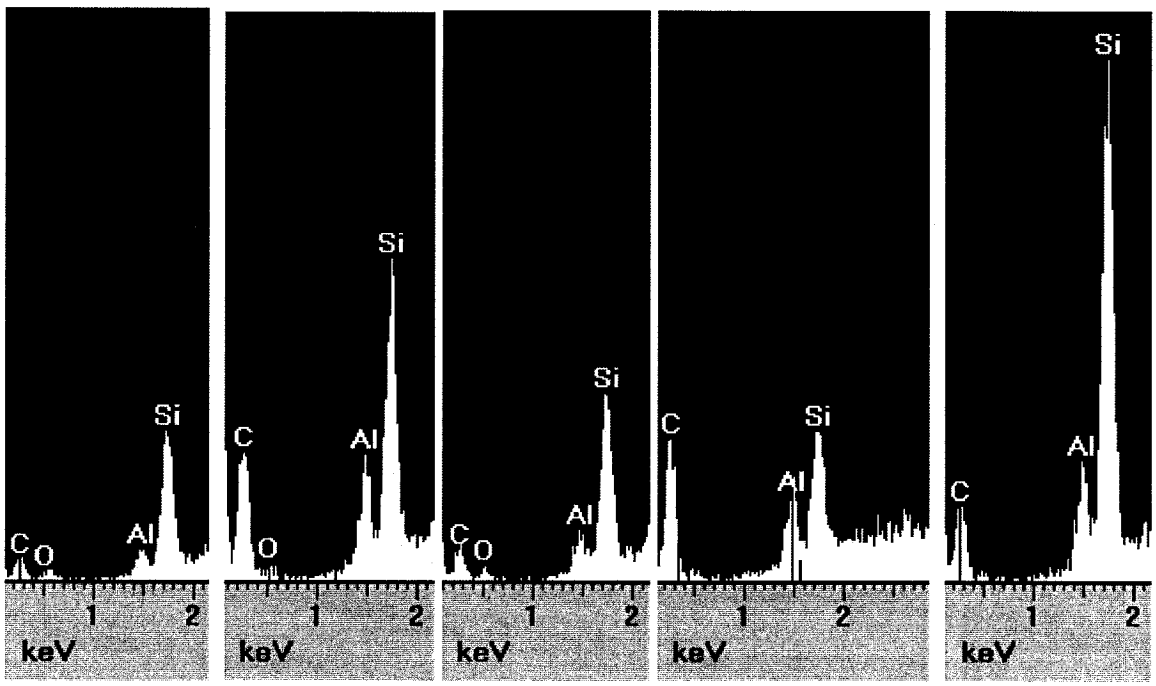

(b) 10-1EDS 10-2EDS 10-3EDS 10-4EDS 10-5EDS

Figure 6.18 SEM image and EDX spectrum of the EPMM3 membrane cross section (a) SEM

Image with magnification 250 (b) EDX spectra of the 10-1EDS, 10-2EDS, 10-3EDS, 10-4EDS, 10-5EDS particles.

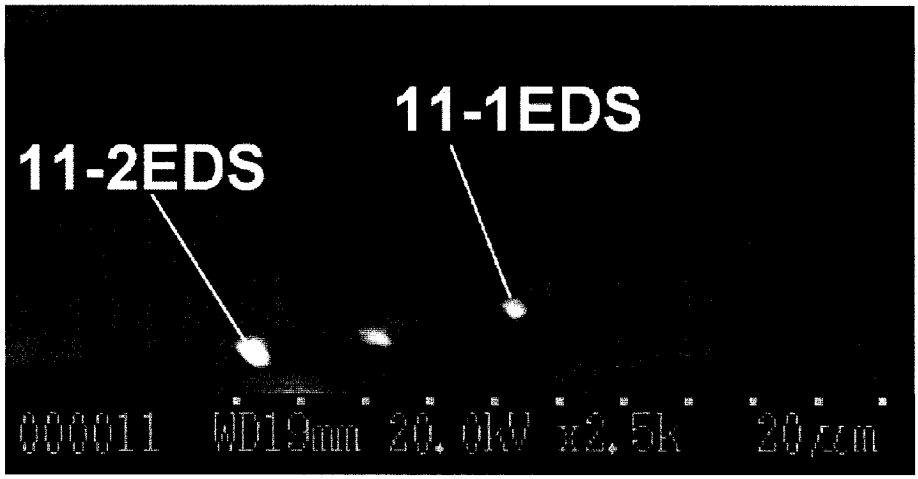

(a)

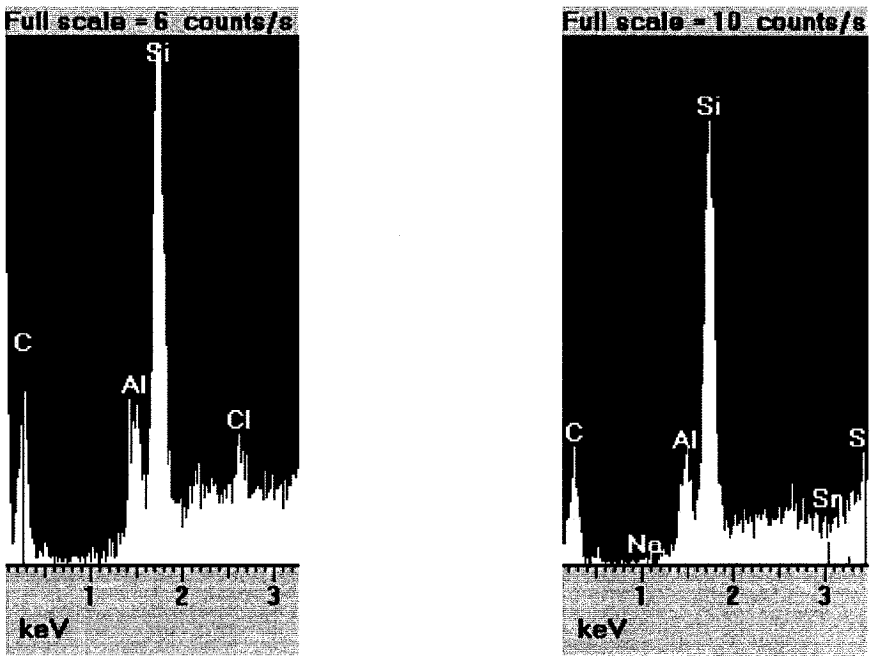

(b) 11-1EDS EDX 11-2EDS

Figure 6.19 SEM image and EDX spectrum of the EPPM3 membrane cross section: (a) SEM image with magnification 2500; (b) EDX spectrum of the 11-1EDS and 11-2EDS particles.

6.4 Gas Transport Properties

The gas permeation measurements were performed using a constant pressure system equipped with a gas chromatography unit. The gas transport properties of all the membranes were determined in both gas mixtures and single gas permeation tests. A complete experiment for a given membrane consisted of tests with air as a gas mixture and oxygen and nitrogen as single gases.

6.4.1 Single gas permeation

The oxygen and nitrogen permeabilities through the PPO, multi-layered and EPMM membranes were measured using a constant pressure system equipped with a gas chromatography unit. The method to determine the gas permeability was described in section 4.3.6

A summary of the gas permeation properties of PPO, the multi-layered membrane and the EPMM membranes along with other literature data is presented in Table 6-6 for the purpose of comparison. The average and standard deviation values for the permeabilities and selectivity of each membrane were determined from each membrane. The standard deviations of the permeabilities values are higher than those of the permeability ratio. This can be due to the fact that the variation in membrane permeability is attributed to errors associated with the determination of the thickness of the membrane and the flow rate measurement, whereas the deviation in the membrane selectivity is ascribed to an error only related to measurement of the flow rate.

Table 6-6 Summary of gas permeation properties of the PPO, the multi-layered and EPMM membranes along those of PPO membranes in the literature data

Membrane	PPO Intrinsic viscosity [η] dL/g	Permeability O_2		Permeability N_2		Permeability ratio O_2/N_2	
		(Barrer)	St.Dev	(Barrer)	St.Dev		St.Dev
Reference: Savis (2004)							
PPO	1.58	10.05	0.74	2.98	0.42	4.22	
Reference: K.TOI and G.MOREL							
PPO	Data not available	Data not available		3.81	Data not available	Data not available	
Reference: Baker (2004)							
PPO	Data not available	16.8	Data not available	3.8	Data not available	4.4	Data not available
Reference: Chowdhury (2001)							
PPO	1.79	16.71	Data not available	3.52	Data not available	4.76	Data not available
Present work							
PPO (P=120psi)							
Coupon 1		17.42	1.58	3.79	0.36	4.59	0.12
Coupon 2		18.5	1.68	4.1	0.39	4.51	0.13
multi-layered(P=120psi)							
Coupon 1		10.68	0.58	2.21	0.12	4.83	0.09
Coupon 2		11.34	0.61	2.305	0.13	4.92	0.09
EPMM2 (P=120psi)							
Coupon 1		15.87	0.978	3.62	0.23	4.38	0.05
Coupon 2		15.40	0.94	3.26	0.19	4.72	0.07
EPMM3(P=120psi)							
Coupon 1		15.38	0.754	3.13	0.18	4.91	0.18
Coupon 2		16.10	0.90	3.45	0.23	4.67	0.16
PPO (P=90psi)							
Coupon 1		17.53	1.56	3.48	0.33	5.04	0.05
Coupon 2		18.25	1.70	4.082	0.43	4.47	0.05
multi-layered(P=90psi)							
Coupon 1		11.10	0.61	2.27	0.14	4.90	0.17
Coupon 2		10.48	0.57	2.01	0.13	5.2	0.18
EPMM2(P=90psi)							
Coupon 1		15.60	0.99	3.35	0.23	4.66	0.11
Coupon 2		15.24	0.90	2.82	0.21	5.41	0.13
EPMM3(P=90psi)							
Coupon 1		15.13	0.81	3.03	0.17	4.99	0.18
Coupon 2		15.73	1.13	3.15	0.17	4.99	0.19
PPO (P=60psi)							
Coupon 1		16.25	1.51	3.11	0.33	5.23	0.25
Coupon 2		17.90	1.62	3.72	0.36	4.81	0.22
multi-layered (P=60psi)							
Coupon 1		12.01	0.64	2.26	0.19	5.31	0.37
Coupon 2		11.21	0.6	2.00	0.17	5.61	0.36
EPMM2(P=60psi)							
Coupon 1		15.42	1.05	2.91	0.41	5.3	0.29
Coupon 2		14.87	0.89	3.05	0.35	4.88	0.18
EPMM3(P=60psi)							
Coupon 1		14.02	0.75	2.50	0.17	5.61	0.31
Coupon 2		15.12	0.91	2.77	0.21	5.45	0.29

Generally, ideal selectivity and permeability allow a useful comparison of different materials, so that one can focus on the intrinsic properties of the gases and polymers. Permeability is composed of two terms, solubility coefficient, S, and diffusion coefficient, D. Consequently, Ideal selectivity can be expressed as a product of solubility mobility selectivity, $[S_A]/[S_B]$, and diffusive mobility selectivity, $[D_A]/[D_B]$, When a polymer, such as PPO, does not have polar groups that especially attract one of the components, the solubility selectivity is largely determined by the relative condensability of two components. Condensability of the components are reflected by their critical temperatures. Here, oxygen has higher critical temperature (154 K) than nitrogen (126 K). Therefore, this makes oxygen more condensable and more soluble in the PPO than nitrogen. A typical solubility selectivity of 1.275 for this pair in the PPO at ambient temperature was reported by Aguilar and Paul (1993). Clearly, this solubility selectivity is not sufficient to produce a high separation factor for this gas pair, hence, favorable mobility selectivity is required to achieve a reasonable separation factor. The mobility selectivity of this gas pair is customized by controlling the diffusion coefficient of oxygen relative to nitrogen. In the main, determination of the mobility selectivity requires consideration of the molecular sieving dimensions of two gases to be separated. The kinematic dimensions of the oxygen and nitrogen are 3.46 Å and 3.64 Å, respectively. The diffusion coefficient can be written in terms of the average jump length and average jumping frequency. For these penetrants having a similar size, the jump length is considered to be similar, so the jumping frequency of oxygen relative to nitrogen in the polymer determines the mobility selectivity of these gases. Therefore, segmental mobility of the PPO has a key role in the separation of this gas pair. Lack of polar groups in the PPO structure results in a weaker inter-chain interaction and a higher degree of chain mobility and

flexibility, however, it is still able to produce sufficiently sensitive size selective gaps to modify jumping frequency of oxygen over nitrogen. These gaps or empty spaces form free volume of the polymer. Based on literature data, the free volume of polyphenylene oxides contains a continuous interconnected three-dimensional network of intermolecular microcavities. These microcavities are similar to a "throat and cavity" type, where a cavity may have several throats. The effective diameter of these throats is 0.4 nm at 77 K and 0.45 nm at 293 K (Ilinitch et al., 1999). Therefore, the gas transport in PPO membranes occurs through these microcavities. PPO shows a mobility selectivity of oxygen over nitrogen of 3.22 at the ambient temperature (Aguilar and Paul, 1993). Consequently an ideal selectivity of 4.1 will be expected for PPO. As is shown in the Table 6-6, there is a wide range of permeability and selectivity values reported for poly (2, 6-dimethyl-1, 4-phenylene oxide).This could be due to the fact the membranes were tested under different conditions that are not reported by authors. In this study, an oxygen/nitrogen ideal selectivity of 4.54 and oxygen permeability of 18 (at P=120 psi) were observed for PPO.

The following sections are concerned with the gas transport properties of the multi-layered PPO and the EPMM membranes.

6.4.1.1 Multi-layered membranes

To predict the properties of the layer of the multi-layered membrane, which contains inorganic particles, we applied a resistance model approach (Henis and Tripodi, 1981).

$$\left(\frac{P}{l}\right)_i = \left(\frac{l_1}{P_{1,i}} + \frac{l_2}{P_{2,i}}\right)^{-1} \tag{6-6}$$

Where $P_{1,i}$ and $P_{2,i}$ are the permeability of first layer and second layer respectively, l_1 and l_2 are the thickness of the first layer and second layer, respectively.

Table 6-7 shows the gas transport properties of the top layer, which was made of PPO material. This top layer has an effective separation thickness of approximately 5 μm. These values were taken from a PPO membrane which was made at the same condition and concentration as the top layer in the multilayered membrane.

Table 6-7 Summary of gas transport properties of the top (second) layer

Pressure	Permeability O_2 (Barrer)	Permeability N_2 (Barrer)	Permeability ratio O_2/N_2
P=120 psi	16.872	3.472	4.86
P=90 psi	16.25	3.176.	5.12
P=60 psi	15.912	2.775	5.73

The gas transport properties of the bottom layer obtained from the resistance model were tabulated in Table 6-8

Table 6-8 Summary of the gas transport properties of the bottom layer

Pressure	Permeability O_2 (Barrer)	Permeability N_2 (Barrer)	Permeability ratio O_2/N_2
P=120 psi	9.931	2.037	4.87
P=90 psi	9.765	1.942.	5.03
P=60 psi	10.706	1.986	5.39

The results indicate that the gas transport properties of the bottom layer are close to those of the top layer. In fact, the presence of the inorganic material in the bottom layer does not affect the gas transport properties of the multi-layered membrane in the single gas permeation test. However, this multi-layered membrane gave a different separation factor from the PPO membrane as seen in section 6.4.2.1 below.

6.4.1.2 EPMM1 membrane

The EPMM1 membranes do not have selectivity for oxygen over nitrogen. No successful membranes of this type could be produced. This result can be due to the intrinsic properties of the inorganic material formed in the EPMM1 membrane or its effect on the PPO chains. In the first case, the inorganic material formed through the condensation polymerization of TEOS at high pH had an intrinsically macro porous structure which is not applicable for gas separation. In the latter, as was observed in the XRD analysis section, the major d-spacing of the PPO chains in the EPMM1 membrane enlarges to 6.65Å. This can cause a drastic decrease in selectivity for this gas pair as both molecules have similar sizes. Moreover, the microscopic picture of the EPMM1 membrane which is shown in Figure 6.20 illustrates the aggregation of the inorganic particles leading to phase separation.

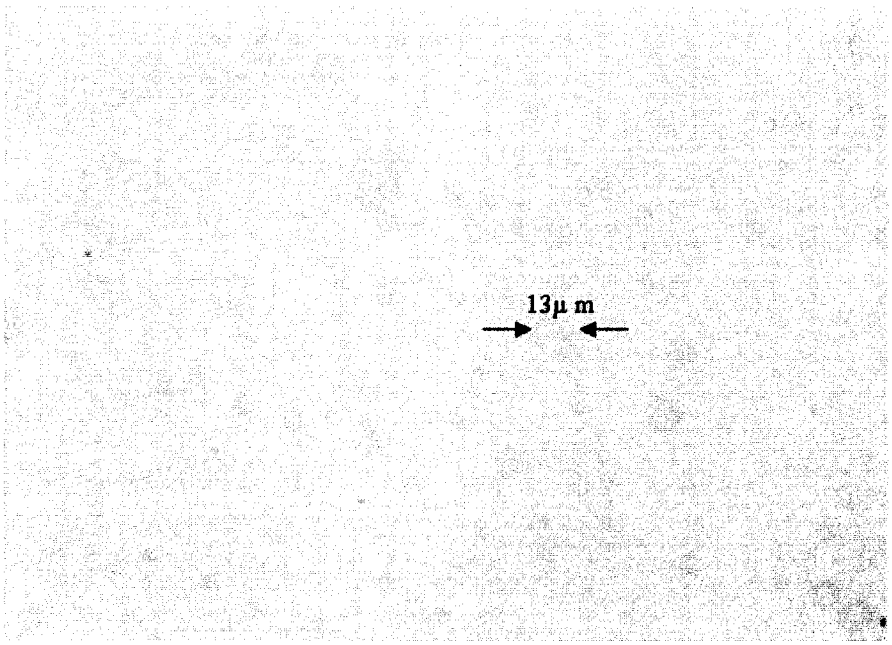

Figure 6.20 The microscopic image of the EPMM1 membrane with a magnification of 200.

6.4.1.3The effect of TEOS loading on the gas permeation properties of EPMM2 and EPMM3 membranes

As seen in Table 6-6, the oxygen permeability of the EPMM2 and EPMM3 membranes significantly decreased for all pressures in comparison with that of the unmodified PPO. An increase in TEOS loading up 5% (PPO vs. EPMM2) results in a decrease in oxygen permeability by approximately 12%. On the other hand, the increase in the TEOS loading from 5 % to 10 % (EPMM2 vs. EPMM3) does not have a great impact on the oxygen permeability, especially at high pressures, so that a slight decrease in the oxygen permeability was observed for the EPMM3.

The nitrogen permeability data presented in Table 6-6 follows the same pattern, which was observed for oxygen permeability data. A reduction of approximately 13% is observed in the nitrogen permeability data at all pressures, when the TEOS loading reaches up to 5 % (PPO vs. EPMM2). At high pressures, the nitrogen permeability of the EPMM3 membrane is close to that of the EPMM2 membrane, whereas at the low pressure, 60 psi, a decrease of 11% is observed when the TEOS loading increases from 5% to 10% (EPMM2 vs. EPMM3).

The results of X –ray diffraction analysis showed that the d-spacing of the membranes remained constant; however, the peak intensity reported in Table 6-2 shows that the crystalinity of the EPMM membranes is less than that of PPO membrane. As was described in the literature review, crystalline phases are impermeable and incapable of gas sorption, so their presence in a material causes a decrease in the permeability of the gases. However, this description is not completely true for PPO. The gas permeability data showed that the gas permeabilities of the semicrystaline PPO are higher than those of the amorphous EPMM membranes. The same results were observed for semicrystaline PPO, semicrystaline

polydiphenyl-PPO and their amorphous random copolymers by Alentiev et al. (1998). This can be interpreted to mean that the local transport parameters of the crystalline and amorphous phases of PPO do not strongly differ .It was supposed that the crystalline lattice of PPO is packed loosely and, therefore, it takes part in gas transport.

Moreover, the reduction in the gas permeability of the EPMM membranes owing to a decrease in the fractional free volume caused by the presence of aluminum silicate or residual solvent in these membranes. The decrease in the fractional free volume of the EPMM2 membrane was shown by the result of the DSC analysis.

As shown in Table 6-6, the O_2 over N_2 selectivity was calculated for EPMM membranes at three different pressures. There are modest increases for the ideal O_2/N_2 separation factor which may reflect the changes in diffusion. As was mentioned in the O_2/N_2 separation through PPO, mobility selectivity, $[D_A]/[D_B]$, is a favorable term in the separation of this pair gas. The diffusivity selectivity is primarily equal to the product of the energetic and entropic selectivity (Zimmerman and Koros, 1999). The materials with the well-defined and rigid pores, for example zeolites, signify the high entropic selectivity which is unachievable by more disordered polymeric structure. The main objective of the formation of aluminum silicate in PPO structure is to increase entropic selectivity of the modified PPO membranes.

O_2 and N_2 are diatomic molecules, and have a spherocylindrical structures as shown , in Figure 6.21. The length and the width values of oxygen and nitrogen were taken from Bussary and Aubert-frecon 1991, and Hirschfelder et al., 1954, respectively.

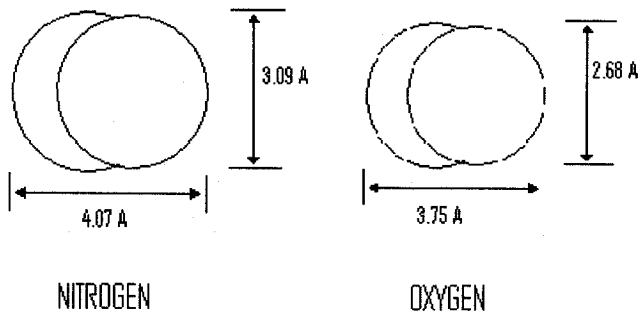

Figure 6.21 The length and width of O_2 and N_2 molecules.

Both O_2 and N_2 can rotate about their two axes in the open pores of the aluminum silicate. Once entering the pore constriction, where the pore size is between the kinematics diameters of nitrogen and oxygen, oxygen can maintain its two dimensional rotation while larger size of nitrogen prevent it from rotating about two rotational axes. Therefore, oxygen encounters only a slight entropy decrease upon entering the constricted region, while nitrogen experiences larger entropy changes. Therefore, this yields an increase in the entropy selectivity and consequently diffusivity selectivity. In the present research, at the low pressure, 60 psi, an increase of 10% was observed in the O_2/N_2 selectivity for the EPMM3 membrane in comparison with that of the unmodified PPO. This can be due to entropy selectivity increases which are produced by the presence of aluminum silicate in the PPO matrix. On the other hand, at high pressures, a slight increase in the selectivity of this pair gas was observed. This can be described that the pore constriction of the aluminum silicate will be open more, since the aluminum silicate produced in the PPO matrix, unlike zeolites, does not have solid pore walls. Therefore, nitrogen will be able to rotate about two rotational axes in the pore constriction so that this causes a reduction in the entropy selectivity.

Although for EPMM2, both oxygen and nitrogen permeability significantly decrease, a slight increase in the ideal O_2/N_2 selectivity was observed. This indicates that pore size of

aluminum silicate and its effect on the PPO chain mobility can restrict the rotation of this pair gas about their rotational axes which can not affect significantly on the entropy selectivity.

As was observed in the thermal analysis section, residual solvent was detected the DSC analysis of the EPMM membranes. It is therefore important to consider the effect of the residual solvent on the gas permeation data. Residual solvents can act in concentration-dependent behavior. Below certain concentrations, they may function as antiplasticizer so that they reduce the chain mobility. They occupy Langmuir sorption site and hence decrease free volume and consequently cause a decrease in gas permeability. In some cases, this reduction in permeability is accompanied by an increase in selectivity which is pronounced for gas pairs differing significantly in molecular size (Maeda and Paul, 1987). At higher concentrations, they act like plasticizers so that they increase chain mobility and permeability and decrease selectivity.

In order to clarify exactly the effect of the aluminum silicate on the gas permeation properties of the emulsion mixed matrix membranes, the elimination of the residual solvent is strongly recommended. The membranes used in this work were treated at 120 °C under vacuum for 48 h. This temperature was used in order to minimize the thermal degradation of PPO. Perhaps lower vacuum pressures could be used to remove the residual solvent or a more volatile surfactant could be used.

6.4.2 Gas separation test

We examined gas mixture (air) in order to better assess the true potential of these synthesized membranes for air separation. A summary of the gas separation properties of the PPO, the multi-layered, and the EPMM membranes are tabulated in Table 6-9.

Table 6-9 The gas separation properties of the PPO, the multi-layered membrane, and the EPMM membranes.

Membrane	Separation factor O_2/N_2		Ideal selectivity O_2/N_2		Permeability O_2		Permeability N_2	
		St.Dev		St.Dev	(Barrer)	St.Dev	(Barrer)	St.Dev
Blank PPO								
coupon 1	3.01	0.003	4.249	0.009	15.47	1.44	3.64	0.37
coupon 2	3.00	0.004	4.227	0.010	15.51	1.30	3.67	0.35
multi-layered membrane								
coupon 1	2.65	0.008	3.520	0.011	8.71	0.730	2.47	0.28
coupon 2	2.6	0.006	3.427	0.015	8.64	0.690	2.52	0.31
EPMM2								
coupon1	3.131	0.004	4.557	0.014	12.55	1.02	2.75	0.22
coupon2	3.154	0.007	4.605	0.018	12.64	1.03	2.74	0.21
EPMM3								
coupon1	2.695	0.027	3.707	0.037	12.02	1.06	3.25	0.28
coupon2	2.721	0.030	3.758	0.044	12.12	1.01	3.23	0.25

6.4.2.1 Multi-layered membrane

Although a similarity of gas permeation properties of the multi-layered membrane with those of PPO was observed in gas permeation test, gas separation data of the multi-layered membrane illustrates a different characteristic from unmodified PPO membrane in gas separation test. The significant difference observed between the multi-layered membrane and unmodified PPO membrane is the difference in their selectivities. The selectivity of the multi-layered membrane is approximately 19 % less than that of the unmodified PPO.

6.4.2.2 The Effect of the ultrasound energy density on the ideal separation factor for EPMM3 membrane

Figure 6-22 illustrates the effect of ultrasound energy density used in the second step of the W/O emulsion preparation. As seen in the Figure 6.22 the ideal selectivity increases with increasing the energy density. This could be due to several reasons; that more TEOS is transferred to the water phase, that the nanoparticles in the mixed matrix membrane are smaller, or that the reaction was more complete at the higher energy densities. Another

explanation would be that at longer sonication times lead to the disengaging of the solid aluminium slilicate from the aqueous phase leading to a more compatibilized nanoparticle-polymer system.

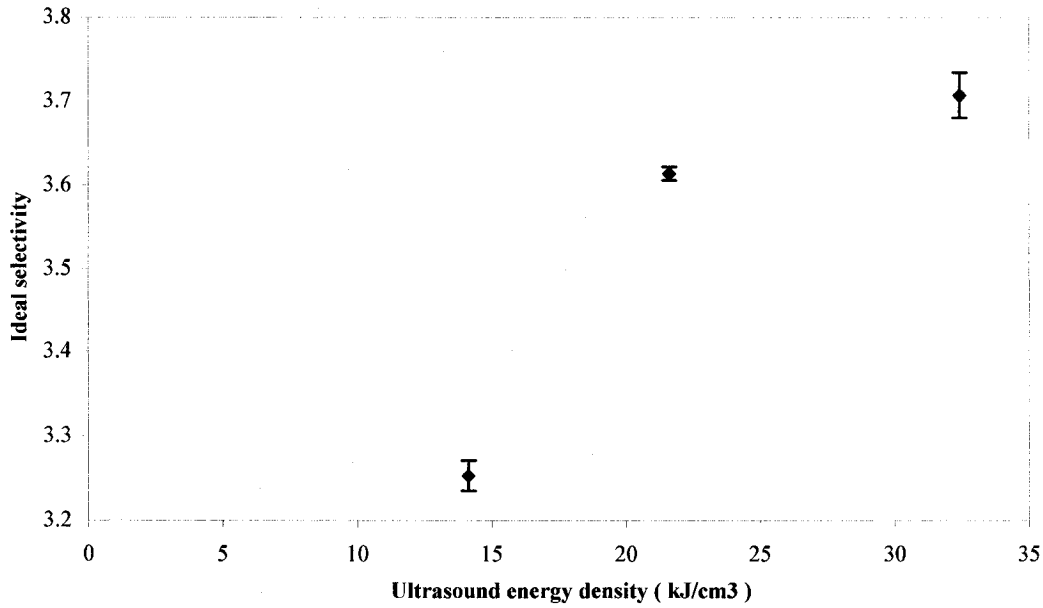

Figure 6.22 The Effect of the ultrasound energy density on the ideal separation factor for EPMM3 membrane.

6.4.2.3 The effect of the TEOS contents on the gas separation properties of the EPMM2 and EPMM3 membranes

The gas separation factor and ideal selectivity of the EPMM membranes are reported in Table 6-9. The EPMM2 membrane shows a higher separation factor and selectivity, in comparison with those of unmodified PPO membrane, while the EPMM3 membrane illustrates lower separation factor and selectivity. A drastic reduction of oxygen permeability is observed when TEOS loading increases up to 5 % (PPO vs. EPMM2). The oxygen permeability decreases to less of an extent with increasing TEOS loading from 5% up to 10% (EPMM2 vs. EPMM3).

The nitrogen permeability shows different trend as the oxygen permeability. The nitrogen permeability decrease with increasing TEOS loading up to 5% (PPO vs. EPMM2), and then it increases when the loading increase up to 10 % (EPPM2 vs. EPPM3).

CHAPTER 7

CONCLUSIONS AND RECOMMENDATIONS

7.1 Conclusions

By performing the polycondensation of tetraethylorthosilicate (TEOS) in the presence of aluminum hydroxonitrate within the emulsified aqueous phase in a dilute solution of poly (2,6-dimethyl-1,4-phenylene oxide) (PPO) in trichloroethylene (TCE), we have demonstrated that it is possible to grow inorganic nanoparticles that are well dispersed in a polymer matrix. Such prepared membranes, which can be referred to as Emulsion Polymerized Mixed Matrix (EPMM) membranes, represent a new category of the materials not limited to the inorganic/polymer system employed in this project.

In the current research we have produced EPMM membranes with an inorganic loading up to 10% based on the initial amount of TEOS. The presence of the particles measuring less than one micron cross section in the membrane was confirmed by SEM analysis. In addition, the EDX analysis showed that the observed particles contained both Si and Al, thus confirming that TEOS had been hydrolyzed by aluminum hydroxonitrate. Moreover, the presence of inorganic components in the membranes was also confirmed by the TG analysis. The latter showed that the minimum conversion of TEOS, based on the mass balance of SiO_2, was 71.7%.

The integrity of the EPMM membranes was confirmed in gas separation tests with air, in which the ideal selectivity for O_2/N_2 separation was observed to be as high as 4.56,

which is 7% greater than the ideal selectivity of a blank PPO membrane. The full extent of the potential of the membranes prepared in the current project could be diminished by the presence of a residual solvent detected in the DSC analysis. On the other hand, it is important to emphasize that the observed selectivity of the EPMM membranes is not due to the presence of the residual solvent. Therefore, the new method developed in this project successfully overcame the major challenge of making inorganic/polymer materials for gas separation, i.e., to avoid the formation of nonselective voids at the inorganic/polymer interface.

The DSC analysis indicated that the glass transition temperature of the EPMM materials strongly depends on the inorganic loading. The respective T_g of EPMM2 and EPMM3 membranes, which correspond to 5% and 10% inorganic loading based on TEOS, respectively, are 204.0°C and 182.5°C. In contrast, the blank PPO membrane had T_g equal to 217.5°C. On the other hand, based on X-ray diffraction analysis, the inorganic loading does not significantly affect *d*-spacing of the EPMM materials. However, based on the normalized intensity of the major peak obtained from X-ray crystallography, the crystalinity of the membrane decreased slightly with inorganic loading.

We have applied a new method for estimation of the fractional free volume of the membranes at the glass transition temperature, which requires measuring the specific heat capacity jump at the glass transition temperature. The specific heat capacity jump of the membranes was measured using modulated DSC. A mathematical correlation between the specific heat capacity jump at glass transition temperature and fractional free volume at glass transition temperature was obtained by combination of Wunderlich equation (1960) and Hirai and Eyring (1958). The validity of the approach was evaluated with the value of fractional

free volume obtained from the group contribution method. In this method, a fraction free volume of 0.201 was obtained for PPO membrane at glass transition temperature. This value of fractional free volume agrees with the value of 0.1988 obtained from the group contribution method, which is reported by Aguilar Vega and Paul (1993). The fraction free volume of the EPMM membranes shows the inorganic phase in the membranes has a great impact on the fractional free volume. The fractional free volume of EPMM2 at the glass transition temperature is 0.1 which is 49.75% lower than the fractional free volume of the blank PPO membrane at the glass transition temperature.

7.2 Recommendations

The following are recommendations formulated, based on the results of this research, for future work:

- The performance of various surfactants should be investigated to minimize the size of the primary emulsion and improve its stability
- The effect of the ultrasound homogenizer energy, which is applied in the second step of the W/O emulsion preparation, on the EPMM membrane properties should be further studied. This study can be done through TGA analysis and gas separation test.
- The potential effects of the residual solvent should be removed by heat treatment around T_g, in order to have a better understanding of the effect of the aluminum silicate on the gas permeation properties of the EPMM membranes and to have better prediction of the gas permeation mechanism governing on the EPMM membranes.
- The potential application of this novel method in preparation of EPMM membranes with high loading of the inorganic material should be studied.

- The EPMM membranes should be characterized by testing other gases such as methane and carbon dioxide, and their potential application in other membrane separations, for example, pervaporation, reverse osmosis etc., should be investigated as well.
- The use of a SEM with higher magnification (e.g. 30,000) is strongly recommended in order to observe the distribution of the inorganic particles embedded in the polymer matrix.
- The estimation of the Cliff-Lorimer factor for Si and Al elements in EDX analysis is suggested to evaluate the weight fraction of Al and Si elements in the inorganic particles embedded in the polymer matrix. This would provide a better estimation of the extent of this reaction.

References

Abismail, B., Canselier, J.P, Wilhelm, A.M., Delmas, H., Gourdon, C., "Emulsification by ultrasound: drop size distribution and stability", *Ultrasonics Sonochemistry,* **6,** 75-83, 1999.

Acrivos, A., Shah, M. J., Petersen, E. E., "On the Flow of a Non-Newtonian Liquid on Rotating Disk", *Journal of Applied Physics*, **31**, 963, 1960.

Akers, P.J., Allen, G., and Bethell, M.J., *Polymer*, **9**, 575, 1968.

Akitt, J.W., and Farthing, A., "Aluminum-27 Nuclear Magnetic Resonance studies of the Hydrolysis of Aluminum (III). Part4. Hydrolysis using Sodium Carbonate".,*J. Chem. Soc., Dalton Trans.*, 1617, 1981.

Alentiev, A., Drioli, E., Gokzhaev, M., Golemme, G., Ilinich, O., Lapkin, A., Volkov, V., and Yampolskii, Y., "Gas permeation properties of phenyleneoxide polymers", *Journal of Membrane Science,* **138,** 99-107, 1998.

Augilar-Vega, M., and Paul, D.R., "Gas transport properties of polyphenylene ethers", *J. Polym. Sci.: Part B: Polym. Phys.* **31,** 1557, 1993.

.

Aycock, D., "Polyphenylene ether, in Encyclopedia of Polymer Science and Technology", Volume 13, Interscience Publisher, New York, 1974.

Baes, C.F and Mesmer, R.E., The Hydrolysis of Cations (Wiley, New York, 1976).

Baker, R. W., Membrane Technology and Applications, John Wiley & Sons, Ltd, 2004.

Baker, R.W. and Wijmans, J.G., Membrane Separation of OrganicVapours from Gas Streams, in Polymeric Gas Separation Membranes, 1994.

Barrales-Rienda, J. M., and Pepper, D. C., "Intrinsic Viscosity and Dimensions of Poly (Phenylene oxide)", *Polymer Letters.*, **4**, 939-941, 1966.

Barrer, R. M., Barrie, J. A., and Slater, J., "Sorption and diffusion in ethyl cellulose. Part III Comparison between ethyl cellulose and rubber" *Journal of Polymer Science*, **27** 177, 1958.

Becher, P., Emulsion, Theory and Practice, second ed. Reinhold, New York, 1965.

Behrend, O., Schubert, H., Ax, K., "Influence of continuous phase viscosity on emulsification by ultrasound" *Ultrasonics Sonochemistry*, **7**, 77-85, 2000.

Bird, B. R., Stweart, W. E. and Lightfoot, E. N., "Transport Phenomena" John Wiley and Sons, 1960.

Bornside, D.E., Macosko, C.W., and Scriven, L.E., "On the Modelling of Spin Coating" *J. Imaging Technol.*, **13**, 122, 1987.

Bornside, D.E., Macosko, C.W., and Scriven, L.E., "Spin coating : one dimensional Model" *J. Appl Phys.*, **66**, 5185, 1989.

Bottero, J.Y.,Cases,J.M.,Fiessinger,F., and Poirier., "Studies of hydrolyzed aluminum species and compensation of aqueous solutions.", *J.Phys.Chem,* **84**,2933, 1980.

Brinker, C.J., Scherer, G.W., "Sol-Gel Science: The Physics and Chemistry of Sol-Gel Processing." Academic Press, San Diego, 1990.

Bussery, B., Aubert-Frecon, M., "Semi-imperical investigationof the angular dependence of the interaction energy betweentwo ground-state oxygen molecules", *Chem. Phys. Lett.*, 179, 393-397, 1991.

Caro, J., Noack, M., Kölsch P., and Schäfer R., "Zeolite membranes-state of their development and perspective", *Microporous and Mesoporous Materials,* **38,** 3-24, 2000.

Chakraborty, A.K., "Aluminosilicate formation in various mixtures of tetraethylorthosilicate (TEOS) and aluminum nitrate (ANN)", Thermochimica Acta, **427**, 109- 116, 2004.

Crank, J. "The mathematics of diffusion", 2nd ed. Clarendo, Oxford, 1975.

Dietz, W.A. "Response Factors for Gas Chromatographic Analyses", *Journal of gas chromatography,* **5**, 68, 1967.

Elferink, W.J., Nair, B.N, de Vos, R.M., Keizer, K.,Verweij, H., "Sol-Gel Synthesis and Charaterization of Microporous Silica Membrane I: SAXS study on the Growth of Polymeric Structures", *Journal of Colloid and Interface Science.,***178**, 565-570, 1996.

Eliseev, A. A, Kalinin, S. V., Pivalov, V. I., Vertegel, A. A., and Tretyakov, Yu. D., "The Effect of Copolymerization of Tetraethylorthosilicate and Aluminum Hydroxonitrate". *Journal of Solid State Chemistry,* **147**, 304-308, 1999.

Emslie, A. G., Bonner F. T., Peck, L. G., "Flow of a Viscous Liquid on a Rotating Disk", *Journal of Applied physics*, **29**, 858, 1957.

Ficheux, M.F, Bonakdar, L., Leal-calderon, F., and Bibette, J. "Some stability Criteria for double emulsions" *Langmuier* , **14**, 2702-2706, 1998.

Furrer, G., Ludwig, C., and Shindler, P. W., "On the Chemistry of the Keggin Al_{13} Polymer", *Journal of Colloid and Interface Science*, **Vol 149**, No 1, March1, 1992.

Ghosal, K., and Freeman, B. D. "Gas Separation Using Polymer Membranes: An Overview", *Polymers for Advanced Technologies*, **5**, 673, 1993.

Hay, A. S., Blanchard, H. S., Enders, G.F., and Eustance, J. W., "Polymerization by Oxidative Coupling", *J. American Chemical Society*, **81**, 6335, 1959.

Hay, A. S., and Dana, D. E. *J. Polym. Sci. Part A:*, **27**, 837, 1989.

Hay, A. S., *Macromoleculaes*, 2, 107, 1969.

Hay, A. S, *Adv. Polym. Sci.*, **4**, 496, 1967.

Henis Jay, M. S. and Tripodi, M. k., "Composite Hollow Fiber Membranes for gas Separation: The Resistance Model Approach", *Journal of Membrane Science,* **8**, 233-246, 1981.

Hirai, N. and Eyring, H., "Bulk Viscosity of Liquids", *Journal of Applied Physics,* **29**, 810, 1958.

Hirai, T., Kawamura, Y., and Komasawa, I. "Preparation of Y_2O_3 nanoparticulate thin films using an emulsion liquid membrane system". *Journal of Colloid and Interface Science* **275** , 508-513, 2004.

Hou, W., Papadopoulos, K. D. "W/O/W globules stabilized with Span 80 and Tween 80", *Colloids Surf A: Physico-chemical and engineering Aspects.* **125**, 181-187, 1997.

Hirschfelder, J.O., Curtiss, C. F., Bird, R. B., Molecular Theory of Gases and Liquids; John Wiley & Sons. Inc. New York, 1954.

Huang, Y.X., Senos, A. M. R., Rocha, J., Baptista, J. L., "Gel formation in mullite precursors obtained via tetraethylorthosilicate (TEOS) pre-hydrolysis", *Journal of Material Science,* **32,** 105-110, 1997.

Jia, L. and Xu, J, *Polym J.*, **23**, 417, 1991.

Jiang, R., Kunz, H. R., Fenton, J. M., "Composite silica/Nafion membranes prepared by tetraethylorthosilicate sol-gel reaction and solution casting for direct methanol fuel cells", *Journal of Membrane Science,* **272**, 116-124, 2006.

Jiao, J. and Burgess, D. J., "Rheology and Stability of Water-in-Oil-Water Multiple Emulsions Containing Span 83 and Tween 80, *AAPS PharmScie,* **5,** 1, 2003.

Joly, C., Goizet, S., Schrotter, J.C., Sanchez, J., Escoubes, M., "Sol-gel polyimide-silica composite membrane gas transport properties", *Journal of membrane Science*, **130**, 63-74, 1997.

Joscelyne, S.M., Tragaradth, G., "Membrane emulsion –a literature review" *Journal of membrane science*, **169**, 107-117, 2002.

Karasz, F. E., O Reilly, J. M., "Thermal Properties Of Poly (2,6-Dimethyl Phenylene ether)" *Journal of polymer Sci. polym. Lett.* **3**, 561-563, 1965.

Kenneth, S., "the chemistry of ultrasound" Encyclopedia Britannia, Chicago, 1994, pp 138-155.

Kesting, R. E. and Fritzsche, A.K., "Polymeric Gas Separation Membranes", John Wiely & Sons, Inc., 1993.

Kim, D. S., Park, H. B., Rhim, J. W., Lee, Y. M., "Preparation and characterization of crosslinked PVA/SiO_2 hybrid membranes containing sulfonic acid groups for direct methanol fuel cell applications", *Journal of Membrane Science*, **240**, 37-48, 2004.

Kim, J. H., Lee, Y. M., "Gas permeation properties of poly (amide-6-b-ethylene oxide) - silica hybrid membranes", *Journal of Membrane Science*, **193**, 209-225, 2001.

Koros, W.J "Model for sorption of mixed gases in glassy polymers" *Journal of Polymer Science, Polymer Physics Ed.,* ***18***, 981, 1980.

Koros, W.J and Fleming, G.K. "Membrane-based gas separation" *J. Membrane Sci.*, **83**, 1, 1993.

Koros, W.J. and Paul, D.R. "Transient and steady state permeation in poly (ethylene terephetalate) above and below glass transition temperature" *Journal of Polymer Science, Polymer Physics Ed.,* **16**, 2171, 1978b.

Krause, S. in Paul, D. R. and Newman S., eds., *Polymer Blends I*, Academic Press, Inc., Orlando, Fla., 1978, p. 6.

Krevelen Van, D.W., "Properties of Polymers" 3rd edn. Elesvier, Amsterdam. 1990.

Landry, C. J. T., Coltrain, B.K., Teegarden, D.M., Long, T.E, Long, V.K., "Use of organic copolymers as compatibilizers for organic-inorganic composites", *Macromolecules* **29**, 4712, 1996.

Lauterborn, W., Ohi, C.D., "Cavitation bubble dynamics", Ultrasonics *Sonochemistry,* **4,** 65-75, 1997.

Livage, J., Babonneau, F., Sanchez, C., in "Sol-Gel Optics, Processing and Applications", (Lisa C. Klein, Ed.), pp.39-58, 1994.

Maeda, Y. and Paul, D. R., "Effect of Anti plasticization of Selectivity and Productivity of Gas Separation Membranes", Journal of Membrane Science, **30**, 1-9, 1987.

Mahajan, R. and Koros J. W., "*Factors controlling successful Formation of Mixed-Matrix Gas Separation*", Ind. Eng. Chem. Res, **39**, 2692-2696, 2000.

Mears, P., "Polymers: structure and bulk properties", Van Nostrand, New York, 1965.

Mahajan, S. S., "Structure modification of poly(2,6- dimethyl- 1,4-phenylene oxide)", Poly-Plast. Tec. Eng. **30**, 27, 1991.

Meyerhofer, D., "Characteristics of resist films produced by spinning", *Journal of Applied .Physics*, **49**, 3993, 1978.

Michaels, A.S, and Bixler, H.J, "Solubility of gasesin polyethylene. Flow of gases through polyethylene, *J. Polym. Sci.,* **50**, 393-413, 1961.

Neduzhii. S. A.,"Investigation of emulsification brought on by sonic and ultrasonic oscillations", *Soviet Physics-Acoustics*, **7**, 221-235, 1961.

Paul, D.R, and Korous, W.J "Effect of partially immobilizing sorption on permeability and diffusion time lag" *Journal of Polymer Science, Polymer. Phys.* Ed. **14,** 675, 1976.

Peurrung.. L. M. and Graves. D. B., *J. Electrochem.* Soc. **138**, 2115, 1991.

Plate, N., and Yampol'skii, Y., "Polymeric Gas Separation Membranes" Edited by Paul D. R., and Yampol'skii Y., CRC Press, London, p.156,1994.

.

Polotskaya, G. A., AGranova, S. A., Gazdina, N. V., Kuznetsov, YU. P., and Nesterov, V. V., "Effect of Molecular Weight Parameters on Gas Transport Properties of Poly(2,6-dimethyl-1, 4-phenylene oxide), *Journal of Applied Polymer Science*, **62**, 2215-2218, 1996.

Rao, M.B. and Sircar, S., "Nanoporous carbon membranes for separation of gas mixtures by selective surface flow", *J. Membr. Sci.*, **85** 253-264, 1993.

Ranby, B.G, Chan, K.S, and Brumberger, H., "Higher order transitions in poly(4-methyl-1-pentene)" *J. Polym. Sci.* **58,** 545, 1962.

Shinoda, K, Yoneyama, T, Tsutsumi, H. "Evolution of emulsifier blending", *J Disper Sci Technol.,***1**, 1-12 , 1980.

Shultz, A. R., "Unperturbed Dimensions of Poly(2-methyl-6-phenyl-1,4-phenylene Oxide) and Poly(2,6-diphenyl-1,4-phenylelene Oxide) Chains," *J. Polym. Sci. : Part A-2*, **8**, 883, 1970.

Srikant, S. K., Arjumand, A. K., Aralaguppi, M. I., Kariduraganavar M. Y., "Synthesis and Characterization of Hybrid Membranes Using Poly (vinyl alcohol) and Tetraethylorthosilicate for the pervaporation Separation of Water- Isopropanol Mixtures" , *Journal of Applied Polymer Science*, **94**, 1304-1315, 2004.

Smolders, C.A., Duval, J.M., Folkers, B., Desgrandchamps, G., and Mulder, M. H. V., "Adsorbent filled membranes for gas separation. Part 1. Improvement of the gas separation properties of polymeric membranes by incorporation of microporous adsorbents" *Journal of Membrane Science*, **80**, 189-198, 1993.

Spangler, L. L., Torkelson, J. M., Royal J. Scot., "Influence of Solvent and Molecular Weight on Thickness and Surface Topography of Spin-Coated Polymer Films", *Polymer Engineering and Science*, **30**, 644, 1990.

Story B., J. and Koros, W.J., "Sorption and transport of CO_2 and CH_4 in chemically modified poly(phenylene oxide)", *Journal of Membrane Science,* **67,** 191-210, 1992.

Swaddle, T. W., Salerno, J., and Treglon, P. A., "Aqueous Aluminates, Silicates, and Aluminosilicates", *Chemical Society Reviews*, **23,** 319-325, 1994.

Szostak, R. "Molecular Sieves Principal of Synthesis and Identification", Blackie Academic 7& Professional 1998.

Takada, K., Matsuya, H., Masuda, T., and Higashimura, T, *J. Appl. Polym. Sci.*, **30**, 1605, 1985.

Thomas, L. C., "Modulated DSC Technology", TA Instrument, 2006.

Toi, K., Morel, G., and Paul, D. R., "Gas Sorption and Transport in Poly(phenylene oxide) and Comparison with other Glassy Polymers., *J.Appl.Polym.Sci.*, **27**, 7, 1982.

Tonelli, A.E., "Conformational characteristics and flexibility of poly(2,6-disubstituted-1,4 phenylene oxides) and polycarbonate of Diphenylol-2, 2-propane," *Macromolecules*, **5**, 558, 1972.

Tonelli, A.E., "Intramolecular Flexibility of Poly(2,6-disubstituted-1,4-phenylene Oxides),", *Macromolecules*, **6**,503, 1973.

Tran, A. "Development of and gas permeation study of homo and copolymers from the family of polyphenylene oxides", 2004.

Wehrli, B., Wieland, E., Furrer, G., Aquatic Sci. **52**, 3, 1990.

Wen, J., Wikes G. L., Chem Matter, **8**, 1667, 1996.

Wenig, W., Hammel, R., MacKnight, W.J., Karasz, F.E., "Morphological studies of semicrystalline poly(2,6-dimethyl-phenylene oxide)," *Macromolecules* **9**, 253,1976.

Wijmans, J.G., Baker, R.W. "The solution-diffusion model: a review", *Journal of Membrane Science.*, **107**, 1, 1995.

Winstone, W. S., Kamalesh, Ho., Sirkar, K., "Membrane Handbook", 1992.

Wrasidlo, W. "Transitions and relaxations in poly(1,4-phenylene ether)", *J. Polym. Sci.*, **Part A-2 58,** 1719, 1972.

Wood, R.W., Loomis, A.L., Phil. Mag.4 (1927) 417.

Wu, C., Xu, T., and Yang, W., "Synthesis and characterizations of new negatively charged organic-inorganic hybrid materials: effect of molecular weight of sol-gel precursor", *Journal of Solid State Chemistry*, **177,** 1660-1666, 2004.

Yonkoski, R.K and Soane, D. S. "Model for spin coating in microelectronic applications" *J. Appl. Phys.* **72,** 725, 1992.

Wunderlich, B., "Study of The Change in Specific Heat Of Monomeric and Polymeric Glasses During The Glass Transition", *J. Chem. Phys.*, **64**, 1052, 1960.

Zhang, S., Wu, C., Xu, T., Gong M., Xu, X., "Synthesis and characterizations of anion exchange organic-inorganic hybrid materials based on poly(2,6-dimethyl-1, 4-phenylene oxide) (PPO), *Journal of Solid State Chemistry,* **178**, 2292-2300, 2005.

Zimmerman, C. M., Koros, W. J., "Entropic Selectivity Analysis of a Series of Polypyrrolones for Gas Separation Membranes", *Macromolecules,* **32**, 3341-3346, 1999.

Zolanddz, R. and Fleming, G.K., "Gas Permeation" in Membrane Hand book, eds. HO, W. S. W. and Sirkar, K. K., Van Nostrand Reinhold, New York, NY, 1992.

APPENDIX A

W/O/W DOUBLE EMULSION

The Tables A.1 to A.4 indicate the quantities of ingredients used in preparation of W/O/W double emulsions. As seen in the all Tables the primary emulsion composition was kept constant. The different external phase compositions were prepared in order to prepare stable double W/O/W emulsions.

Table A.1 the external phase includes only pure water

Primary Emulsion		**External phase**	
Span 83	0.3400 g	The volume ratio of external phase to primary emulsion	5
Kerosene	1.7 cm^3	External phase (pure water) volume (cm^3)	17
Internal phase	1.7 cm^3	SDS (g)	0.017
Span 83	20%(W/V)	SDS (w/V)	0.1%
Energy density	$\frac{600W \times 0.8 \times 40\text{sec}}{3.4\text{cm}^3} = 5.65\,\text{kJ}/\text{cm}^3$		

Table A.2 the external phase includes TEOS and EtOH

Primary Emulsion		**External phase**	
Span 83	0.3507 g	The volume ratio of external phase to primary emulsion	5
Kerosene	1.8 cm^3	External phase volume (cm^3)	18
Internal phase	1.8 cm^3	TEOS (cm^3)	0.4
Span 83	20%(W/V)	EtOH (cm^3)	9.3
Energy density	$\frac{600W \times 0.8 \times 40\text{sec}}{3.6\text{cm}^3} = 5.3\,\text{kJ}/\text{cm}^3$	Water (cm^3)	8.3
		SDS (g)	0.018
		SDS (W/V)	0.1%

Table A.3 the external phase includes only TEOS

Primary Emulsion		**External phase**	
Span 83	0.3428 g	The volume ratio of external phase to primary emulsion	5
Kerosene	1.7 cm^3	External phase volume (cm^3)	17
Internal phase	1.7 cm^3	TEOS (cm^3)	0.4
Span 83	20%(w/V)	Water (cm^3)	16.6
Energy density	$\frac{600W \times 0.8 \times 40\text{sec}}{3.4\text{cm}^3} = 5.65\,\text{kJ}/\text{cm}^3$	SDS (g)	0.017
		SDS (W/V)	0.1%

Figure A.1 illustrates a ternary –phase diagram of TEOS, H_2O and isopropanol provided in this study.

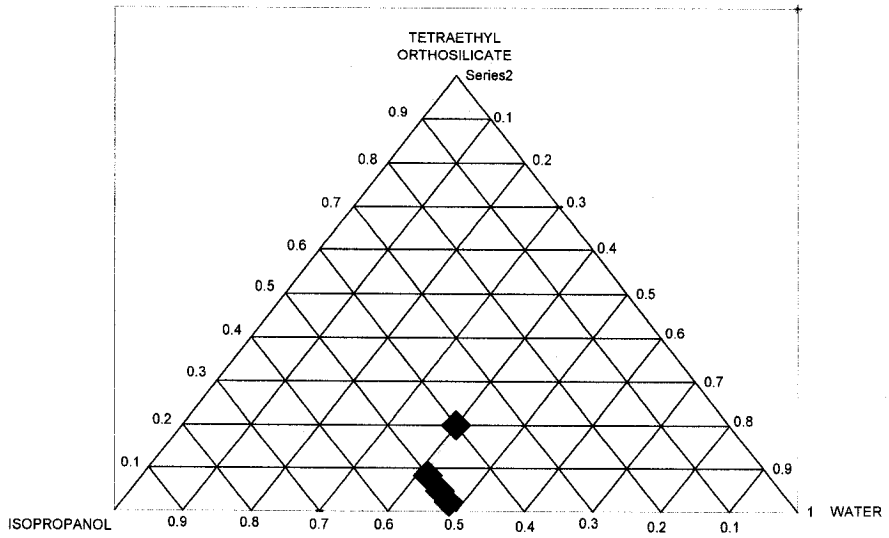

Fig A.1 Ternary phase diagram of TEOS, isopropanol and water

Table A.4 The external phase includes TEOS and Isopropanol

Primary Emulsion		**External phase**	
Span 83	0.522 g	The volume ratio of external phase to primary emulsion	10/6
Kerosene	2.61 cm^3	External phase volume (cm^3)	8.7
Internal phase	2.61 cm^3	TEOS (cm^3)	0.2
Span 83	20.42%(W/V)	Water (cm^3)	6
Energy density	$\frac{600W \times 0.8 \times 40\sec}{5.22cm^3} = 3.678 kJ/cm^3$	SDS (g)	0.0087
		SDS (W/V)	0.1%

APPENDIX B

B.1 Modulated Differential Scanning Calorimetry

A modulated DSC differs from a standard DSC in that in addition to a linear heating rate a sinusoidal heating rate is also applied to the sample. The linear heating rate allows the determination of the total heat flow. The sinusoidal heating rate allows the determination of the fraction of the total heat flow that responds to a changing heating rate. This fraction of the total heat flow is called the reversing heat flow or the heat capacity component of the total heat flow. The heat flow that does not respond to a changing heating rate is called a non reversing heat flow and is determined by subtracting the revering heat flow from the total heat flow.

The heat flow in the modulated DSC can be described in the following equation:

$$\frac{dH}{dt} = C_p \frac{dT}{dt} + f(T,t) \qquad \text{B1}$$

Where: dH/dT is total heat flow [mW], C_p is the heat capacity of the sample [mJ/°C], dT/dt is the heating rate [°C/s], and $f(T,t)$ is the heat flow that is a function of temperature and time. A convectional DSC measures only the total heat flow. When two or more transitions occur at the same time, it may be impossible to interpret the convectional DSC results. This problem is solved in the modulated DSC by splitting the total heat flow into two terms. The first term on the right hand side of Eq. (B1) is the reversing heat flow, which is also called the heat capacity component. The second term is the nonreversing heat flow, which is also called the kinetic component. (Thomas, Leonard C., 2006).

B.2 Modulated DSC results

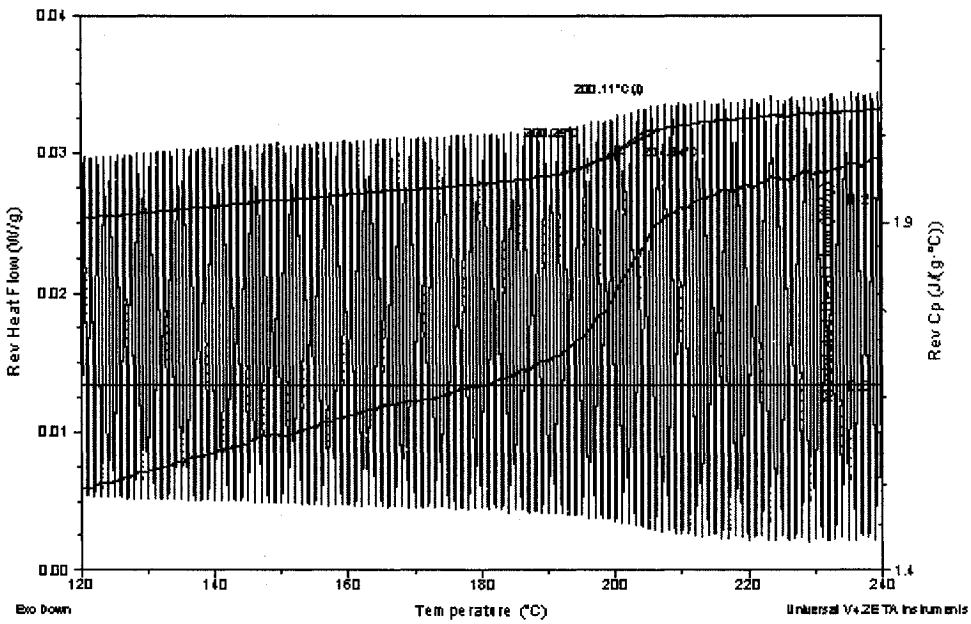

Figure B.1 Modulated DSC analysis of EPMM1 membrane

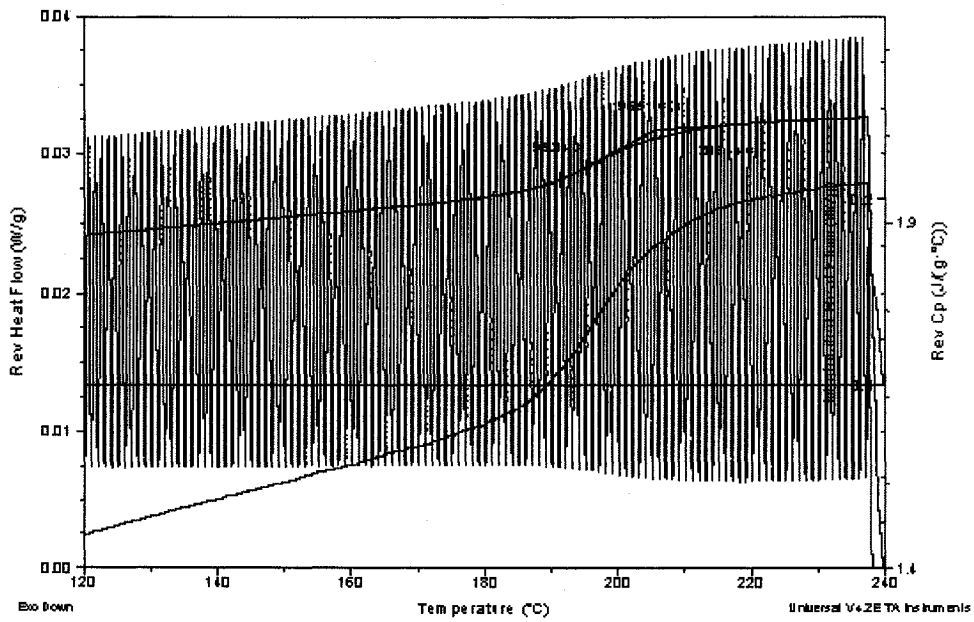

Figure B.2 Modulated DSC analysis of EPMM2 membrane

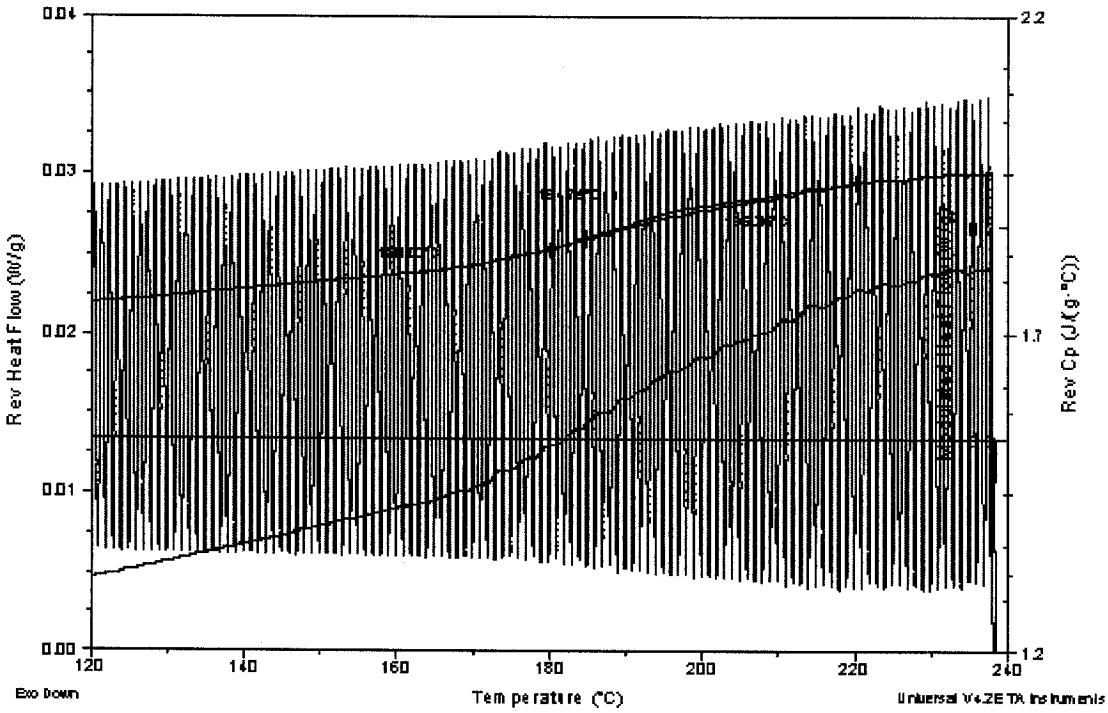

Figure B.3 Modulated DSC analysis of the EPMM3 membrane

Appendix C

Sample calculation

Initial blank PPO sample (mg)	5.302
Residual blank PPO sample (mg)	0.024
Initial EPMM3 sample (mg)	5.047
Residual EPMM3 sample (mg)	0.130
In organic residue of EPMM3 sample	0.107

Initial solution of EPMM3 membrane			
Initial solution	g	mol	Weight percent
TEOS (gr)	0.1	0.000480	8.555
PPO (gr)	1		85.554
Aluminum nitrate	0.012960	0.000034	1.109
Water	0.034561	0.001920	2.956
$Na_2 CO_3$	0.004011	3.78448E-05	0.343
N-octanol	0.017344	0.000133	1.483
Total			100

At 700 ° C for 100% conversion	mol	mol percent	g
SiO_2	0.000480	89.698	0.028841
Al_2O_3	1.72805E-05	3.229	0.001762
Na_2O	3.78448 E-05	7.0720	0.002346
Total	0.000535133	100	0.032950

TGA analysis

EPMM3 sample	mg	m mol
TEOS	0.4318	0.00207
PPO	4.3183	
Aluminum nitrate	0.0559	0.000149
Na_2CO_3	0.0173	0.000163
water	0.1492	
N-octanol	0.0749	0.000575
Total	5.0476	

At 700 ° C for 100% conversion	m mol	mol percent	m g
SiO_2	0.00207	89.6987	0.1245
Al_2O_3	7.46233E-05	3.229	0.007
Na_2O	0.000163	7.072	0.010
Total	0.002310	100	0.14229

Conversion based on SiO_2

$$\frac{0.107-(0.007+0.010)}{0.1245}\times 100 = 71.63\%$$